Membrane-active Compounds from Dinoflagellate-Structure-based Mechanism of Action of Amphidinol 3

(渦鞭毛藻由来の膜透過化物質・アンフィジノール３の構造を基盤とした作用機構に関する研究)

Respati Tri Swasono

Osaka University

Membrane-active Compounds from Dinoflagellate - Structure-based Mechanism of Action of Amphidinol 3.

(渦鞭毛藻由来の膜透過化物質・アンフィジノール３の構造を基盤とした作用機構に関する研究)

Respati Tri Swasono

Department of Chemistry
Graduate School of Science
Osaka University
2010

Membrane-active Compounds from Dinoflagellate - Structure-based Mechanism of Action of Amphidinol 3.

(渦鞭毛藻由来の膜透過化物質・アンフィジノール３の構造を基盤とした作用機構に関する研究)

A thesis submitted to the Graduate School of Science of Osaka University in partial fulfillment of the requirements for the degree of

Doctor of Philosophy (Ph.D.)
in Chemistry

by

Respati Tri Swasono

Department of Chemistry
Graduate School of Science
Osaka University

Abstract

Seventeen members of the amphidinol family (AMs) have been isolated from dinoflagellate of the genus Amphidinium. Unlike other natural or synthetic antifungal compounds, AMs lack nitrogenous polycycles or macrocyclic structures in their structures. These unique features make AMs an interesting model to gain a better understanding of the molecular mechanism of antifungal action. Among AM homologues, amphidinol 3 (AM3) significantly exceeds other homologues in the antifungal activity. The absolute configuration of AM3 was previously determined by extensive NMR experiments on the basis of *J*-based configuration analysis (JBCA) method, modified Mosher method, and HPLC analysis of the degradation products.

AM3 undergoes conformational changes in organic solvents while it takes relatively fixed configuration in a membrane model. By using NMR data of peracetyl AM3, the configuration of C50-C51 of AM3 as *threo*, which remained uncertain in the previous study, can be confirmed. The assignment supports that AM3 takes a turn structure around the two tetrahydropyran rings to form a hairpin-like shape. This conformational preference of AM3 is considered to play a crusial role for toroidal pore formation.

Like other polyene antibiotics, sterols commonly play an essential role in the selective toxicity of AM3. To examine more closely the effects of sterol on the affinity of AM3 to liposomal membranes, a dodecylamine-modified sensor chip was used to carry out kinetic analysis for AM3 binding to sterol-containing and sterol-free palmitoyloleoylphosphatidylcholine (POPC) liposomes by surface plasmon resonance (SPR).

Among other kinetic models, the two-state reaction scheme best reproduced the SPR sensorgrams, which indicated that the interaction is composed of two steps, which correspond to partition to the membrane and internalization to form stable complexes. The association constant for the first step (k_{a1}) and affinity constant (K_A) of AM3 in 5% cholesterol-containing membrane

exceeds that in the cholesterol-free one by 180- and 1000-fold, respectively. Although effect of ergosterol on the initial binding process is not as dramatic as in the case of cholesterol, ergosterol stabilizes formation of complex in the second step. As a result, K_A value of AM3 in 5% ergosterol-containing membrane exceeds that in the sterol-free one by about 5000-fold. These effects of cholesterol and ergosterol may account for the respective potent cytotoxicity and antifungal activities. Interestingly, AMs lack anti-bacterial activity, which is probably due to the absence of sterols in bacterial membranes. Moreover, AM3 showed higher affinity to ergosterol membrane than cholesterol one, particularly, in dissociation process; K_{A2} of the former was significantly larger than those of the latter. These observations indicate that AM3 forms more stable complex in the presence of ergosterol and may provide a clue for developing a new antifungal drug.

List of Abbreviations

1D	one-dimensional
2D	two-dimensional
Ac	acetyl
AM	amphidinol
AmB	amphotericin B
BuOH	butanol
C_6D_6	deuterated benzene
CD_3OD	deuterated methanol
CID	collision-induced dissociation
CFP	ciguatera fish poisoning
Cho	cholesterol
d	deuterated
δ	NMR chemical shift in ppm
DMPC	1,2-dimyristoyl-*sn*-glycerol-3-phosphocholine
DMSO	dimethyl sulfoxide
DQF-COSY	double-quantum filtered correlation spectroscopy
DSP	diarrhetic shellfish poisoning
EC_{50}	effective concentration 50%
EDC	1-ethyl-3-(3-dimethylaminopropyl)carbodiimide
eggPC	egg york phosphatidylcholine
Erg	ergosterol
ES	Erd-Schreiber
ESI	electrospray ionization
EtOAc	ethyl Acetate
EtOH	etanol
g	gram(s)
GC	gas chromatography
GC-MS	gas chromatography-mass spectrometry

h	hour(s)
HETLOC	heteronuclear long-range coupling
HMBC	heteronuclear multiple-bond correlation
HSQC	heteronuclear single-quantum correlation
HPLC	high performance liquid chromatography
Hz	hertz
IC_{50}	inhibition concentration 50%
J	spin coupling constants in Hz
LUV	large unilamellar vesicle
MPA	α-methoxyphenylacetic acid
MTPA	2-methoxy-2-trifluoromethyl-2-phenylacetic acid
Me	methyl
MEC	minimum effective concentration
MeOH	methanol
MHz	megahertz
min	minute(s)
MLV	multi lamellar vesicle
MS	mass spectrometry
m/z	ratio mass to charge (in mass spectroscopy)
NMR	nuclear magnetic resonance
NOE	nuclear Overhauser effect
NOESY	nuclear Overhauser effect spectroscopy
NHS	*N*-hydroxysucciimide
ODS	octadecylsilyl
PBS	phosphate buffered saline
PC	phosphatidylcholine
PEG	polyethylene glycol
POPC	1-palmitoyl-2-oeoyl-*sn*-glycerol-3-phosphocholine
PSP	paralytic shellfish poisoning
pyr-d_5	deuterated pyridine
rt	room temperature

RU	response (resonance) unit
SDS	sodium dodecylsulfate
SPR	surface plasmon resonance
SUV	small unilamellar vesicle
THP	tetrahydropyran
TLC	thin layer chromatography
TOCSY	total correlation spectroscopy
UV	ultraviolet

Table of Contents

List of Figures

List of Tables

Chapter 1

General Introduction-Bioactive Compounds from Marine Dinoflagellates of the Genus *Amphidinium*

1.1 Dinoflagellate Toxins

Marine microorganisms namely bacteria, cyanobacteria, dinoflagellates, and others are considered as the real producers of marine toxins including fish and algal poisons as well as bioactive substances isolated from marine invertebrates like sponges and tunicates.[1,2] In particular, marine dinoflagellates frequently produce toxins that cause seafood poisonings and massive fish death. These poisoning cases including paralytic shellfish poisoning (PSP), diarrhetic shellfish poisoning (DSP), neurotoxic shellfish poisoning (NSP), and ciguatera fish poisoning (CFP) have been received a lot of attention because of their socioeconomic impacts.

PSP, DSP, and NSP in humans are caused by ingestion of shellfish containing toxins. These toxins are accumulated by shellfish grazing on dinoflagellate toxins. The first and most toxic PSP toxin chemically characterized was saxitoxin (STX), which is produced mainly by dinoflagellates of the genus *Alexandrium.* DSP toxins can be divided into different groups depending on their chemical structures. The first group, acidic toxins, includes okadaic acid (OA) and its derivatives, dinophysistoxins (DTXs). The second group, neutral toxins, consists of polyether-lactones of the pectenotoxin family (PTXs). The third group includes a sulfated polyether and its derivatives, yessotoxins (YTXs). Neurotoxic shellfish poisoning (NSP) is caused by polyether brevetoxins produced by the unarmoured dinoflagellate *Karenia brevis* (formerly *Gymnodinium breve* or *Ptychodiscus brevis*). The brevetoxins are toxic to fish, marine mammals, birds and humans, but not to shellfish. In addition to shellfish poisoning, ciguatera fish poisoning (CFP) has been known for centuries. The poisoning is induced by

accumulation of causative toxins, such as the ciguatoxins, through the food chain, from small herbivorous fish grazing on the coral reefs into organs of bigger carnivorous fish that feed on them.[3] Table 1-1 shows examples of seafood poisonings, causative dinoflagellates and their main toxins.[4]

Table 1-1. Several seafood poisonings caused by marine dinoflagellates and their main toxins.[4]

Seafood poisoning	Causative dinoflagellates	Main toxins
Paralytic shellfish poisoning (PSP)	*Alexandrium catenalla, A. cohorticula, A. fundyense, A. fraterculus, A. leei, A. minutum, A. tamarense,A. andersonii, A. ostenfeldii, A.tamiyavanichii, Gymnodinium catenatum, Pyrodinium bahamanse* var *compressa*	Saxitoxins (STXs), Gonyautoxins (GTXs)
Diarrhetic shellfish poisoning (DSP)	*Dinophysis acuta, D. caudate, D. fortii, D. norvegica, D. mitra, D. rotundata, D. sacculus, D. mile, D. tripos, Prorocentrum lima, P. arenarium, P.belizeanum, P. cassubicum, P. convacum, P.faustiae, P. hoffmannianum,P. makulosum, Protoceratium reticulatum, Coolia* sp., *Protopperidium ocenicum, P. pellucidum,Phalacroma rotundatum.*	Okadaic acid, dinophysis toxins (DTXs), yessotoxins (YTXs), pectenotoxins (PTXs)
Neurotoxic shellfish poisoning (NSP)	*Karenia brevis, K. papilonacea, K. sellformis, K. bicuneiformis, K. concordia, Procentrum borbonicum*	Brevetoxins (PbTxs)
Ciguatera fish poisoning (CFP)	*Gambierdiscus toxicus, Ostreopsis* spp., *O. lenticularis, O. siamensis.*	Ciguatoxins (CTXs), Maitotoxins (MTXs), palytoxin, gambierol

Moreover, marine dinoflagellates are known to produce some of the largest and most complex polyketide secondary metabolites which have been found to be useful tools for probing biological and pharmacological phenomena.

These compounds are characterized by the presence of polycyclic ethers and/or polyhydroxy groups.[5,6]

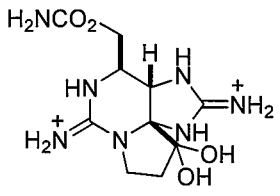

Saxitoxin

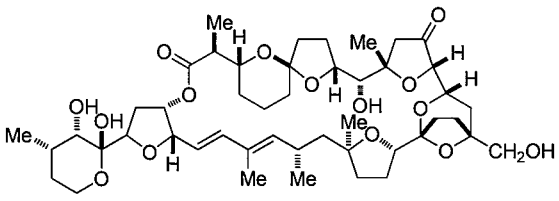

Pectenotoxin 1

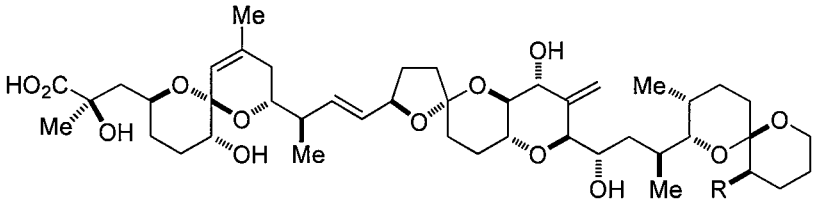

Okadaic acid: R = H

Dinophysistoxin 1: R = Me

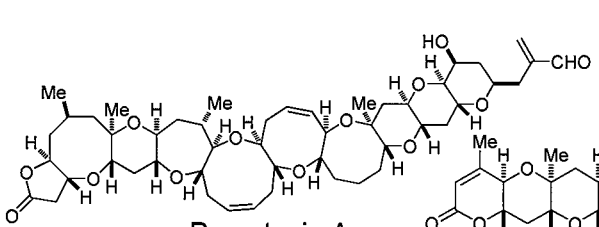

Brevetoxin A

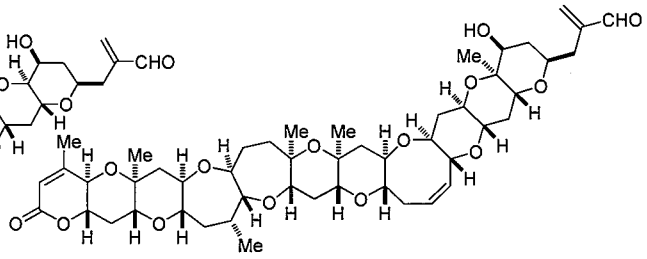

Brevetoxin B

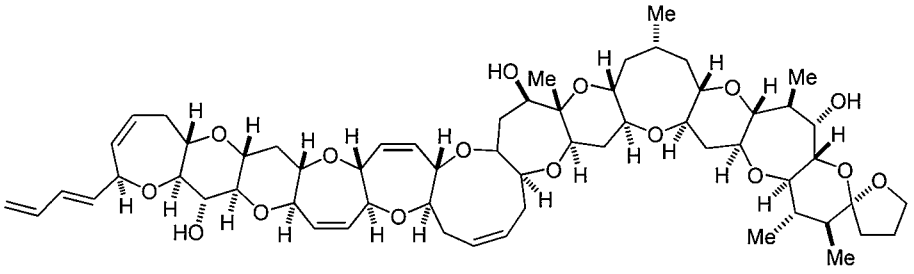

CTX4A

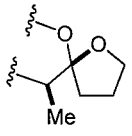

CTX4B

Ciguatoxins

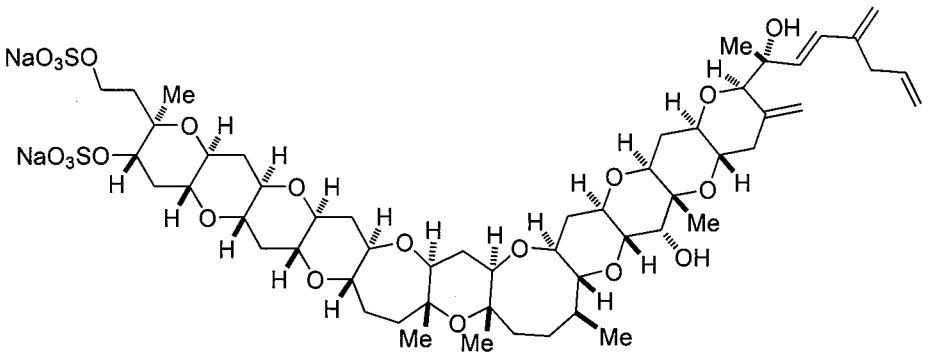

Yessotoxin

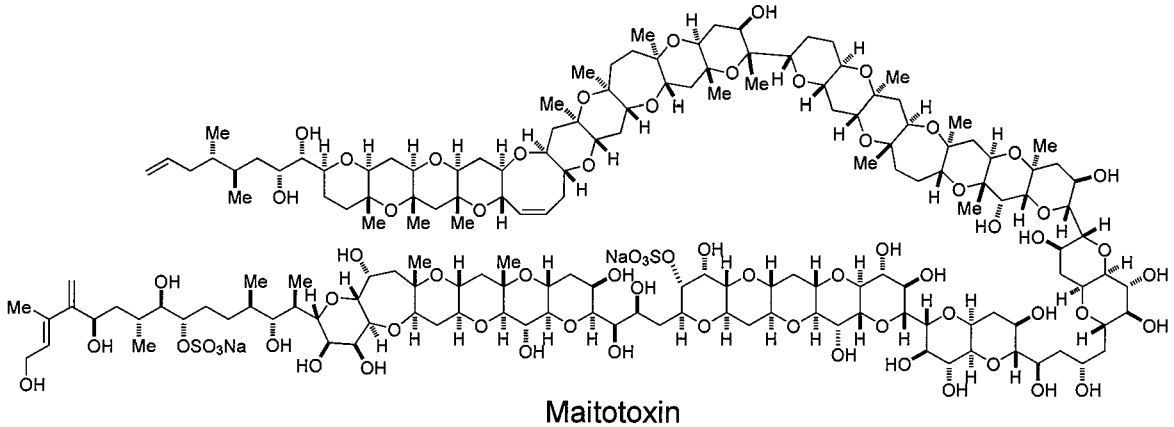

Maitotoxin

1.2 Bioactive Compounds from the Dinoflagellates of Genus *Amphidinium*

Among other dinoflagellates, the genus *Amphidinium* attracts much attention because of their production of numerous bioactive compounds with diverse structures and highly specific activities. Dinoflagellates of the genus *Amphidinium* Clapare´de & Lachmann belong to the order Gymnodiniales and the family Gymnodiniaceae and contains approximately 120 species.[7] The symbiotic dinoflagellate *Amphidinium* sp., isolated from the inner tissue of acoel flatworms *Amphiscolops* sp., produces a large number of macrolides, among them amphidinolides B, C, and a linear polyketide, amphidinin A. Many of these compounds show potent cytotoxicity against murine lymphoma L1210 cells and human epidermoid carcinoma KB cells.[8] Furthermore, colopsinol A, a new class of polyketide compound bearing a gentiobioside (*β*-D-glucopyranosyl-(1→6)-*β*-D-glucopyranoside) moiety and a sulfate ester, was isolated from the same

dinoflagellate. It is interesting to note that quite different types of polyketides such as colopsinol A and the amphidinolides are produced from the same dinoflagellate. Colopsinol A exhibits potent inhibitory activity against DNA polymerases α and β with IC_{50} values of 13 and 7 μM, respectively. However, there is no cytotoxic activity observed (IC_{50} > 10 μg/ mL) against L1210 murine leukemia cells and KB human epidermoid carcinoma cells *in vitro*.[9] In contrast to colopsinol A, amphidinolides B shows potent cytotoxicity against L1210 and KB cells with IC_{50} values of 0.00014 and 0.0042 μg/ mL, respectively.

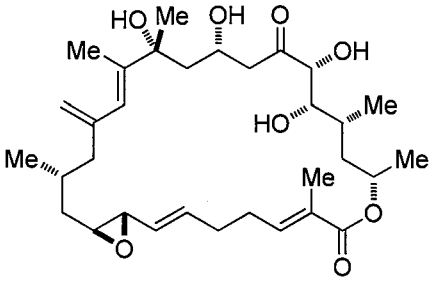

Amphidinolide B

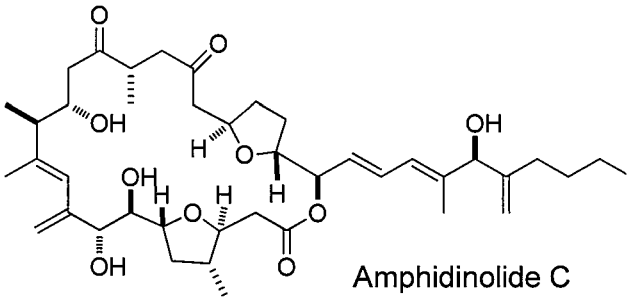

Amphidinolide C

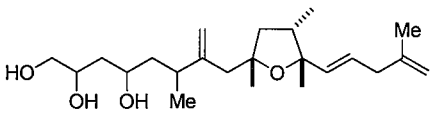

Amphidinin A

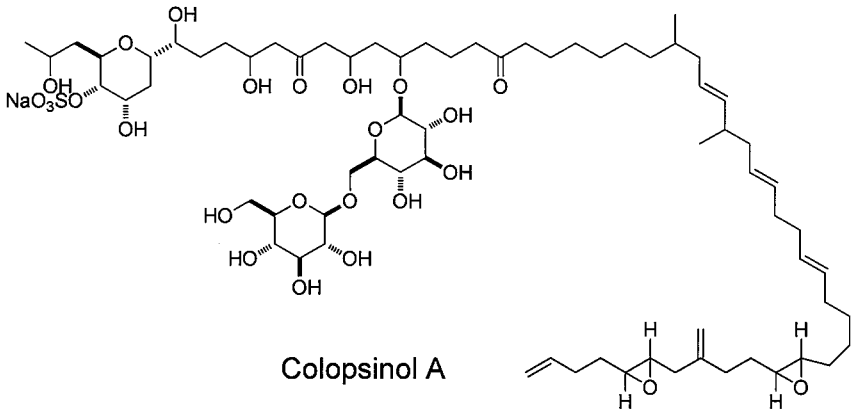

Colopsinol A

1.3 Family of Amphidinols

1.3.1 Amphidinols

An early report of hemolytic and antifungal activities from extracts of *Amphidinium klebsii* led to the isolation and identification of amphidinol 1 (AM1)

in 1991.[10] Since then, nearly 20 closely related toxins known as the amphidinols (AMs) have been isolated from various marine dinoflagellates belonging to the genus *Amphidinium*.[11-17] In general, all members in this group of natural products are characterized by a long polyhydroxy chain and polyolefins, which provide their amphiphilic properties. The hydrophilic and hydrophobic portions are connected by an intermediate C19 section containing two tetrahydropyran rings separated by a short C7 aliphatic chain. The structure of this connection is largely preserved among the different amphidinols. Most structural varieties resulted from alterations in the length and substitution pattern of the polyol portion (C23-C37) and from variations in the length (C16-C18) and degree of unsaturation of the polyene section.[17]

Amphidinol 1 (AM1) was isolated from *A. klebsii* collected in Okinawa, Japan and subsequently AM2, AM3, AM4, AM5, and AM6 were isolated from a different strain of *A. klebsii* separated from Aburatsubo-Bay, Kanagawa Japan (Biological specimen of the dinoflagellate was deposited in the National Institute of Environmental Studies, with the number of NIES 613). Isolation of AM7 and AM8 have not been elucidated.[13] Later, AM7 was isolated again from the same strain of *A. klebsii* and found to possess the smallest molecular weight among the known AM homologues.[14] Moreover, two closely related homologues of AM7, AM14 and AM15, were also isolated from the same strain of dinoflagellate (NIES 613).[16]

Meanwhile, *A. carterae* separated from Kauaroa, South Island, New Zealand, was reported to produce five amphidinol analogues, AM9 to AM13. This was the first isolation of new amphidinol analogues from *A. carterae* collected outside of Japan. This strain produces AM9 most abundantly.[15] More recently, a novel amphidinol with hemolytic activity, AM17 has been isolated from a strain of *A. carterae* collected in Little San Salvadore Island, Bahamas.[17] Above results indicated that amphidinol productivity and profile of *Amphidinium* spp. differed from strain to strain, as observed in other toxigenic dinoflagellates.

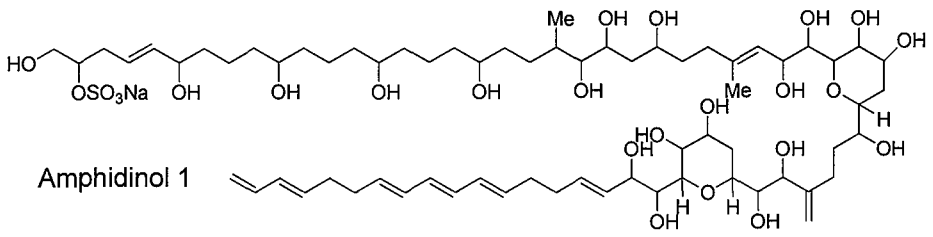

Amphidinol 1

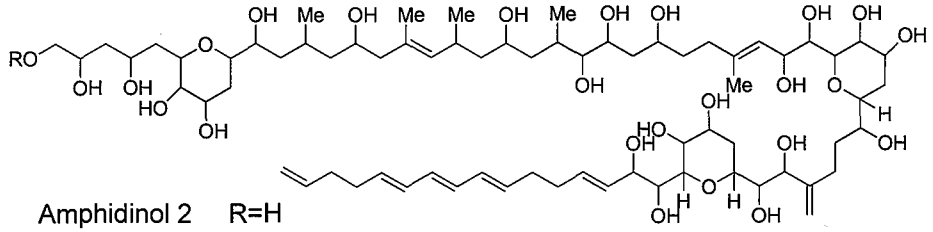

Amphidinol 2 R=H

Amphidinol 11 R=SO_3Na

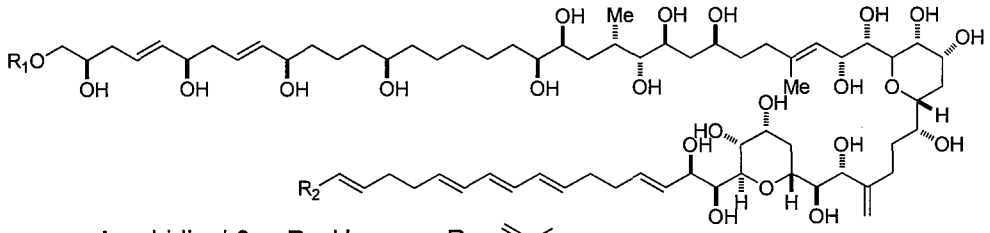

Amphidinol 3 R_1=H R_2=

Amphidinol 4 R_1=H R_2=H

Amphidinol 12 R_1=SO_3Na R_2=H

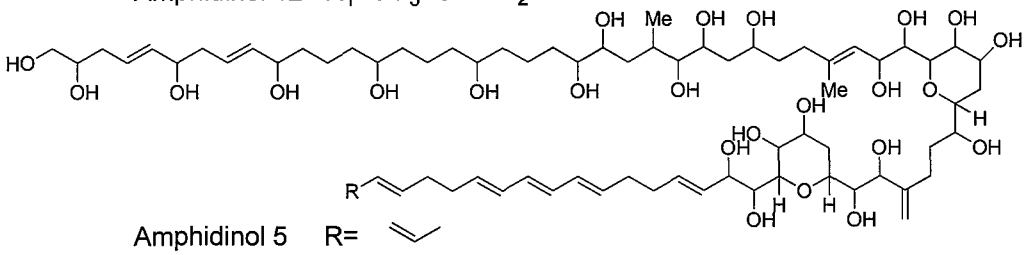

Amphidinol 5 R=

Amphidinol 6 R=H

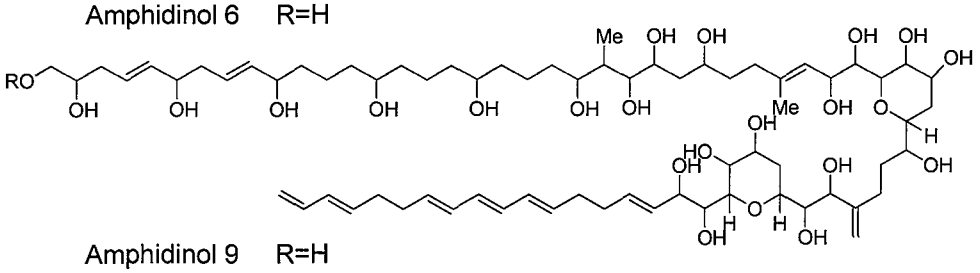

Amphidinol 9 R=H

Amphidinol 13 R=SO3Na

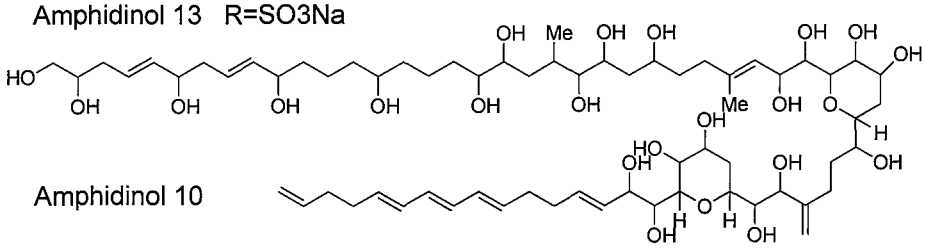

Amphidinol 10

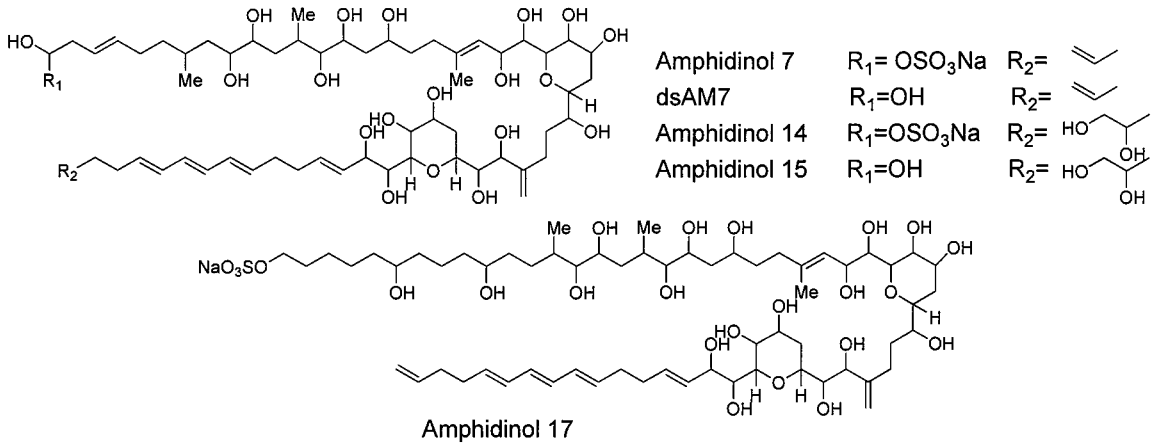

1.3.2 Amphidinol congeners

Other closely related analogues of amphidinols have been reported; among them, luteophanols,[18, 19] lingshuiols,[20] and karatungiols[21] display cytotoxic and antifungal activities, whereas carteraol E from another strain of *A. carterae* shows ichthyotoxicity.[22] More recently, the structure of similar compounds called karlotoxins that belongs to a group of fish-killing toxins produced by *Karlodinium veneficum* were described. the dinoflagelate *Karlodinium veneficum* (syn. *Karlodinium micrum*) which is also previously known by several names as *Gymnodinium galatheanum, Gymnodinium micrum,* or *Gynodinium veneficum* has recently attracted more attentions especially after massive fish-killing event at Hyrock Fish Farm in Maryland in 1996. *Karlodinium veneficum* is distributed worldwide and reported to produce water-soluble toxins called with hemolytic, cytotoxic, and ichthyotoxic activities.[23,24] This was the first report of such a compound from a dinoflagellate other than the genus *Amphidinium.*[25]

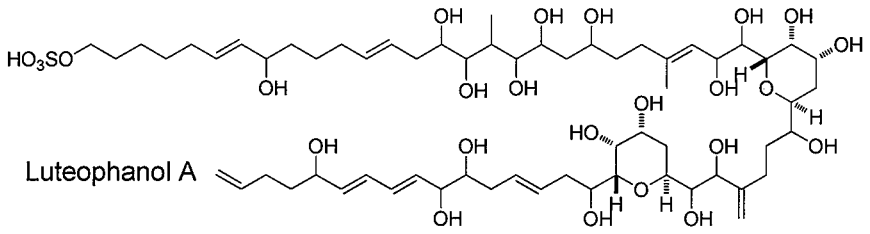

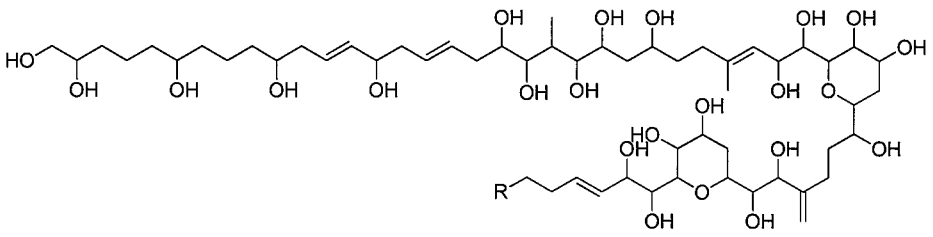

R =

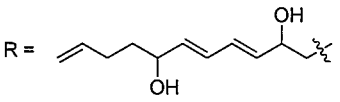

Luteophanol B

R =

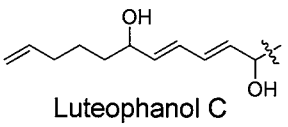

Luteophanol C

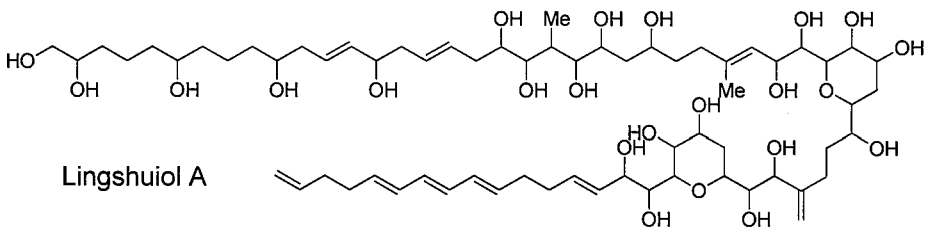

Lingshuiol A

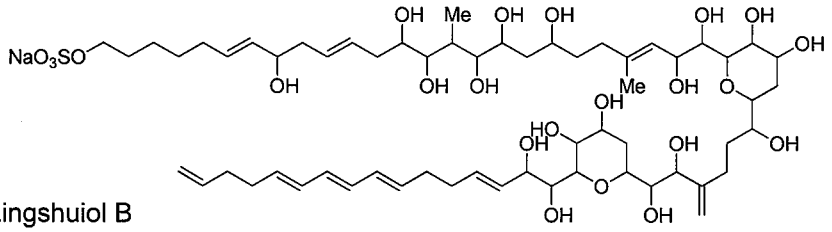

Lingshuiol B

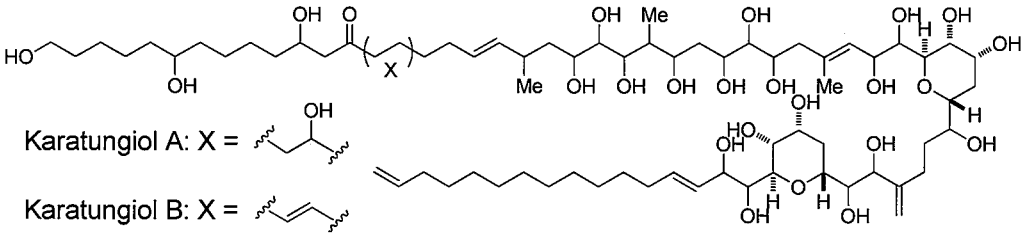

Karatungiol A: X =

Karatungiol B: X =

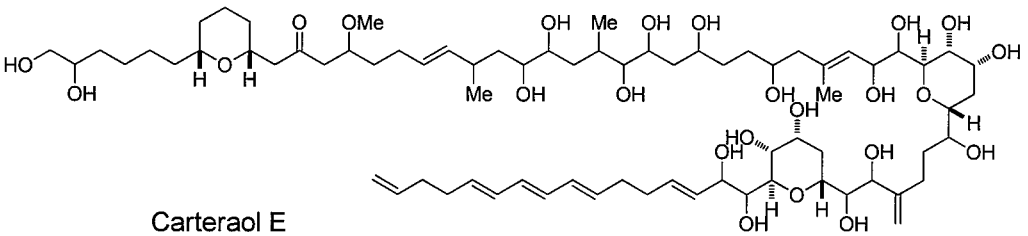

Carteraol E

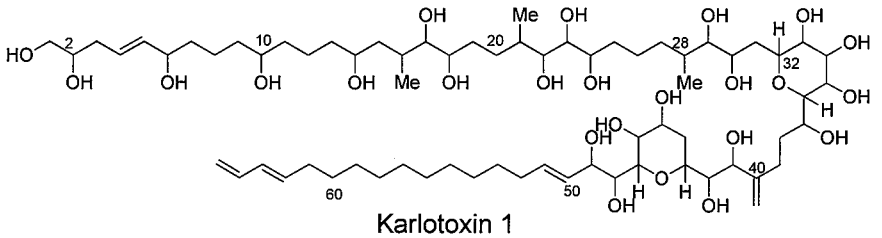

Karlotoxin 1

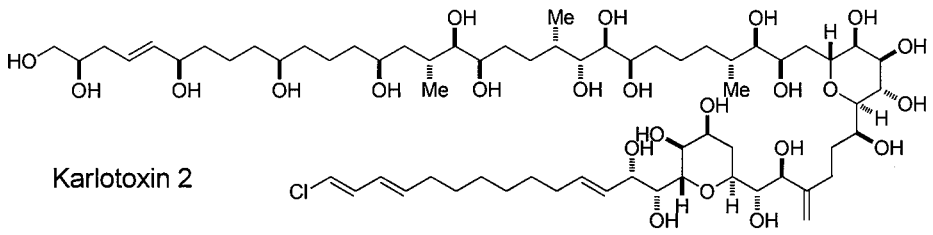

1.3.3 Structure elucidation of amphidinols

Structure elucidation of AMs was accomplished mainly by intensive analysis of 1D and 2D NMR spectra as well as high resolution MS spectra. Large portions of the structure were elucidated by detail analysis of COSY, TOCSY and HMBC spectra. The number of hydroxyl groups was estimated by measuring the ^{13}C chemical shift of the hydroxyl-bearing carbons using CD_3OH/C_5H_6N (2:1) and CD_3OD/C_5H_6N (2:1) as solvents. The hydroxyl-bearing carbons located in the tetrahydropyran rings were confirmed by NOE experiments and $^3J_{H,H}$ measurements across the rings.[10]

Further verification of the NMR-derived structure was performed by tandem mass spectrometry (MS/MS).[26] The negative collision-induced dissociation (CID) is known to produce product ions due to cleavages at α and β positions to hydroxyl groups, while the positive CID mode give rise to ion peaks diagnostic of the conjugated polyene system.[10]

Understanding of chemical structure of natural products, especially the stereochemistry, is crucial for studying the molecular basis of their mechanism of actions. In the next chapter, determination of the absolute structure of amphidinol 3 and closely related compound karlotoxin 2 will be discussed in more details.

1.3.4 Structure-activity relationship of amphidinols

Amphidinols exhibit a variety of biological activities such as antifungal, hemolytic, cytotoxic, ichthyotoxic, anti-diatom, and anti-dinoflagellate activities.[10-17] AM1, which posseses a sulfate ester, was initially isolated as a potent

antifungal and hemolytic agent. The interest has been to determine the role of sulfate ester in its bioactivity. However, as shown in Table 1-2 AM2 to AM6 retain strong activities despite the lack of the sulfate ester moiety. Therefore, the presence of the sulfate ester does not seem to be necessary for the antifungal and other activities.

Table 1-2. Reported bioactivities of AM1[10]-AM6.[13]

	Hemolytic activity (EC_{50} in μM)	Antifungal activity (MEC in μg/disk)	Anti-diatom (MEC in μg/mL)
AM1[10]	ca.0.050	6	-
AM2	0.91	6	1.0
AM3	0.0094	4	0.1
AM4	0.185	6	0.4
AM5	0.230	6	0.5
AM6	0.580	6	1.0

The isolation of AM7, which has a sulfate ester and known as the smallest molecular weight among AM homologues, was expected to provide new information on structure–activity relationship. AM7 showed antifungal activity against *Aspergillus niger* with MEC of 10 μg/disk and hemolytic activity with EC_{50} of 3 μM (Table 1-3). In comparison with AM3, the most potent homologue in antifungal and hemolytic activities, AM7 showed less potent antifungal and hemolytic activities. The structure-activity relationship for the polyhydroxyl part was more closely examinated by preparing desulfo-AM7 (dsAM7) from AM7 by hydrolysis of the sulfate ester. As a result, the hemolytic activity of dsAM7 was significantly higher than that of AM6, which possesses a much longer polyhydroxyl chain, but should be a little lower than that of AM4 (or AM3). The major structure differences among AM4, AM6, and dsAM7 reside mainly in the

length of the polyhydroxyl chain. This tendency in hemolytic activity implies that the length of the polyhydroxyl side chain of AM3 (and AM4) most effectively disrupts erythrocyte membrane among AMs tested.[14]

Structure of AM14 and AM15 are very close to AM7 except for the polyene terminal moiety. However, in contrast to AM7, AM14 revealed no antifungal activity and AM15 showed only marginal activity at a higher dose; neither AM14 nor AM15 induced hemolysis up to 50 μM. Thus, the terminal hydrophobic segment appears to play an important role in the activity of amphidinols.[16]

Table 1-3. Reported bioactivities of AM3, AM6, AM7, dsAM7, AM14, and AM15.[16]

	Hemolytic activity (EC_{50} in μM)	Antifungal activity (MEC in μg/disk)
AM3	0.4	6
AM6	2.9	6
AM7	3.0	10
dsAM7	1.2	8
AM14	>50	>60
AM15	>50	60

Moreover, biological activities of AM9 are comparable with those of AM4. The location of hydroxyl groups seems to have less influence on activity as they have the same polyene terminal but different polyol substitutions pattern. Hemolytic and antifungal activities of AM11, AM12, and AM13 were less potent than those of AM2, AM4, and AM9. As in the case of AM7, attachment of the sulfate ester at C1 markedly reduced their activities. A similar result was also observed for AM17, another sulfated analogue, which only showed weak hemolytic activity.

Table 1-4. Reported bioactivities of AM2, AM4, AM9-13,[15] and AM17.[17]

	Hemolytic activity (μM)	Antifungal activity (μg/disk)	Cytotoxicity (μg/mL)
AM2	1.16	44.3	14.8
AM4	0.207	58.2	25.3
AM9	0.176	32.9	36.5
AM10	6.53	154	35.2
AM11	28.9	256.6	23.0
AM12	3.00	>100	26.8
AM13	2.02	132	32.5
AM17[17]	4.90	inactive	-

1.4 Summary of Previous Work and Current Findings on the Mode of Action of Amphidinol

Since the first report on the isolation and identification of AM1 by Yasumoto's group, about 20 congeners including those having closely related structures have hitherto been reported. Their unique structural characteristics, which are comprised by long carbon chains encompassing multiple hydroxyl groups and polyolefins, provide the amphiphilic nature of these molecules. Amphiphilic properties of AMs are important for their membrane-permeabilizing activity. Permeabilization of the phospholipid membrane by AMs is thought to be responsible for their potent antifungal activity. AMs increase membrane permeability by directly interacting with lipid bilayers.

Previous studies in the author's group showed that AMs permeabilize the membrane more efficiently in the presence of sterol.[11,13,27-29] The size of the pore/lesion formed in the erythrocyte membrane was estimated to be 2.0-2.9 nm in diameter which was significantly larger than those of other antifungals such as amphotericin B (AmB).[27] Recently, it has been reported that the membrane-permeabilizing activity of AM3 is hardly affected by membrane thickness. These results supports the toroidal pore formation by AM3, rather than barrel-stave pore,

because the stability of a barrel-stave pore as exemplified by an ion channel of AmB is influenced by the membrane thickness to much greater extent than that of a toroidal pore.[29]

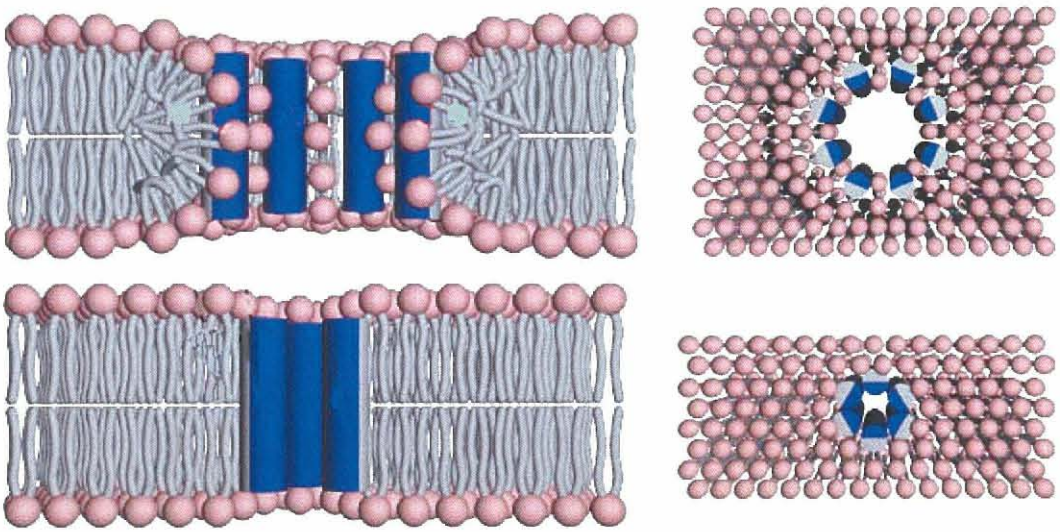

Figure 1-1. Cartoon of two pore models; toroidal (top) and barrel-stave model (bottom).[30]

Moreover, structure-activity relationship have examined using intact AMs and chemically modified AM derivatives with structural variations in polyhydroxy and polyene sections. It was found that polyene and polyhydroxy moieties play respective roles in binding to the lipid bilayer membrane and in forming an ion permeable pore/lesion across the membrane.[16] Conformational analysis of AM3 carried out on the basis of high-resolution ^{1}H NMR data using SDS[28] and bicelles[31] as membrane models, revealed that the central region of AM3 takes a hairpin conformation while the hydrophobic polyene chain is immersed in the hydrophobic interior. This conformational and positional preference of AM3 may account for formation of a toroidal pore in biological membranes.

Despite those important findings, some information about structure and mode of action of amphidinols including sterol effect on their membrane-permeabilizing activity remain unclear. This work will present reevaluation of

AM3 structure performed on the basis of NMR data of peracetyl AM3, followed by study of AM3 affinity to liposomal membranes in the presence and absence of sterol examined by Surface Plasmon Resonance (SPR). Thus, confirmation of AM3 structure, in particular for the contentious portions around the tetrahedropyran rings (C32-C51), which play an essential role in the hairpin conformation, can be established. Furthermore, SPR experiments disclosed that sterols, in particular ergosterol, markedly enhance the binding of AM3 to phospholipid membrane. Based on these results, the stereochemistry confirmation and the possible mechanism of action of AM3 are presented.

References:

1. Shimizu, Y. *Chem. Rev.*, **1993**, *93*, 1685-1698.
2. Kobayashi, J.; Kubota, T. *J. Nat. Prod.*, **2007**, *70*, 451-460.
3. FAO, *Marine Biotoxins*. FAO food and nutrition papers, FAO: Rome, 2004.
4. Camacho, F. G.; Rodriguez, J. G.; Miron, A. S.; Garcia, M. C. C.; Belarbi, E. H.; Christi, Y.; Grima, E. M. *Biotechnology Advances,* **2007**, *25*, 176-194.
5. Yasumoto, T.; Murata, M. *Chem. Rev.*, **1993**, *93*, 1897-1909.
6. Murata, M.; Yasumoto, T. *Nat. Prod. Rep.*, **2000**, *17*, 293-314.
7. Murray, S.; Patterson, D. J. *Eur. J. Phycol.*, **2002**, *37*, 279-298.
8. Kobayashi, J.; Tsuda, M. *Nat. Prod. Rep.*, **2004**, *21*, 77-93.
9. Kobayashi, J.; Kubota, T.; Takahashi, M.; Ishibashi, M.; Tsuda, M.; Naoki, H. *J. Org. Chem.*, **1999**, *64*, 1478-1482.
10. Satake, M.; Murata, M.; Yasumoto, T.; Fujita, T.; Naoki, H. *J. Am. Chem. Soc.*, **1991**, *113*, 9859-9861.
11. Paul, G. K.; Matsumori, N.; Konoki, K.; Sasaki, M.; Murata, M.; Tachibana, K. In Harmful and Toxic Algal Blooms, Sendai, July, 1996; Intergovernmental Oceanographic Commission of UNESCO: Sendai, 1996; 503-506.
12. Paul, G. K.; Matsumori, N.; Murata, M.; Tachibana, K. *Tetrahedron Lett.*, **1995**, *36*, 6279.
13. Paul, G. K.; Matsumori, N.; Konoki, K.; Murata, M.; Tachibana, K. *J. Mar. Biotechnol.*, **1997**, *5*, 124-128.
14. Morsy, N.; Matsuoka, S.; Houdai, T.; Matsumori, N.; Adachi, S.; Murata, M.; Iwashita, T.; Fujita, T. *Tetrahedron,* **2005**, *61*, 8606-8610.
15. Echigoya, R.; Rhodes, L.; Oshima, Y.; Satake, M. *Harmful Algae,* **2005**, *4*, 383-389.
16. Morsy, N.; Houdai, T.; Matsuoka, S.; Matsumori, N.; Adachi, S.; Oishi, T.; Murata, M.; Iwashita, T.; Fujita, T. *Bioorg. Med. Chem.*, **2006**, *14*, 6548-6554.
17. Meng, Y.; Wagoner, R. M. V.; Misner, I.; Tomas, C.; Wright, J. L. C. *J. Nat. Prod.*, **2010**, *73*, 409-415.
18. Kubota, T.; Ishibashi, M.; Nakamichi, H.; Kosaka, T.; Ishikawa, T.; Kobayashi, J. *J. Org. Chem.*, **1997**, *62*, 3820-3823.
19. Kubota, T.; Tsuda, M.; Doi, Y.; Takahashi, A.; Nakamichi, H.; Ishibashi, M.; Fukushi, E.; Kawabata, J.; Kobayashi, J. *Tetrahedron,* **1998**, *54*, 14455-14464.
20. Huang, X.-C.; Zhao, D.; Guo, Y.-W.; Wu, H.-M.; Trivellone, E.; Cimino, G. *Tetrahedron Lett.*, **2004**, *45*, 5501-5504.
21. Washida, K.; Koyama, T.; Yamada, K.; Kita, M.; Uemura, D. *Tetrahedron Lett.*, **2006**, *47*, 2521-2525.
22. Huang, S.-J.; Kuo, C.-M.; Lin, Y.-C.; Chen, Y.-M.; Lu, C.-K. *Tetrahedron Lett.*, **2009**, *50*, 2512-2515.

23. Deeds, J. R.; Terlizzi, D. E.; Adolf, J. E.; Stoecker, D. K.; Place, A. R. *Harmful Algae,* **2002**, *1*, 169-189.
24. van Wagoner, R. M.; Deeds, J. R.; Satake, M.; Ribeiro, A. A.; Place, A. R.; Wright, J. L. C. *Tetrahedron Lett.,* **2008**, *49*, 6457-6461.
25. Peng, J.; Place, A. R.; Yoshida, W.; Anklin, C.; Hammann, M. T. *J. Am. Chem. Soc.,* **2009**, *132*, 3277-3279.
26. Biemann, K.; Hubert, H. A. *Science,* **1987**, *237*, 992-998.
27. Houdai, T.; Matsuoka, S.; Matsumori, N.; Murata, M. *Biochim. Biophys. Acta,* **2004**, *1667*, 91-100.
28. Houdai, T.; Matsuoka, S.; Morsy, N.; Matsumori, N.; Satake, M.; Murata, M. *Tetrahedron,* **2005**, *61*, 2795-2802.
29. Morsy, N.; Houdai, T.; Konoki, K.; Matsumori, N.; Oishi, T.; Murata, M. *Bioorg. Med. Chem.,* **2008**, *16*, 3084-3090.
30. Toke, O.; Maloy, W. L.; Kim, S. J.; Blazyk, J.; Schaefer, J. *Biophys. J.,* **2004**, *87*, 662-674.
31. Houdai, T.; Matsumori, N.; Murata, M. *Org. Lett.,* **2008**, *10*, 4191-4194.

Chapter 2

Structure Reevaluation of Amphidinol 3, the Most Potent Antifungal Member of Amphidinol Family

2.1 Introduction

Among other homologues, amphidinol 3 (AM3) is the most potent antifungal compound. The stereochemistry of AM3 is of great interest for not only synthetic chemistry but also mechanism of action studies. The absolute configuration of AM3 was previously determined by extensive NMR experiments such as the *J*-based configuration analysis (JBCA) method,[1] modified Mosher method,[2-4] and HPLC analysis of the degradation products.[5] However, the configuration and conformation with respect to the C50-C51 and C38-C39 units remained ambiguous due to an intermediate coupling constant between two vicinal protons, which could be interpreted as alternating rotamers either in *threo*- or in *erythro*- interaction, suggests that those bonds undergo conformational changes.

Recently, the stereochemistry of C2 of AM3 has been revised to be *R* by comparing synthetic specimens with a fragment of AM3 and by GC-MS. A small amount of AM3 in CH_2Cl_2/MeOH was treated with Grubbs catalyst in the presence of ethylene at room temperature. The degradation product was analyzed by GC-MS equipped with a chiral capillary column and showed identical retention time with that of authentic sample, (*R*)-pent-4-ene-1,2-diol. This indicated that the absolute configuration at C2 of AM3 is *R*.[6]

Karlotoxin 2 (KmTx2, Figure 2-1), a congener isolated from the dinoflagellate *Karlodinium veneficum* that shows close structural similarities to AM3, has been reported to have the different absolute configuration for the C34-C51 unit where all the asymmetric centers have opposite configuration to those in AM3.[7] These circumstances prompted us to do further structural confirmation of

AM3, in particular for the contentious portions around the tetrahedropyran rings (C32-C51). The stereochemistry in this region is not only essential for mechanism of action studies but also for synthetic studies of AM3 that have been carried out by several groups all over the world.[6,8-20]

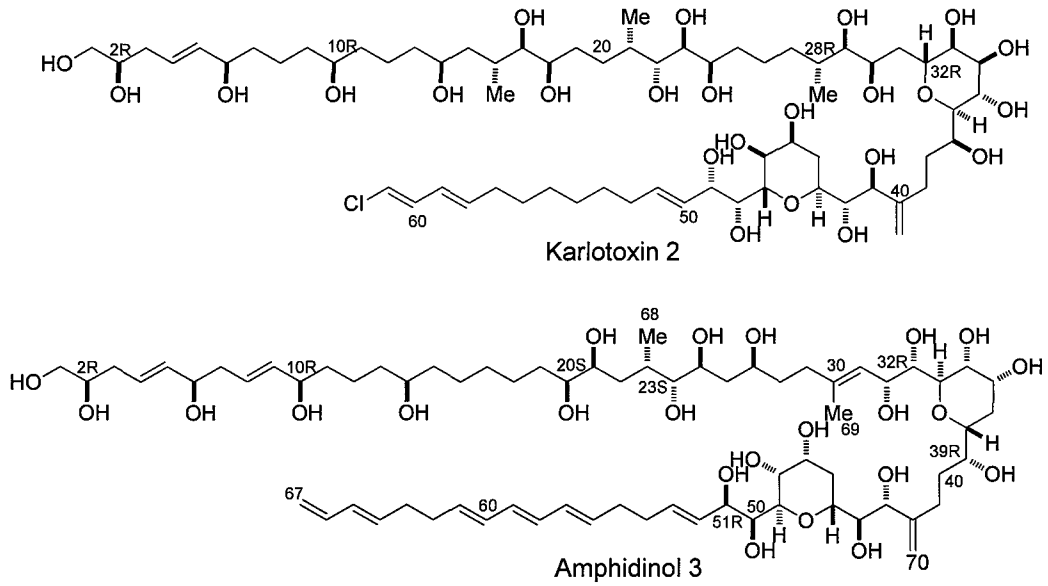

Figure 2-1. Proposed absolute configuration for karlotoxin 2 and amphidinol 3.

2.1.1 Structure and absolute configuration of amphidinol 3

The absolute configuration of AM3 was determined by three methods, namely; (1) the *J*-based method[1,21] was used for acyclic parts with 1,2- and 1,3-chiral centers, C20-C27, C32-C34, C38-C39, C44-C45, and C50-C51; (2) NOE analysis combined with the *J* analysis was used for two ether cycles and their linkage C39-C44; (3) the absolute stereochemistry at C2, C6, C10, C14, C23, and C39 was determined using the modified Mosher method and chromatographic/NMR comparison of the degradation products.[5]

Configuration assignment of C32-C33 was successfully carried out using the *J*-based analysis. As shown in the figure below, the ^{3}J(H-32, H-33) value indicated a *gauche* interaction for the 1,2 diol system.[1] The values for ^{2}J(C32, H-

33) and ^3J(C34, H-32) indicate that H-33 is *anti* to C32-OH and H-32 is *gauche* to C34, respectively. Therefore the *threo* configuration for C32-C33 can unequivocally be established. The *J*-based analysis can also be applied to a system undergoing conformational change like C38-C39, which the ^3J(H-38, H-39) is an intermediate value between *anti* and *gauche*. The two small values for ^3J(C37, H-39) and ^3J(C40, H-38) indicate *gauche* C37/H-39 and *gauche* C40/H-38 interactions in both conformers. Out of the six possible pairs of alternating rotamers from *erythro* and *threo* configurations, only one pair fits all of these requirements. The diastereomeric relationships of C44-C45 and C50-C51 were assigned using the same method.

C32-C33

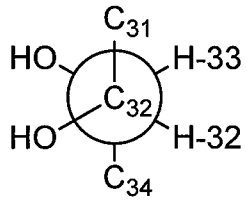

^3J (H-32, H-33) = 1.6
^2J (C32, H-33) = 1
^3J (C34, H-32) = 1

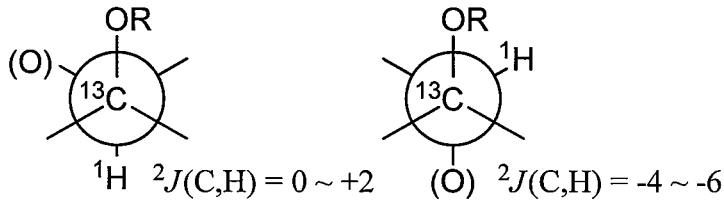

(Geminal ^{13}C-^{1}H coupling constant values; $^2J_{C,H}$ when the dihedral angles between ^{13}C-attached oxygen and the proton are 180° (*anti*) or 60° (*gauche*))

C38-C39

^3J (H-39, H-38) = 5.1
^3J (C40, H-38) = 1
^2J (C37, H-39) = -1

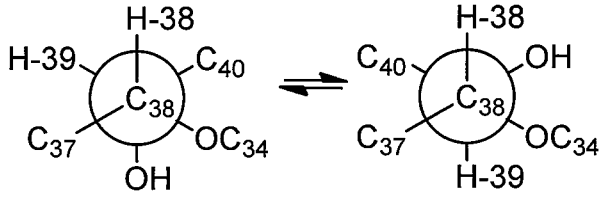

C44-C45

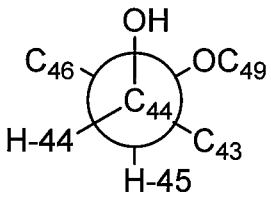

^3J (H-44, H-45) = 1.7
^2J (C44, H-45) = 0
^2J (C45, H-44) = 1

C50-C51

^{3}J (H-50, H-51) = 3.4
^{2}J (C51, H-50) = -2.5
^{3}J (C49, H-51) = 1

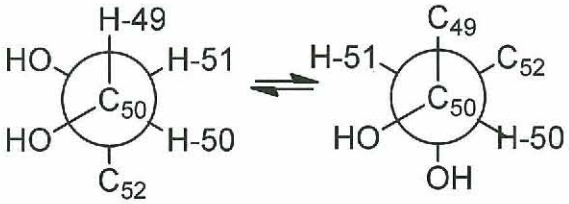

Using the same method, the relative configuration of consecutive chiral centers C20-C27 could be accomplished. Summary of $^{3}J_{H,H}$ and $^{2,3}J_{C,H}$ values are shown in Figure 2-2. All pairs of vicinal carbons, except C24-C25 with two *anti* orientations of H/H, C/H can be assigned on the basis of $^{2,3}J_{C,H}/^{3}J_{H,H}$, which results in elucidation of the 1,2-diastereomeric relationship for the C20-C27 part.

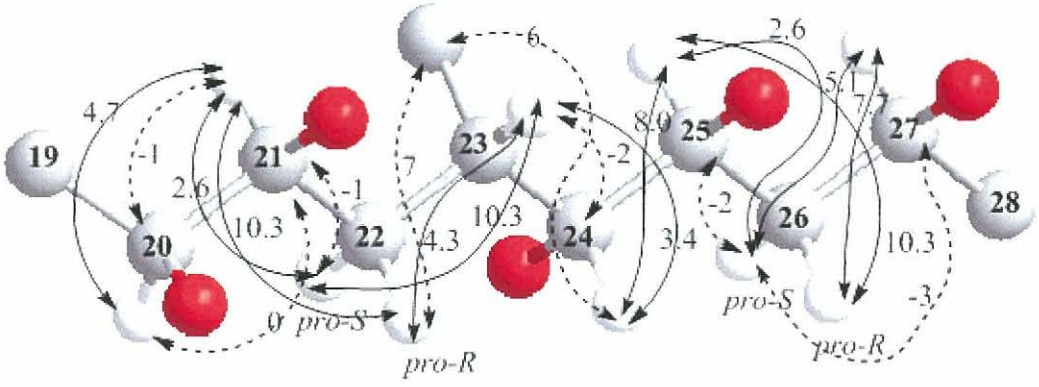

Figure 2-2. Configuration and conformation for C20-C27 of AM3 established on the basis of $^{2,3}J_{C,H}$ and $^{3}J_{H,H}$. Hydrogen atoms of methyl and hydroxyl groups were omitted for clarity. Dashed lines with arrows and numbers indicate $^{2,3}J_{C,H}$ in Hz, and plain lines denote $^{3}J_{H,H}$ in Hz.

Among 14 vicinal methine-methine interactions in the acyclic parts of AM3, there are four H/H-*anti* orientations, which were indicated by large $^{3}J_{H,H}$ values for pairs of H-24/H-25, H-33/ H-34, H-43/H-44, and H-49/H-50. For configuration assignments of these parts, additional NOE information is necessary. Diastereomeric relations between C24 and C25, C33 and C34, C43 and C44, and

C49 and C50 were established by key NOEs between H-23 and C25-OH, H-32 and H-38, C43-OH and H-45, and H-45 and H-51, respectively.

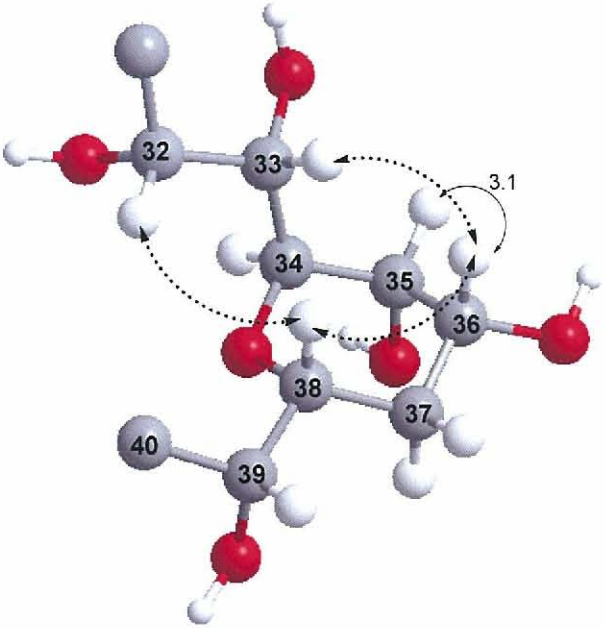

Figure 2-3. Configuration and conformation for C32-C39 of AM3 with key NOEs.

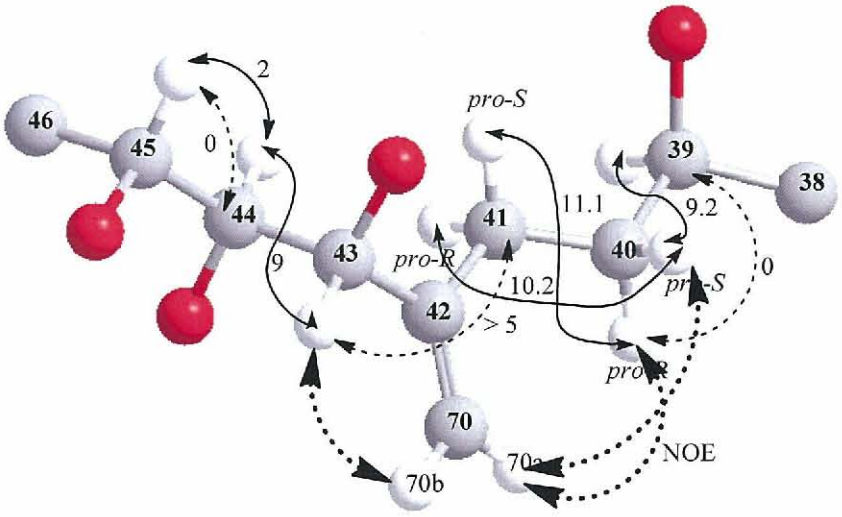

Figure 2-4. Configuration and conformation for C39-C45 of AM3 with key NOEs. Hydrogen atoms of hydroxyl groups were omitted for clarity.

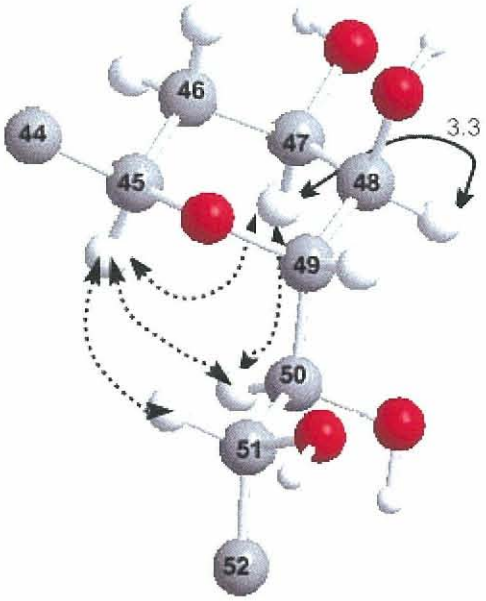

Figure 2-5. Configuration and conformation for C45-C51 of AM3 with key NOEs.

The absolute configurations and those at C2, C6, C10, C14, and C39 were elucidated by the modified Mosher method[2-4] where degradation products of AM3 by $HIO_4/NaBH_4$ were esterified with (*R*)- and (*S*)-MTPA (2-methoxy-2-trifluoromethyl-2-phenylacetic acid) and separation by HPLC, furnished MTPA esters of fragments corresponding to C2-C20 (1b,c), C21-C24 (2) and C33-C50 (3b,c) in Figure 2-6. The configuration of C23 was determined to be 23*S* by comparison of the NMR data of the bis-(*R*)-MTPA esters **2** with (*S*)- and (*R*)-MTPA esters of authentic (*R*)-methyl-1,4-butanediol.

The configuration of C2 was determined using the C1-C4 fragment obtained from the *O*-benzyloxy-methyl derivative of AM3 by treatment with $OsO_4/NaIO_4$. The resulting 1,2-dibenzyloxylmethoxy-butyl *p*-bromobenzoate (4) was chromatographed on a chiral resolution column and determined to be an (*S*)-enantiomer. However, this assignment has recently been revised to be an (*R*) enantiomer as aforementioned.[6]

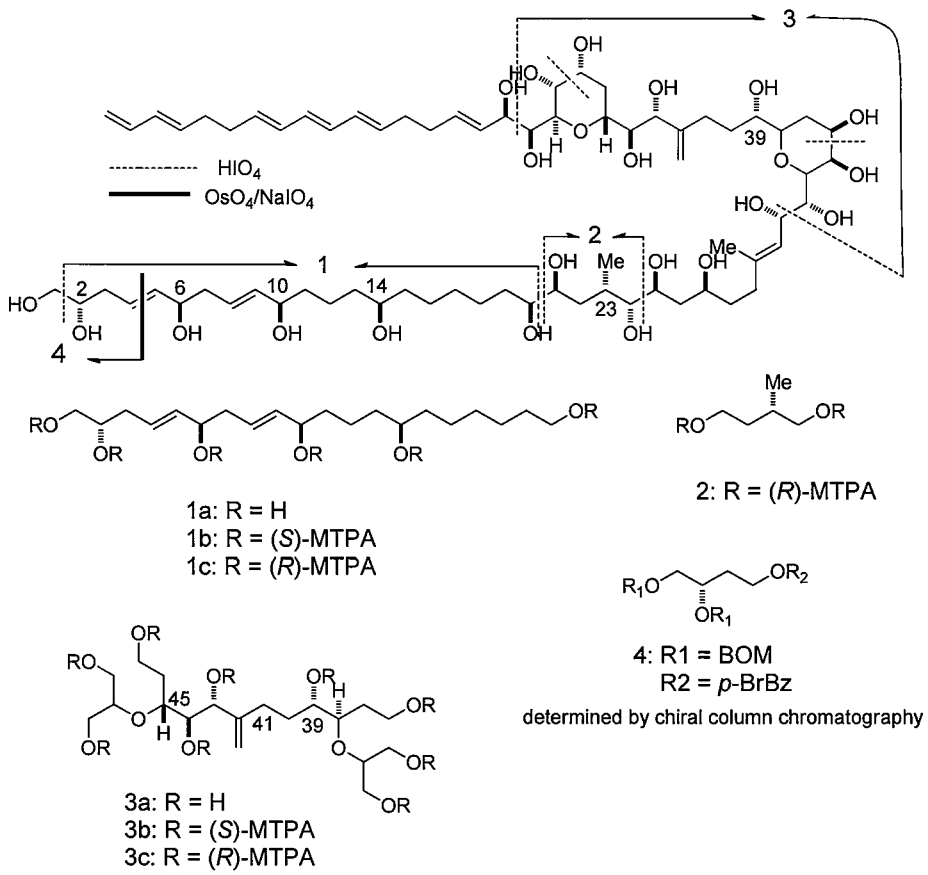

Figure 2-6. Degradation of AM3 followed by esterification with MTPA.

2.1.2 Structure and absolute configuration of karlotoxin 2 (KmTx2)

Most carbon connections in karlotoxin 2 were established using 2D INADEQUATE experiments. The connection between carbons absent of INADEQUATE correlations and the two pyran rings were achieved in addition to validation of the structure by heteronuclear correlations in the HMBC experiments.

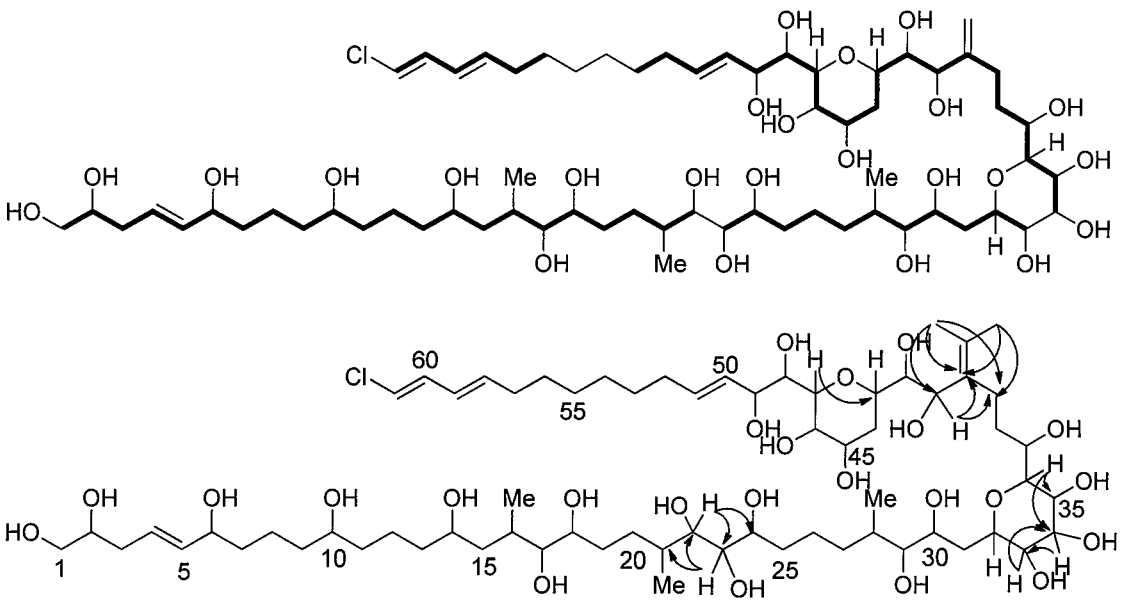

Figure 2-7. Structure of KmTx2; Bold shows the INADEQUATE connections (Top), Key HMBC correlations (Bottom).

2.1.2.1 Determination of the relative configuration of karlotoxin 2

Configuration of C28~C49

The relative configuration of C48-C49 was assigned by $^{3}J_{H,H}$ and $^{2,3}J_{C,H}$. The small ^{3}J(H-48, H-49) value indicated the *gauche* relationship of this two protons. The small $^{2}J_{C,H}$ values of C48/H-49 and C49/H-48 implied *anti*-orientations of the H-49/C48-OH and H-48/C49-OH which was further confirmed by the small $^{3}J_{C,H}$ for C47/H-49 and C50/H-48. The large coupling constant between H-48 and H-47 indicated the *anti* orientation of these two protons; An NOE correlation between H-49 and H-43 revealed the *erythro* relationship of C48 and C47. The configuration of C43~C41 was established using similar methods as depicted Figure 2-8.

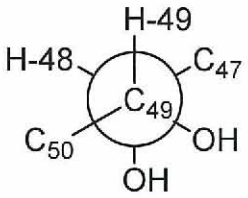

^3J (H-49, H-48) = 3.0
^3J (H-49, H-47) = 0.0
^3J (H-50, H-48) = 3.5
^2J (C49, H-48) = 1.5
^2J (C48, H-49) = small

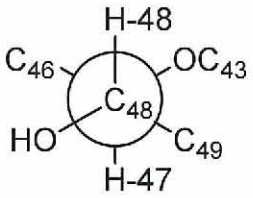

^3J (H-48, H-47) = 10.4
^2J (C48, H-47) = -5.7
^2J (C47, H-48) = -3.6

NOE H-49/H-43

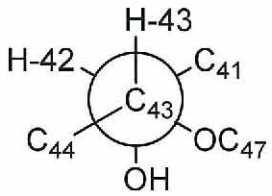

^3J (H-43, H-42) = small
^3J (H-42, H-44) = small
^3J (C41, H-43) = small
^2J (C43, H-42) = small
^2J (C42, H-43) = small

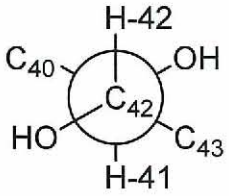

^3J (H-42, H-41) = 9.0
^2J (C42, H-41) = -5.2
^2J (C41, H-42) = -4.3

NOE H-43/H-41

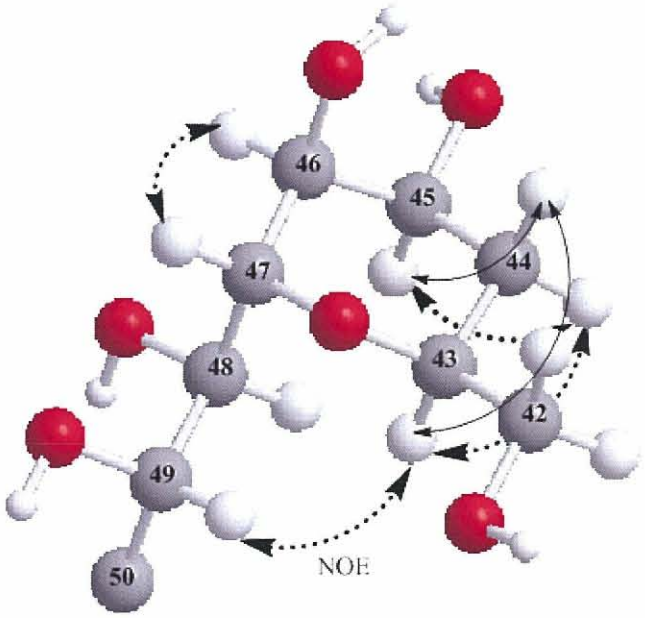

Figure 2-8. Coupling constants and configuration of C41-C43 and C47-C49 of KmTx2 (top), NOE and large $^3J_{H,H}$ (bottom).

The NOE correlation between H-43 and H-49 suggested the *axial* orientation for both H-43 and C48, and equatorial orientation for H-47. The large coupling constants for H-44a/H-43 and H-44a/H-45 in the 1D TOCSY spectrum, revealed the axial orientation of H-43, H-44a, and H-45. The presence of NOE between H-47/H-46 and the absence of NOE between H-44a/H-46 suggested an equatorial H-46, which led to the relative configuration of C43~C47 pyran ring as shown in Figure 2-8. The configuration of the second pyran ring C32-C36 was assigned in a similar method (Figure 2-9).

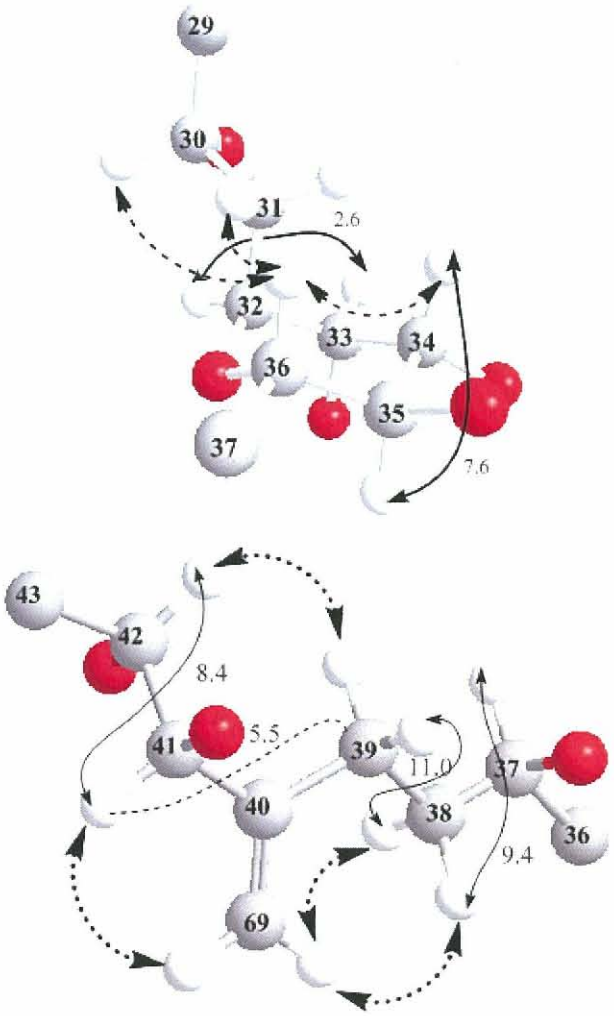

Figure 2-9. Configuration of C32-36 (top) and C37-C41 (bottom) of KmTx2 including NOE correlations.

To correlate the configuration of the two rings, the diastereomeric relationship between C37 and C41 was established. The prominent NOEs between

H-67(H) and the two protons at C38 suggested that C67 is *syn* to C38. The $^{3}J_{H,H}$ values of H-37~H-39 indicated the zigzag conformation of C37~C40 and assigned the diastereotopic methylene protons as shown in Figure 2-9. The *anti* orientation of H-41 and C39 was determined by a large ^{3}J(H-41, C39) and a intense NOE between H-41 and H-67(L). The orientation of C42 and C39 was determined by NOE between H-42 and H-39(H).

The intermediate coupling constant between H-36 and H-37 indicated the presence of two alternating conformers, *gauche* and *anti* orientation of H-36/H-37. The *gauche* orientation of C38/H-36 was suggested by the small ^{3}J(C38, H-36), while C35/H-37 and C37-OH/H-36 were *gauche* or *anti* orientation suggested by the intermediate $^{2}J_{H,C}$. This fits the configuration and conformation shown in Figure 2-10. Similarly, H-28 and H-29 showed an intermediate coupling constant and the relative configuration between C28 and C29 assigned as shown in Figure 2-10.

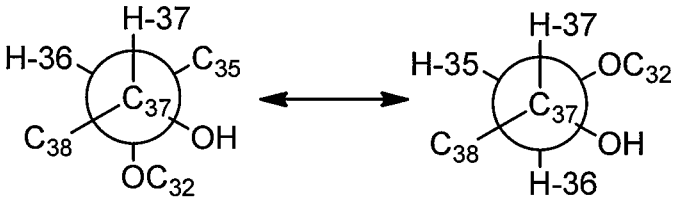

^{3}J (H-37, H-36) = 5.51
^{3}J (H-38, H-36) = small
^{2}J (C37, H-36) = -3.2
^{2}J (C36, H-37) = -2.7

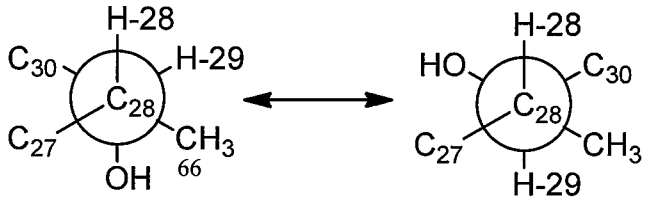

^{3}J (H-29, H-28) = 7.3
^{2}J (C66, H-29) = 2.0
^{2}J (C29, H-28) = -4.6

Figure 2-10. Relative configuration of C36-C37 and C28-C29 of KmTx2.

The configuration of C30 and C32 was correlated based on the diastereospesific assignment for methylene protons of C31 (Figure 2-11). The *gauche* and *anti* relationship of H-31(H)/H-32 and H-31(L)/H-32 were indicated by the small and large coupling constants between H-31(H)/H-32 and H-31(L)/H-32, respectively. The *anti* orientation of C32-O/H-31(H) was determined by the small ^{2}J(C32, H-31), while the *gauche* orientation of C30/H-32 and C32-O/H-31(L) were assigned by the small ^{3}J(H-32, C30) and large ^{2}J(H-31L, C32) (Figure 2-11). H-31(L) to be *gauche* with H-30 and *anti* to C30-OH was suggested by the small ^{3}J(H-30, H-31L) and ^{2}J(C34, H-32L) values. The *anti* orientation of H-33(H) to H-34 was indicated by the large ^{3}J(H-33H, H-34). The relative configuration of C30/C29 was determined to be *threo* by the *gauche* orientation of H-30/H-29 which was indicated by the small coupling constant of H-29/H-30 and the *anti* orientation of H-30/C29-OH and H-29/C30-OH deduced by small ^{2}J(C30, H-29) and ^{2}J(C29, H-30) values. Thus, the relative configuration of C29 ~ C32 was determined as shown in Figure 2-11.

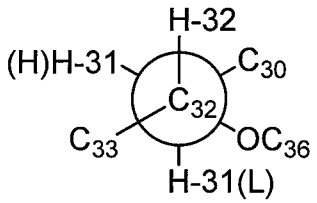

^{3}J (H-32, H-31H) = 2.6
^{3}J (H-32, H-31L) = 11.4
^{3}J (C30, H-32) = 2.7
^{2}J (C32, H-31H) = -0.7
^{2}J (C32, H-31L) = -6.6

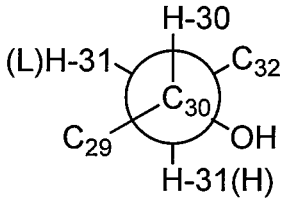

^{3}J (H-30, H-31H) = 10.3
^{3}J (H-30, H-31L) = 2.3
^{3}J (C32, H-30) = 2.5
^{2}J (C30, H-31H) = -5.8
^{2}J (C30, H-31L) = -0.8

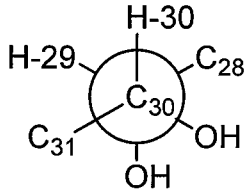

^{3}J (H-30, H-29) = 3.1
^{3}J (C28, H-30) = small
^{2}J (C30, H-29) = -0.5
^{2}J (C29, H-30) = -0.5

Figure 2-11. Relative configuration of C29-C32 of KmTx2.

2.1.2.2 Determination of absolute configuration of karlotoxin 2

The absolute configuration, KmTx2 was deduced by using the degradation products that were then esterified with (*R*)- and (*S*)-α-methoxyphenylacetic acid (MPA). The MPA esters thus were obtained corresponded to C2-C17 (**1a/b**), C18-C22 (**2a/b**), and C24-C29 (**3a/b**) (Figure 2-12). The absolute configurations of C6,

C10, C14, C21, and C28 were proposed to be *R*, *R*, *S*, *S*, *R*, respectively, by comparison of $\Delta\delta^{RS}$ between **1a/b**, **2a/b**, and **3a/b**. In addition, **2a/b** and **3a/b** were synthesized to verify the absolute configurations of C21 and C28.

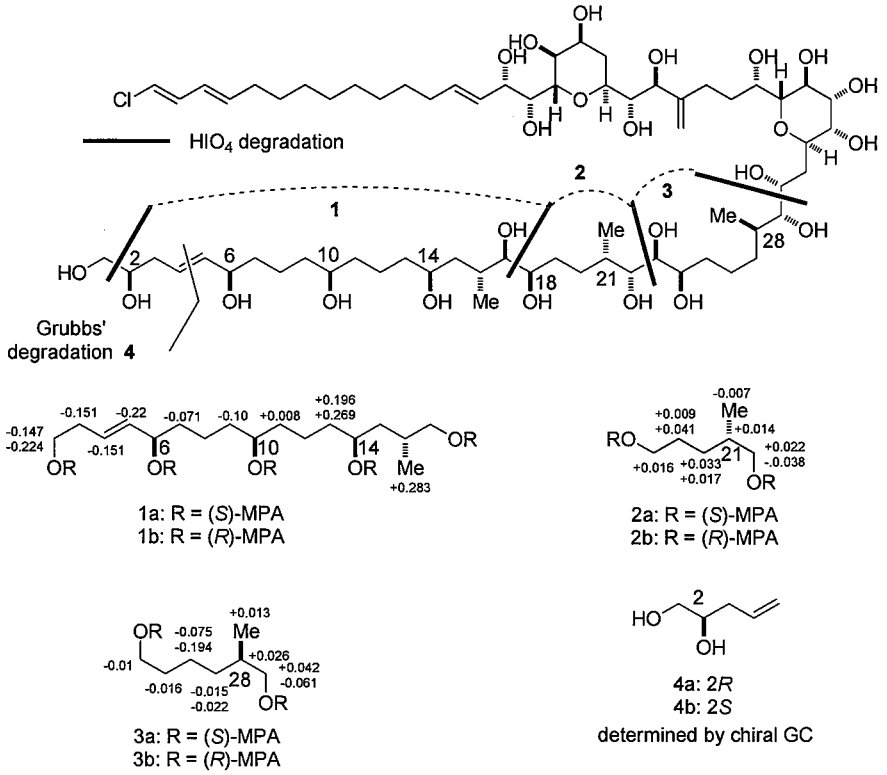

Figure 2-12. Degradation of KmTx2 followed by esterification with MPA; $\Delta\delta^{RS}$ values are also shown.

KmTx2 has structural similarities to AM3 particularly in the region around two tetrahydropyran rings. KmTx2 shares the same C34-C51 substructure of AM3 with the addition of a 35-OH group and less a 33-OH group. The absolute configuration of the C34-C51 unit is proposed to have opposite stereochemistry to that in AM3. Among amphidinol homologues, it is actually a rare case to observe structural variety in this central region. Therefore, this fact prompted further structural confirmation of AM3.

2.2 Structural Confirmation of AM3 Based on NMR Data of Peracetyl Derivative

Structure-activity relationship using naturally occurring AMs and chemically modified AM derivatives has disclosed that the polyolefinic and polyhydroxy moieties play respective roles in binding to the lipid bilayer membrane and in forming an ion-permeable pore/lesion across lipid bilayer membranes.[22-25] In order to gain insight into the membrane-bound structure of AMs, conformational analysis of amphidinol 3 (AM3) has been carried out on the basis of high-resolution ^{1}H NMR data measured for SDS micelles[26] and isotropic bicelles[27]. These experiments have revealed that the central region of AM3 takes a hairpin conformation, while the hydrophobic polyene chain is immersed in the hydrophobic interior (Figure 2-13). The results show that AM3 adopt a turn structure in the portion of the two tetrahydropyran rings. The polyhydroxy chain of AM3 resides in the hydrophilic water-accessible region while hydrophobic polyolefin penetrates into the membrane interior. In such structures, confirmation of the stereochemistry of 1,2 diol systems adjacent to the tetrahydropyran rings is crucial, in particular for C50-C51 portion; yet, the conformation of this part remains uncertain.

Although intramolecular hydrogen bonding hardly causes significant conformational aberration, structural arrangements of six member rings in the region may stabilize formation of intramolecular hydrogen bonding, and as a result, alter the configuration. To eliminate the effect of this intramolecular hydrogen bond, which sometime hampers application of *J*-based method, peracetyl AM3 was prepared to confirm the stereostructure on the basis of its NMR data.

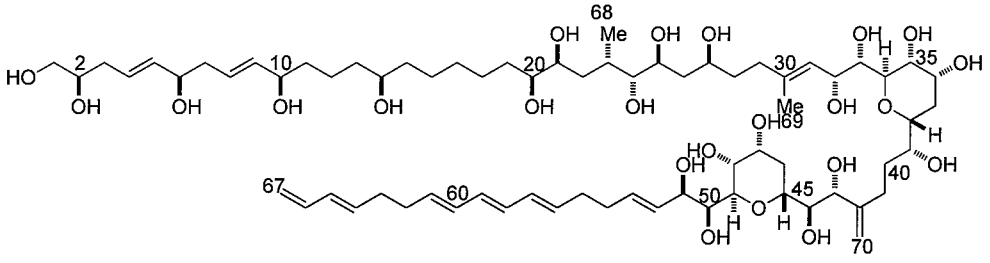

Amphidinol 3 (AM3)[5]

Peracetyl AM3 (All the 21 hydroxyl groups are acetylated)

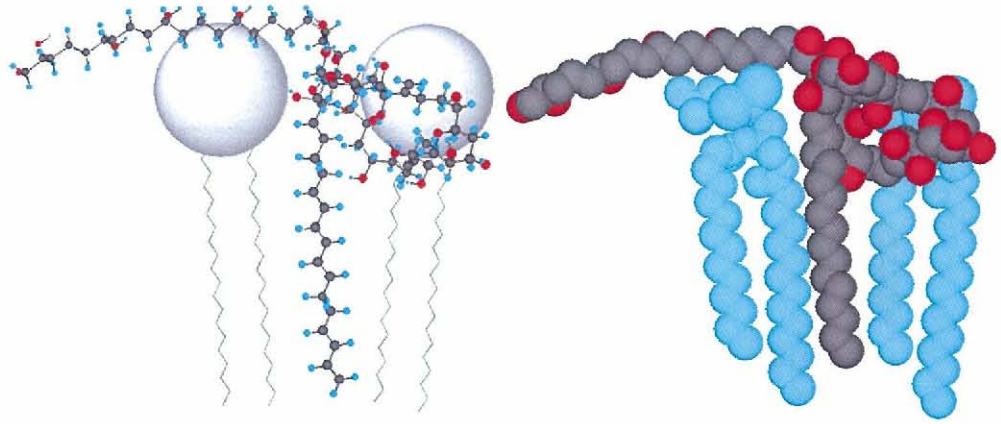

Figure 2-13. Proposed model for membrane-bound structure of AM3. Blue molecules represent DMPC interacting with AM3.

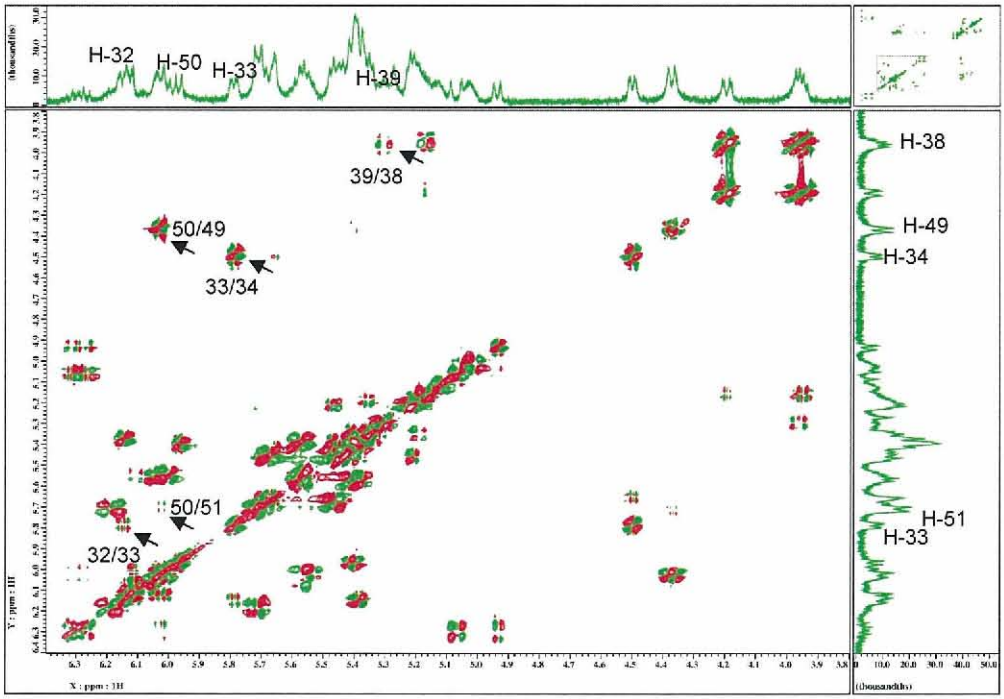

Figure 2-14. Enlargement of DQF-COSY spectrum of peracetyl AM3 in C_6D_6 measured at 500 MHz.

Assignments of ^{1}H and ^{13}C NMR signals were based on DQF-COSY, TOCSY, and HSQC spectra. For measuring $^{2,3}J_{C,H}$ values, HETLOC experiments were performed; In case of small magnetization transfer by TOCSY, intensities of HMBC cross peaks were used to estimate the coupling constant values.

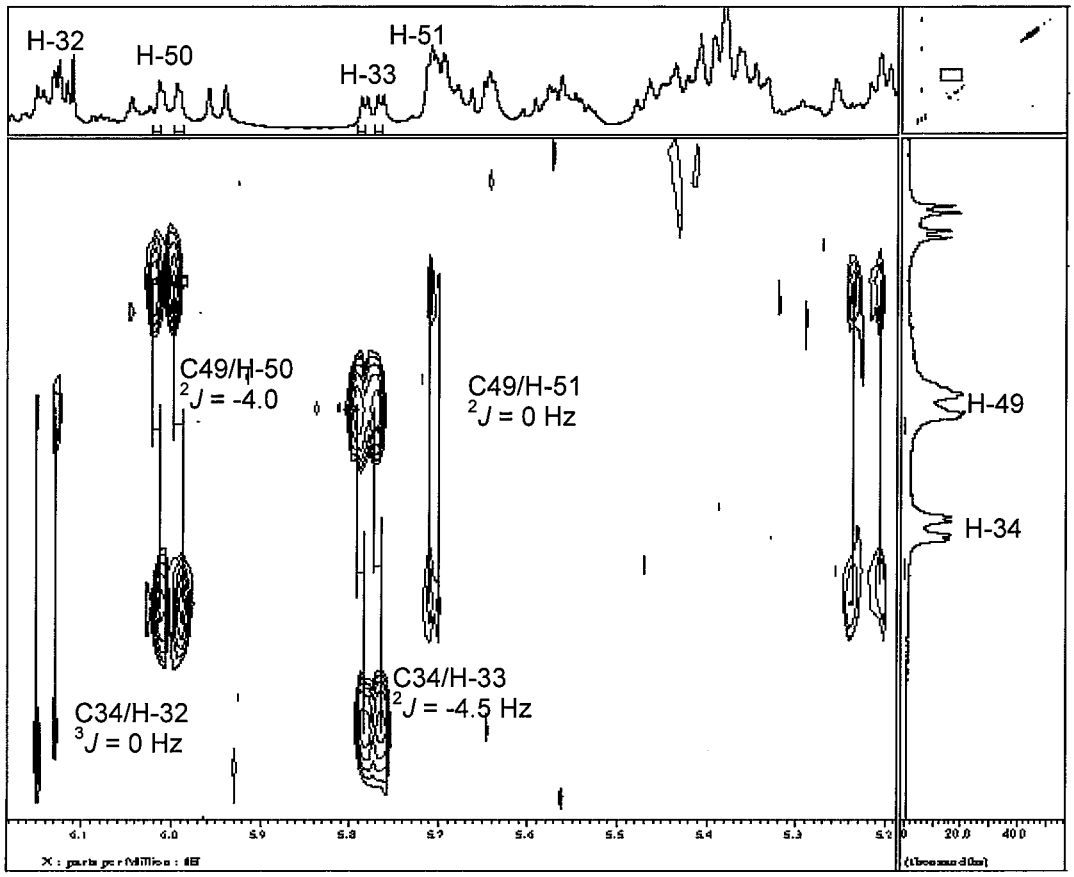

Figure 2-15. Enlargement of HETLOC spectrum of peracetyl AM3 in C_6D_6 measured at 500 MHz.

a AM3

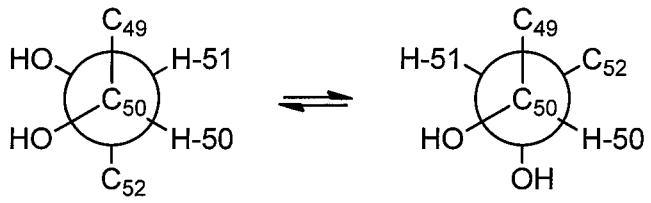

^3J(H-50, H-51) = 3.4 Hz
^2J(C51, H-50) = −2.5 Hz
^3J(C49, H-51) = 1 Hz

b Peracetyl AM3

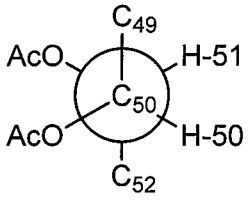

^3J(H-50, H-51) = 1.8 Hz
^2J(C50, H-51) ≅ 0 Hz
^2J(C51, H-50) ≅ 0 Hz
^3J(C49, H-51) = 0 Hz

Figure 2-16. Coupling constants and rotamers for C50-C51 of AM3 and peracetyl AM3. The Newman projections in panel **a** depict that two dominant rotamers alternate each other to give rise to intermediate *J* values.

2.2.1 Relative configuration of 1,2 diol systems adjacent to the tetrahydropyran rings

In contrast to AM3, the C50-C51 portion of peracetyl AM3 did not show conformational alternation as expected. In Figure 2-16**b**, the small ^{3}J(H-50, H-51) value indicated the *gauche* orientation of these two protons to be predominant. The small $^{2}J_{C,H}$ values between C51/H-50 and C50/H-51 further suggested that both H-50/C51-OAc and H-51/C50-OAc adopt *anti* orientation. This was further confirmed by the small ^{3}J(C49, H-51) value, which indicated the *gauche* relationship between H-51/C49. Therefore, the *threo* configuration of C50-C51 was unequivocally established.

Similar assignment could also be applied for C32-C33, which is another key part for the hairpin conformation of AM3. As shown in Figure 2-17, typical *gauche* interaction between H-32/H-33 was revealed by the small ^{3}J(H-32, H-33) values. The values for ^{2}J(C32, H-33) and ^{3}J(C34, H-32) are small, indicating that H-33 is *anti* orientation to C32-OAc and H-32 is *gauche* to C34, respectively. These interactions clearly reveal the *threo* configuration for C32-C33.

a AM3

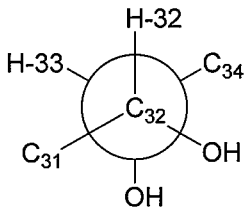

^{3}J(H-32, H-33) = 1.6 Hz
^{2}J(C32, H-33) = 1 Hz
^{3}J(C34, H-32) = 1 Hz

b Peracetyl AM3

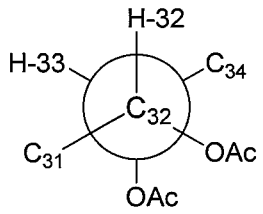

^{3}J(H-32, H-33) = 3 Hz
^{2}J(C32, H-33) ≅ 0 Hz
^{3}J(C34, H-32) = 0 Hz

Figure 2-17. Coupling constants and rotamers for C32-C33 of AM3 and peracetyl AM3.

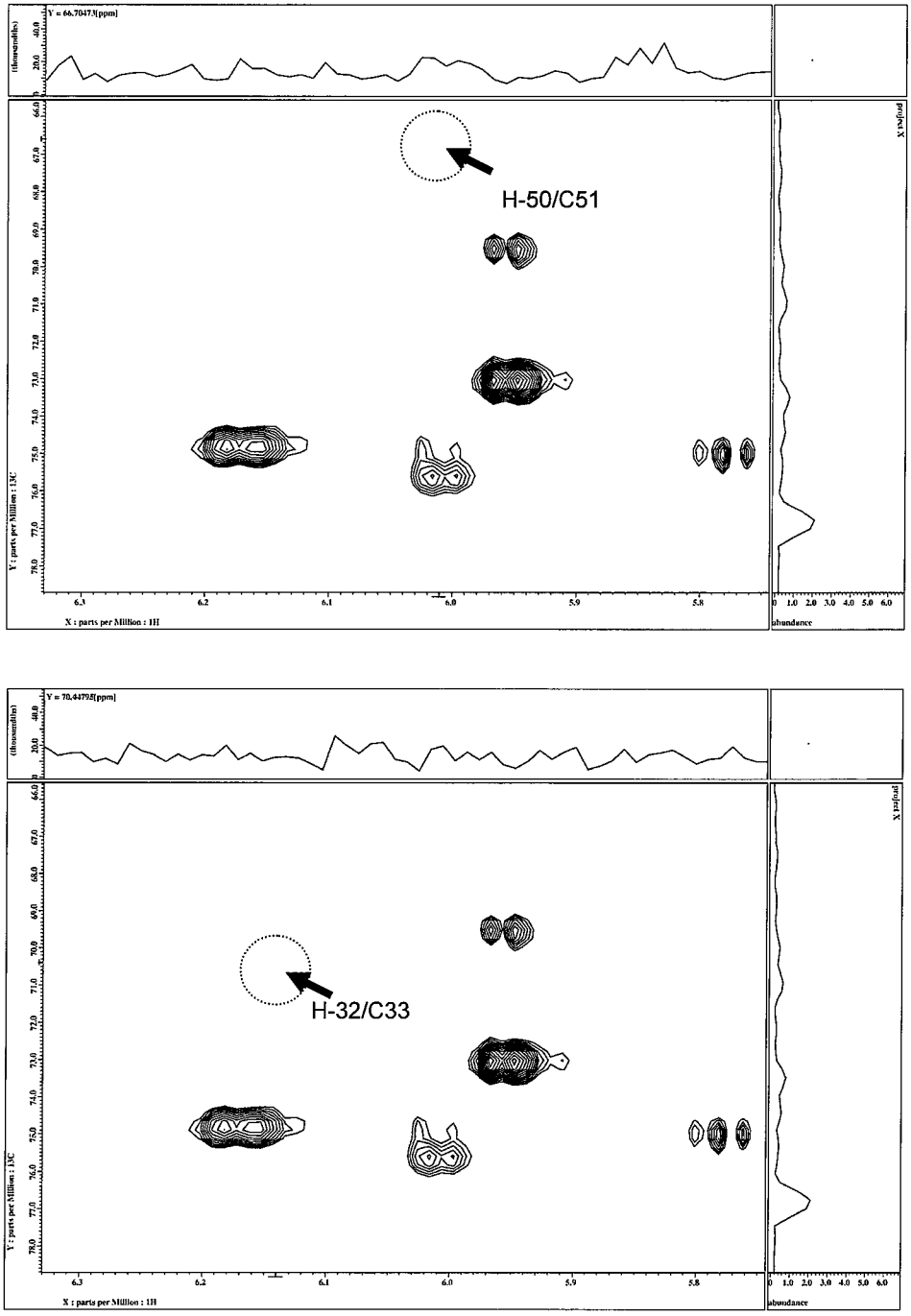

Figure 2-18. Enlargement of HMBC spectrum of peracetyl AM3 showing corresponding slices for H-50→C51 (top) and H-32→C33 (bottom). Sample was dissolved in C_6D_6 and measured at 600 MHz for ^{1}H and 150 MHz for ^{13}C.

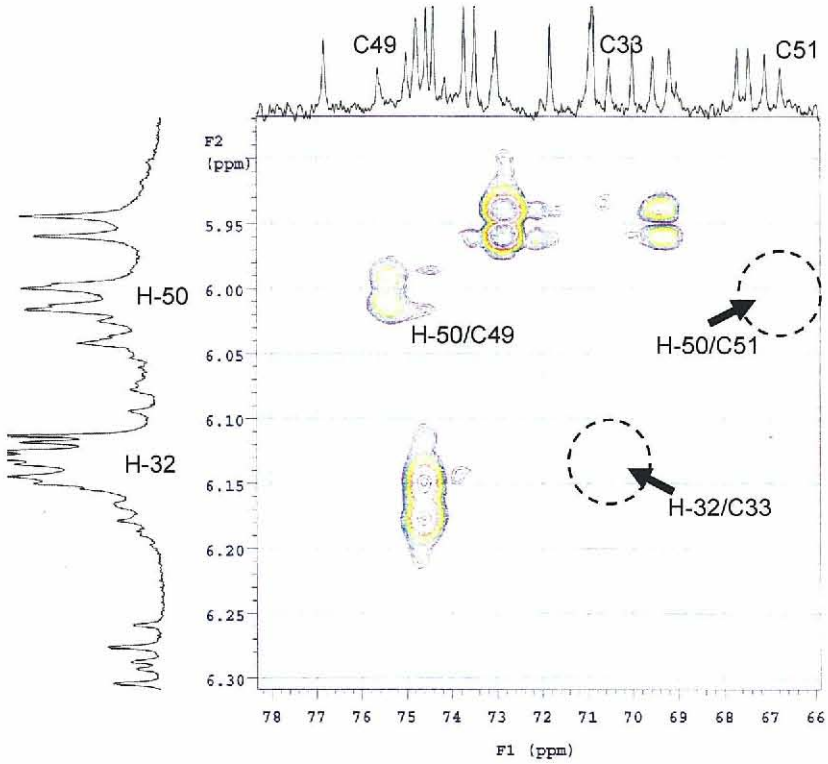

Figure 2-19. Enlargement of HMBC spectrum of peracetyl AM3 in C_6D_6 and measured at 600 MHz for ^1H and 150 MHz for ^{13}C.

2.2.2 Relative configuration of the tetrahydropyran rings and C39-C45 chain

The relative configurations of the two tetrahydropyran rings (Figure 2-20) and the C39-C45 tether (Figure 2-21) were determined mainly using NOEs and *J*-based configuration analysis[1] for peracetyl AM3. Spin-spin coupling constants of peracetyl AM3 used for the configuration study are listed in the Table 2-1 in comparison with those of AM3. Assignments of ^1H and ^{13}C signals, as well as NOEs data of peracetyl AM3 are presented in Table 2-2. The large ^3J(H-33, H-34) and ^3J(H-49, H-50) indicated the *anti* orientation of their adjacent protons; in this case, NOEs are required for the determination of the relative configuration.[1] In the *threo* configuration, an H/H-*anti* orientation allows C/C-*gauche* relationship. The prominent NOEs should be observed on for protons on these *gauche*-oriented carbons. For exo-cyclic bonds C33-C34 and C49-C50, NOEs across the ether bonds H-32/H-38 and H-45/H-51 unambiguously show their relative configurations as previously assigned (Figure 2-20).

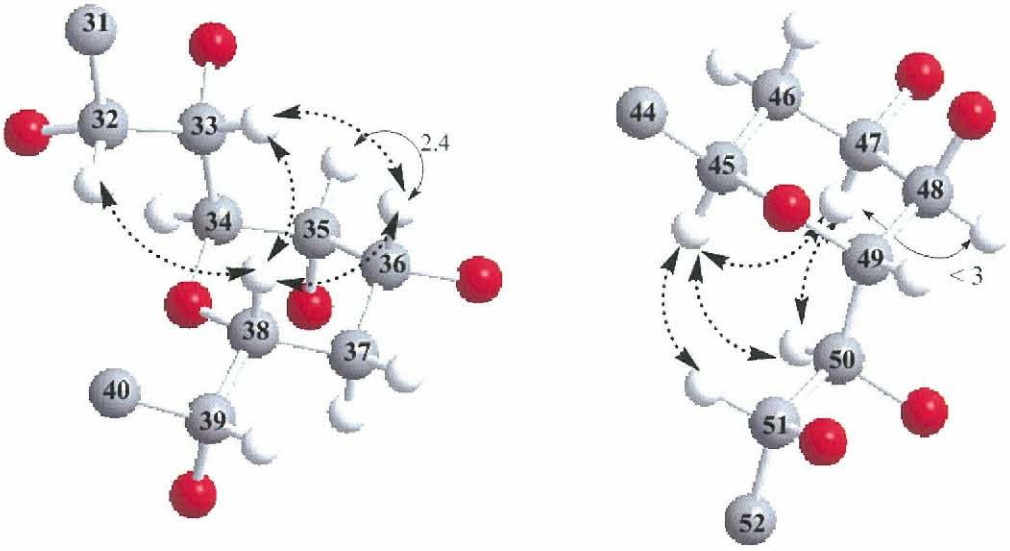

Figure 2-20. Configuration of tetrahydropyran rings of peracetyl AM3 with key NOEs (dashed arrow) and $^{3}J_{H,H}$ in Hz (small plain arrow). Acetyl groups on oxygen atoms were omitted for clarity.

Table 2-1. $^{3}J_{H,H}$ and $^{2,3}J_{C,H}$ values of AM3 and peracetyl AM3.

Bond	AM3[5]		Peracetyl AM3	
	$^{3}J_{H,H}$	$^{2,3}J_{C,H}$	$^{3}J_{H,H}$	$^{2,3}J_{C,H}$
C32-C33	1.6	C32-H33 = 1	3.0	C32-H33 ≅ 0
		C34-H32 = 1		C34-H32 = 0
C33-C34	9.5		9.0	
C35-C36	3.1		2.4	
C38-C39	5.1	C37-H39 = 1	4.6	C37-H39 = 0
		C40-H38 = 1		C40-H38 = 1
C39-C40	9.4 (H^{s})		9.2 (H^{s})	
	3.4 (H^{R})		< 3.0 (H^{R})	
C40-C41	10.2	($H\text{-}40^{s}$-$H\text{-}41^{R}$)	9.0	($H\text{-}40^{s}$-$H\text{-}41^{R}$)
	11.1	($H\text{-}40^{R}$-$H\text{-}41^{s}$)	9.1	($H\text{-}40^{R}$-$H\text{-}41^{s}$)
C42-C43		C41, H-43 > 5		C41, H-43 > 5
C44-C45	1.7	C44, H-45 = 0	< 3.0	C44, H-45 ≅ 0
		C45, H-44 = 1		C45, H-44 ≅ 0
C48-C47	3.3		<3.0	
C49-C50	10.0		9.2	
C50-C51	3.4	C50-H-51 = 0	1.8	C50-H-51 ≅ 0
		C51-H-50 = -3		C51-H-50 ≅ 0
				C49-H-51 = 0

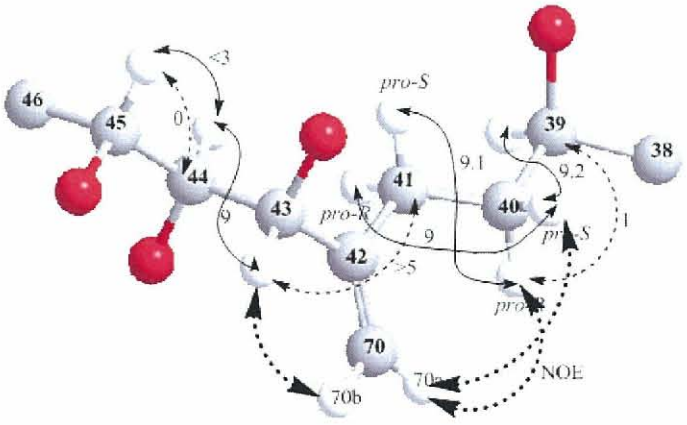

Figure 2-21. Configuration of C39-C45 unit of peracetyl AM3 with key NOEs (dashed arrow), $^{3}J_{H,H}$ (small plain arrow), and $^{2,3}J_{C,H}$ (dashed line) in Hz. Acetyl groups were omitted for clarity.

Table 2-2. NMR data of positions 31-52 of peracetyl AM3.

Position	δ_H	δ_C	NOE
31	5.38	132.1	H-32, 33, 34
32	6.14 dd (9.0, 3.0)	69.0	H-31, 33, 34, 38
33	5.78 dd(9.0, 3.0)	70.4	H-33, 34, 35, 36, 38
34	4.49 dd (8.4, 2.4)	74.8	H-32, 33, 35
35	5.64	66.9	H-33, 34, 36
36	5.42	67.5	H-33, 37, 38
37	1.70, 2.10	28.2	H-36, 38
38	3.96	72.9	H-32, 33, 36, 37
39	5.39	72.9	H-40, 41
40	2.05, 2.26	28.7	H-39, 41, 70
41	2.22, 2.46	27.6	H-39, 40, 43, 44
42	-	145.3	
43	5.95	74.2	H-44, 70
44	5.38	74.4	H-43, 45
45	4.36	69.4	H-44, 46, 47, 50, 51
46	1.26, 1.96	27.5	H-44, 45, 47
47	5.21	74.6	H-45, 48, 50
48	5.70	74.8	H-47, 49
49	4.37 dd(9.6, 1.2)	75.5	H-48
50	6.01 dd(10.2, 1.8)	68.9	H-45, 47
51	5.71 dd (6.0, 1.8)	66.6	H-45, 50, 52, 53
52	6.18 dd(13.2, 7.2)	131.5	H-51, 53

The central region of AM3 (C20-C52) in membrane model was reported to adopt a hairpin conformation (Figure 2-13).[26,27] The hydrophilic polyhydroxy portion of AM3 mainly resides on the surface, while the hydrophobic polyolefinic region penetrated in the membrane interior (Figure 2-13). Conformation research experiments on and around tetrahydropyran rings with the confirmed configuration in this study allows us to deduce the orientation of the polyene side chain with respect to the central hairpin portion and also to the membrane surface. Recently, the membrane-permeabilizing activity of AM2 and AM3 is found to be hardly affected by membrane thickness.[28]

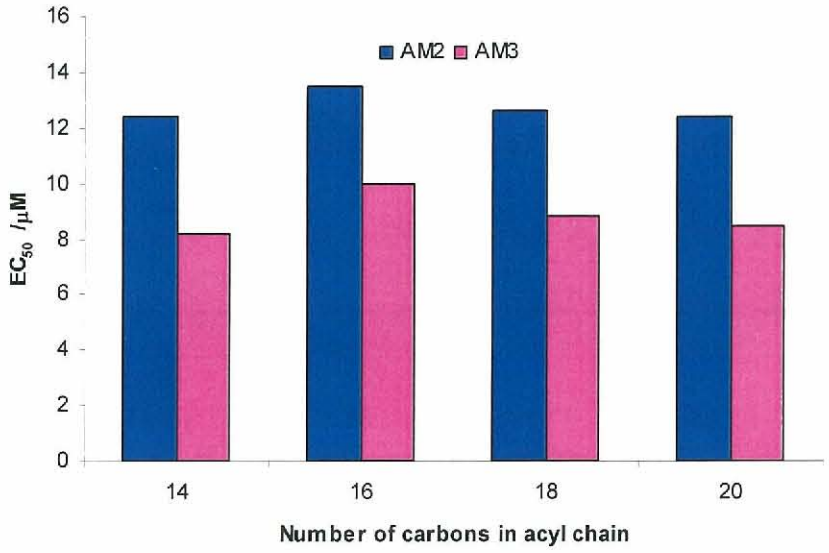

Figure 2-22. Effect of acyl chain length of PC on membrane-permeabilizing activities induced by AM2 (blue bars) and AM3 (purple bars).[28]

The finding supports the toroidal pore formation by AM3 rather than the barrel-stave pore because the stability of a barrel-stave pore as exemplified by an ion channel of AmB is influenced by the membrane thickness to much greater extent than that of a toroidal pore. As aforementioned, large difference in diameter of pores formed by AM3 and AmB also infers the different mechanism of pore formation. In contrast to a barrel-stave assembly, a toroidal-pore involves lipid headgroups as pore lining even when they partially penetrate in the lipid bilayer. In the toroidal assembly, the lipid monolayer continues from the outer leaflet to

inner one so that the pore is lined by both the detergents and the lipid headgroups.

From this consideration, the amphiphilic structure of AM3 is apparently suitable for forming a toroidal pore where the long hydrophilic polyhydorxy chain can induce a positive curvature strain to effectively capture the polar headgroups of membrane surface (Figure 2-13). Finally, the hydrophilic chain of AM3 associates with lipid headgroups to form the inner lining of the toroidal pore.

In conclusion, using the detailed NMR data obtained for peracetyl AM3, the stereochemistry of the C50-C51 and C32-C33 portions of AM3 were successfully to be confirmed. The current results support the previous finding that AM3 takes a turn structure around the two tetrahydropyran rings. This conformation may account for formation of a toroidal pore in biological membranes. In the previous report, the absolute configuration of C34-C51 portion of AM3 was determined on the correlation with C39, whose absolute configuration was deduced from Mosher's esters of the C33-C50 unit of HIO4 degradation products.[5] Similarly, the absolute configuration of C34-C51 unit of karlotoxin 2 was determined on the correlation with C30;[7] the interpretation of ^{3}J(H-31, H-30) = 7.3 Hz as an intermediate or large coupling constant is somewhat controversial, which may possibly give an effect on assignment of relative configuration of C30-C31 and, eventually on the absolute configuration of C34-C51 unit of karlotoxin 2. To confirm the absolute configuration of C34-C51 portions of AM3, the synthetic fragments corresponding to this unit are needed to compare their stereochemistry with those of degradation products from AM3.

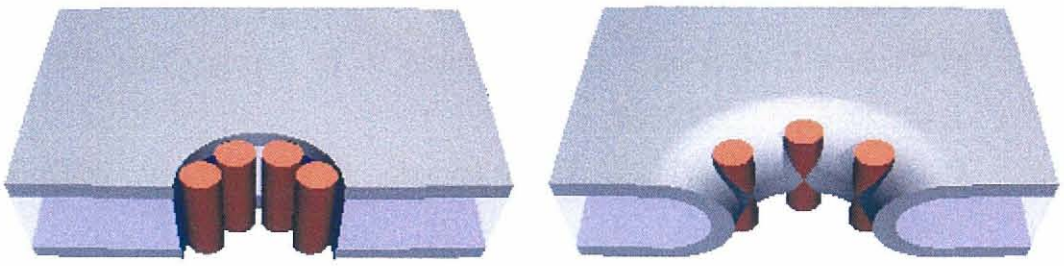

Figure 2-23. Schematics of the barrel-stave model (left) and the toroidal model (right). The dark layers represent the headgroup regions of bilayers. AM3 is represented by the cylinders, adapted from the literature.[29]

References:

1. Matsumori, N.; Kaneno, D.; Murata, M.; Nakamura, H.; Tachibana, K. *J. Org. Chem.*, **1999**, *64*, 866-876.
2. Ohtani, I.; Kusumi, T.; Kashman, Y.; Kakisawa, H. *J. Am. Chem. Soc.*, **1991**, *113*, 4092-4096.
3. Seco, J. M.; Quinoa, E.; Riguera, R. *Chem. Rev.*, **2004**, *104*, 17-117.
4. Hoye, T. R.; Jeffrey, C. S.; Shao, F. *Nature protocols*, **2007**, *2*, 2451-2458.
5. Murata, M.; Matsuoka, S.; Matsumori, N.; Paul, G. K.; Tachibana, K. *J. Am. Chem. Soc.*, **1999**, *121*, 870-871.
6. Oishi, T.; Kanemoto, M.; Swasono, R.; Matsumori, N.; Murata, M. *Org. Lett.*, **2008**, *10*, 5203-5206.
7. Peng, J.; Place, A. R.; Yoshida, W.; Anklin, C.; Hammann, M. T. *J. Am. Chem. Soc.*, **2010**, *132*, 3277-3279.
8. BouzBouz, S.; Cossy, *J. Org. Lett.*, 2001, *3*, 1451-1454.
9. Cossy, J.; Tsuchiya, T.; Ferrie, L.; Reymond, S.; Kreuzer, T.; Colobert, F.; Jourdain, P.; Markó, I. E. *Synlett*, **2007**, *14*, 2286-2288.
10. Colobert, F.; Kreuzer, T.; Cossy, J.; Reymond, S.; Tsuchiya, T.; Ferrie, L.; Markó, I. E.; Jourdain, P. *Synlett*, **2007**, *15*, 2351-2354.
11. Flamme, E. M.; Roush, W. R. *Org. Lett.*, **2005**, *7*, 1411-1414.
12. Hicks, J. D.; Flamme, E. M.; Roush, W. R. *Org. Lett.*, **2005**, *7*, 5509-5512.
13. Hicks, J. D.; Roush, W. R. *Org. Lett.*, **2008**, *10*, 681-684.
14. de Vicente, J.; Betzemeier, B.; Rychnovsky, S. D. *Org. Lett.*, **2005**, *7*, 1853-1856.
15. de Vicente, J.; Huckins, J. R.; Rychnovsky, S. D. *Angew. Chem. Int. Ed. Engl.*, **2006**, *45*, 7258-7262.
16. Huckins, J. R.; de Vicente, J.; Rychnovsky, S. D. *Org. Lett.*, **2007**, *9*, 4757-4760.
17. Paquette, L. A.; Chang, S.-K. *Org. Lett.*, **2005**, *7*, 3111-3114.
18. Chang, S.-K.; Paquette, L. A. *Synlett*, **2005**, *19*, 2915-2918.
19. Bedore, M. W.; Chang, S.-K.; Paquette, L. A. *Org. Lett.*, **2007**, *9*, 513-516.

20. Dubost, C.; Markó, I. E.; Bryans, J. *Tetrahedron Lett.*, **2005**, *46*, 4005-4009.

21. Matsumori, N.; Nonomura, T.; Sasaki, M.; Murata, M.; Tachibana, K.; Satake, M.; Yasumoto, T. *Tetrahedron Lett.*, **1996**, *37*, 1269-1272.

22. Houdai, T.; Matsuoka, S.; Matsumori, N.; Murata, M. *Biochim. Biophys. Acta*, **2004**, *1667*, 91-100.

23. Paul, G. K.; Matsumori, N.; Konoki, K.; Murata, M.; Tachibana, K. *J. Mar. Biotechnol.*, **1997**, *5*, 124-128.

24. Morsy, N.; Matsuoka, S.; Houdai, T.; Matsumori, N.; Adachi, S.; Murata, M.; Iwashita, T.; Fujita, T. *Tetrahedron*, **2005**, *61*, 8606-8610.

25. Morsy, N.; Houdai, T.; Matsuoka, S.; Matsumori, N.; Adachi, S.; Oishi, T.; Murata, M.; Iwashita, T.; Fujita, T. *Bioorg. Med. Chem.*, **2006**, *14*, 6548-6554.

26. Houdai, T.; Matsuoka, S.; Morsy, N.; Matsumori, N.; Satake, M.; Murata, M. *Tetrahedron*, **2005**, *61*, 2795-2802.

27. Houdai, T.; Matsumori, N.; Murata, M. *Org. Lett.*, **2008**, *10*, 4191-4194.

28. Morsy, N.; Houdai, T.; Konoki, K.; Matsumori, N.; Oishi, T.; Murata, M. *Bioorg. Med. Chem.*, **2008**, *16*, 3084-3090.

29. Yang, L.; Harroun, T. A.; Weiss, T. M.; Ding, L.; Huang, H. W. *Biophys. J.*, **2001**, *81*, 1475-1485.

Chapter 3

Sterol Effect on Membrane-Permeabilizing Activity of Amphidinol 3

3.1 Introduction

Permeabilization of the phospholipid membrane by AMs is thought to be responsible for their potent antifungal activity. It was previously revealed that AMs increase membrane permeability by binding to artificial lipid bilayers.[1-3] The structure-activity relationship using naturally occurring AMs and chemically modified AM derivatives has showed that the polyene and polyhydroxy moieties play respective roles in binding to the lipid bilayer membrane and in forming an ion-permeable pore/lesion across the membrane.[4] Hydrophobicity of the polyene moiety of AMs affects the membrane activity dramatically whereas the polyhydrxyl chain moderately alters the antifungal and hemolytic activities. The substitution of the sulfate group is generally inhibitory to the biological activities. Moreover, the distinct partition coefficients (K'_m values) to multilamellar vesicle (MLV) membrane were examined by HPLC quantification for AMs[3]; the K'_m values of AM2, AM3, and AM4 in eggPC preparations were 0.77×10^3, 22.2×10^3 and 2.24×10^3, respectively. The order in K'_m values agrees well with those of the membrane-permeabilizing and antifungal activities, where AM3 binds most efficiently to PC membrane.

The molecular mode of action of AMs has been proposed on the basis of the conformation of AM3 in SDS micelles[3] and isotropic bicelles.[5] These experiments have revealed that the central region of AM3 takes a hairpin conformation while the hydrophobic polyene chain is immersed in the hydrophobic interior. The results imply that (i) AMs bind to bilayer membrane mainly with the polyene portion (C52-C67 of AM3); (ii) the polyhydroxy chain (C1-C20 of AM3) is responsible for formation of lining of the pore/lesion across

the membrane; (iii) the central part (C21-C51 of AM3) adopts hairpin-shape conformation, stabilized by hydrogen bonds under amphiphatic environments.

AMs permeabilize the membrane more efficiently in the presence of sterol.[1-3, 6, 7] In previous report by Paul *et al.*, leakage of calcein by AM3 and AM5 from small unilamellar visicle (SUV) was found to be dependent on sterol. The efficacy of AM5 is found to be 27-fold enhanced by 33% cholesterol upon comparison of EC_{50} values[2] and a similar result have also been observed for AM3.[1] The efficacies of AM2 and AM3 have been measured by fluorescent-dye leakage experiments for POPC liposomes with various cholesterol and ergosterol contents, indicating that, with increasing concentrations of the sterol, the membrane permeability increases significantly. Amount of cholesterol as small as 0.5% (w/w) prominently enhances the AMs activity.[8] It is interesting that in sterol-free liposome composed of POPC, AM3 does not induce membrane-permeabilization up to 20 μM (Figure 3-1).

Table 3-1. Effect of sterol content in the liposome* on membrane-permeabilizing activities induced by AM2 and AM3.[8]

Amount of	EC_{50} (μM)		Amount of	EC_{50} (μM)	
Cho.%(w/w)	AM2	AM3	Erg.%(w/w)	AM2	AM3
0	16	NA#	0	16	NA#
0.5	16	11.8	0.5	12	7.5
5	8.3	3.4	5	6.4	3.4
10	3	2.5	10	3.9	3
30	6	3	30	5.5	2.1

*In all cases, the lipid concentration was 27 μM.
#Leakage did not occur up to 20 μM AM3 tested.

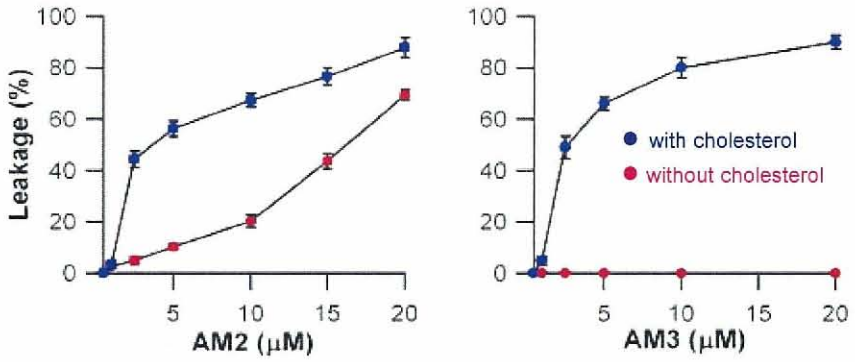

Figure 3-1. Effect of cholesterol on membrane-permeabilizing activities of AM2 and AM3.[7]

All previous findings, especially the effects of sterol on AMs activities, directed us to obtained more evidence about sterol efficacy in potentiation of the AMs activities.

3.2 Surface Plasmon Resonance (SPR) Experiments

Surface plasmon resonance (SPR) has recently emerged as a useful tool for assessing interactions between biomolecules. Among other features, the capability for measuring time course of the interactions from a minute amount of biomolecules becomes a great advantage of this method. Many studies have shown that SPR techniques are useful for investigation of membrane-bound peptides and drugs.[9-11] More recently, the interaction between complex amphiphilic molecule, AmB, and lipid bilayers has successfully been evaluated by devising a new SPR methods for reducing the level of nonspecific interaction between analytes and sensor chip basis. This method greatly facilitated kinetic analysis for AmB binding to sterol-containing PC.[12] To examine more closely the affinity of AM3 to membranes with or without sterol in this study, we utilized the same dodecylamine-modified SPR sensor chip to carry out kinetic analysis for AM3 binding to sterol-containing and sterol-free POPC liposomes.

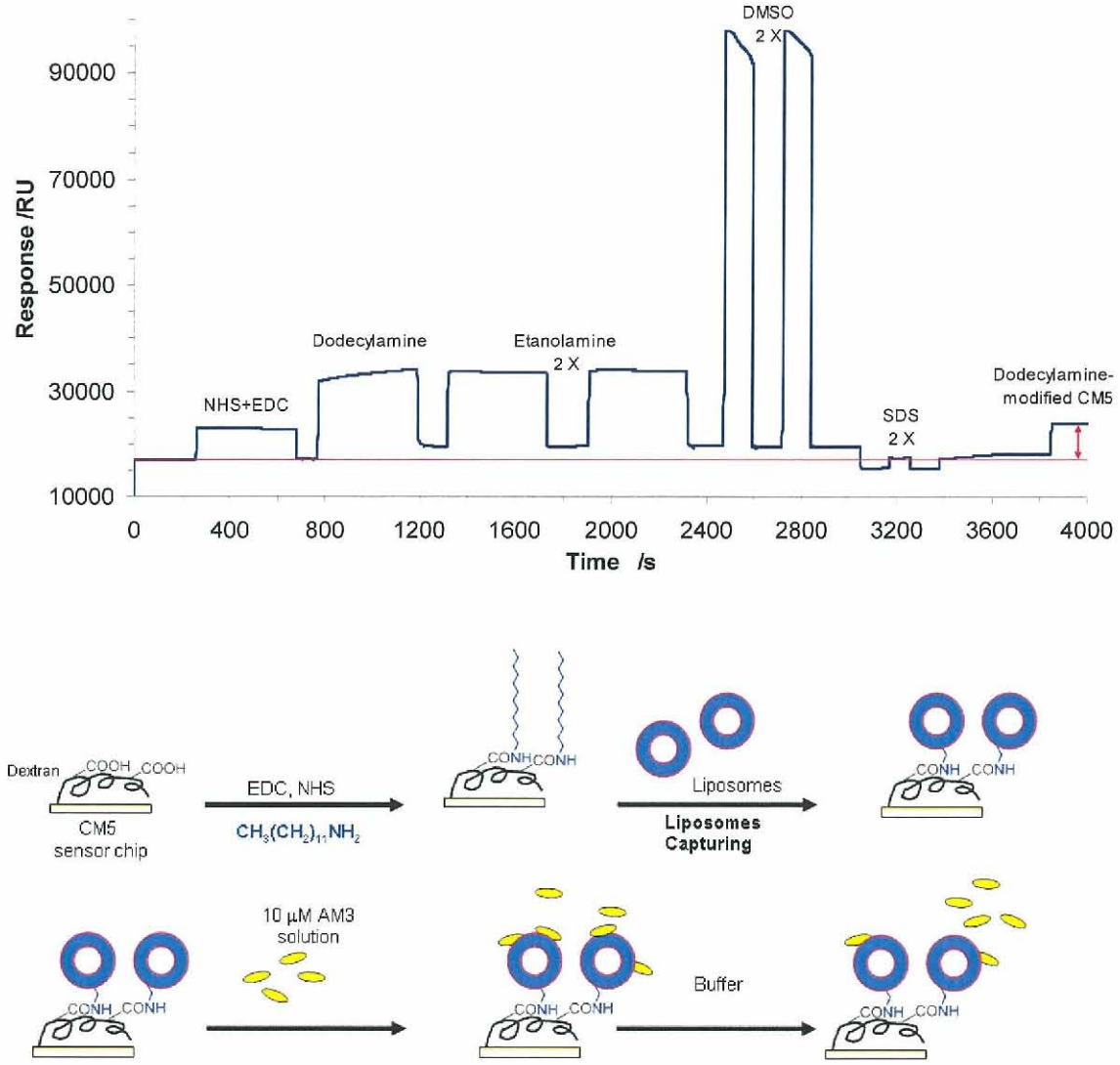

Figure 3-2. Sensorgram of dodecylamine modification on flow cell 2 of CM5 sensor chip and schematic illustration of SPR experiment.

3.2.1 Modification of sensor chip with dodecylamine

The CM5 chip of SPR was modified with dodecylamine to prepare a hydrophobic surface (Figure 3-2). One of two flow cell lanes in the CM5 chip was modified with dodecylamine, while the other lane remained intact for the use of a control run. To the modified lane, POPC and POPC/sterol liposomes were stably captured. When the liposomes at the phospholipid concentration of 0.5 mM were introduced, the SPR response due to liposome association reached about 10,000

RU (Figure 3-3). The sensor chip was tolerant of NaOH treatments (50 mM), and the amount of captured liposomes was essentially unchanged by repetitive washing. For kinetic analysis, the binding of AM3 to liposome membranes was standardized as an amount of AM3 in RU bound to the amount of lipids equivalent to 10,000 RU.

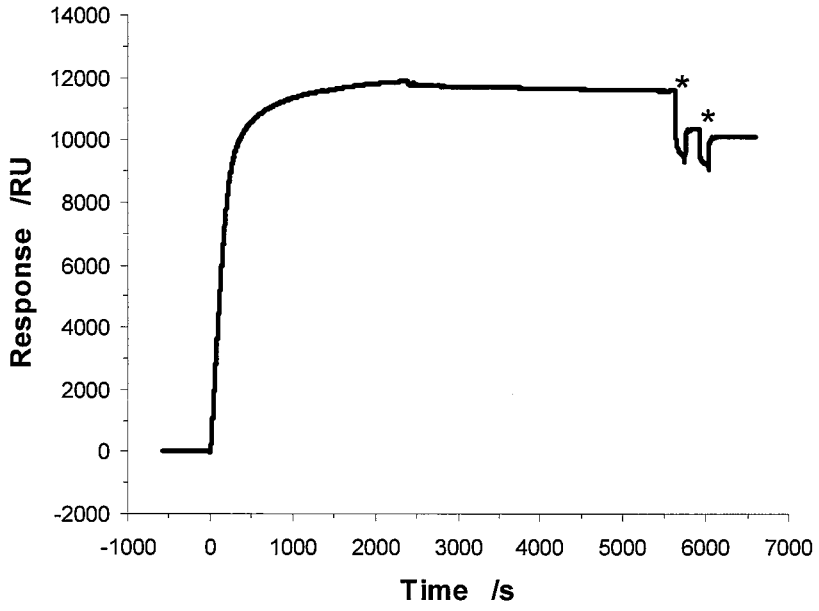

Figure 3-3. Sensorgram for immobilization of 0.5 mM POPC liposome (80 μL) on dodecylamine-modified CM5 sensor chip. Liposome-bound surface was washed twice with 50 mM NaOH for 2 min at 20 μL/min (denoted by asterisks).

Detection of AM3 affinity was carried out in PBS buffer (pH 7.4) as running and injection media. AM3 dissolved in PBS buffer was then passed on the sensor chip treated with liposomes. The SPR response increased immediately after injection due to interaction between AM3 in the sample solution and POPC liposomes immobilized on the surface of the sensor chip. To evaluate AM3 binding to sterol-containing or sterol-free liposomes, the SPR response in the control lane was subtracted from that in the liposome-captured lane. AM3 firmly interacted with the sensor-chip surface and a small portion of AM3 was hardly washed out during regeneration. To eliminate the effect of the remaining AM3, a newly prepared sensor chip always be used.

Typical sensorgrams for interaction of 10 μM AM3 with sterol-free liposomes, 5% cholesterol-containing POPC liposomes and 5% ergosterol-containing POPC liposomes are shown in Figure 3-4 to Figure 3-6. The RU changes upon AM3 addition are largely responsible for the drug-liposome interaction. The kinetic analysis of the drug's binding to membrane was carried out using BIAevaluation software for the reaction models including Langmuir binding, bivalent analyte, and two-state reaction models. Among those, the two-state reaction model best reproduced the experimental sensorgrams as depicted in sensorgrams as smooth red curves.

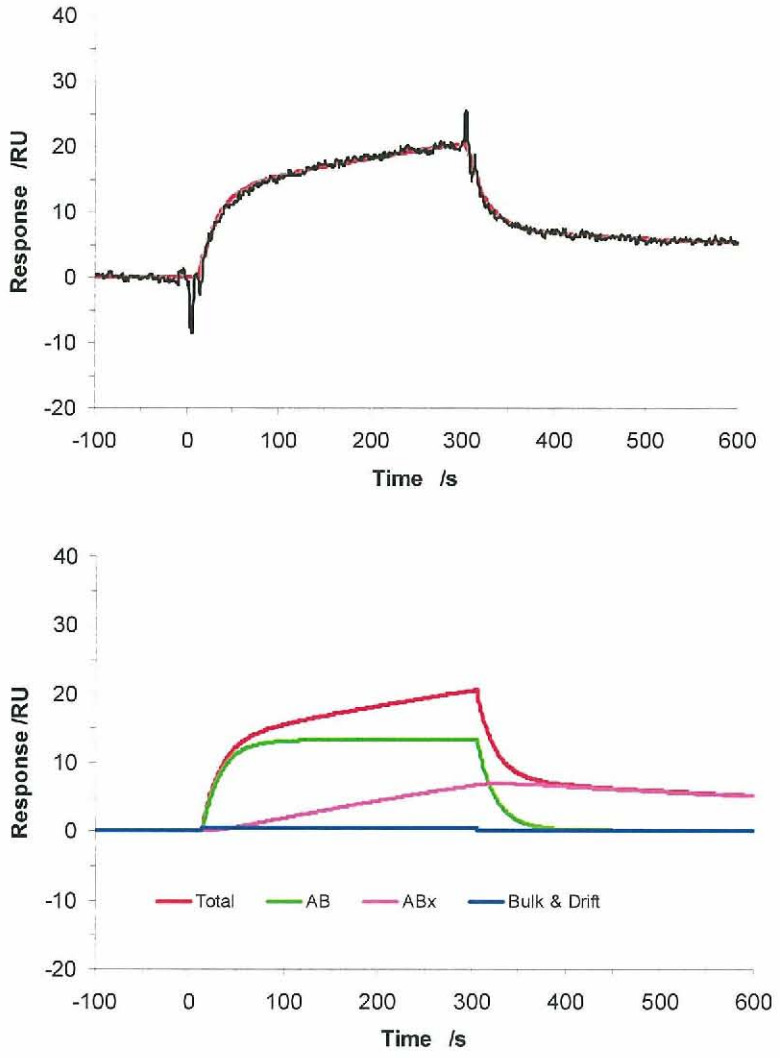

Figure 3-4. Typical SPR sensorgram and its components for interaction of 10 μM AM3 to cholesterol-free POPC. The sensorgram was fitted to the two-state reaction model.

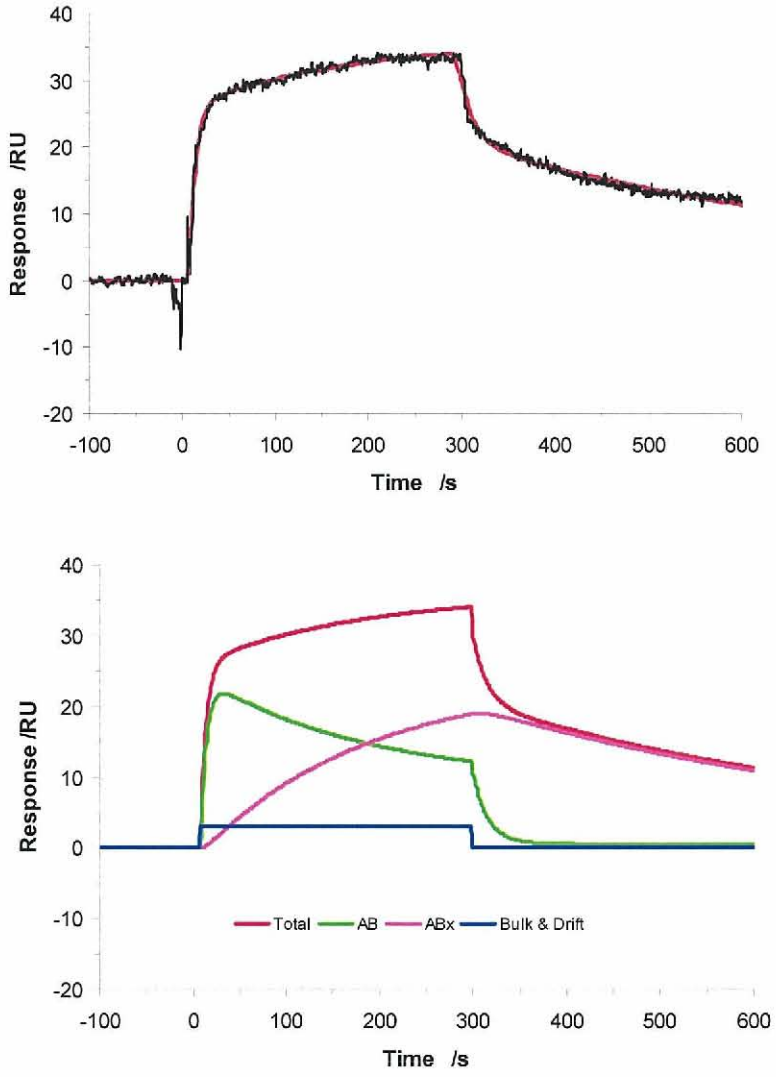

Figure 3-5. Typical SPR sensorgram and its components for interaction of 10 μM AM3 to 5% cholesterol-containing POPC. The sensorgram was fitted to the two-state reaction model.

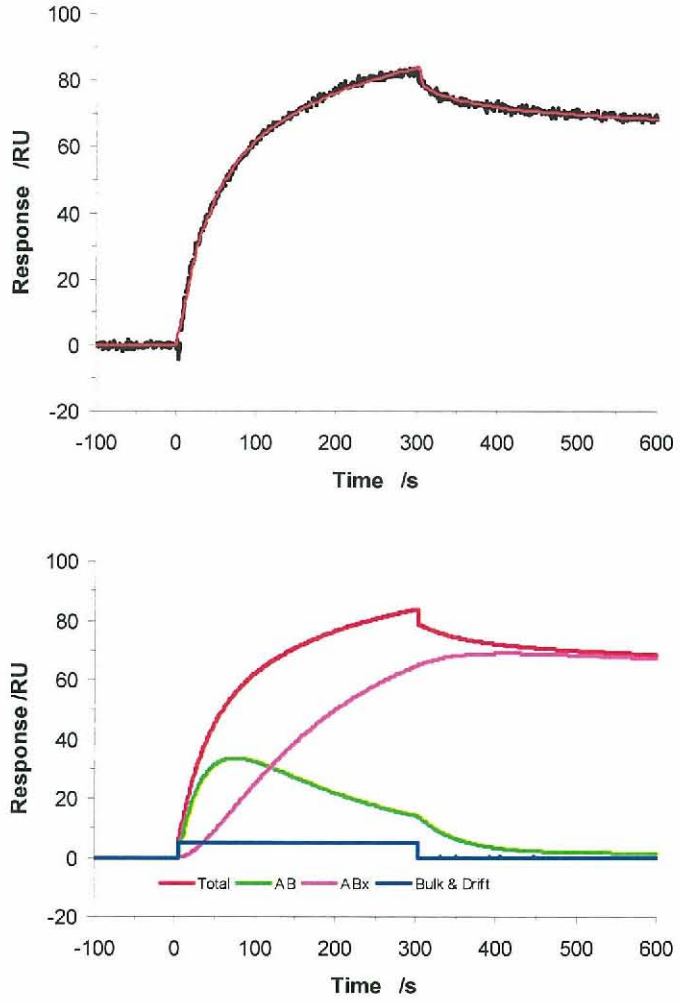

Figure 3-6. Typical SPR sensorgram and its components for interaction of 10 μM AM3 to 5% ergosterol-containing POPC. The sensorgram was fitted to the two-state reaction model.

3.2.2 Kinetic analysis of AM3 interaction to membrane bilayer

The two-state reaction model indicates that the interaction is composed of subsequent two steps; the first step is partition of AM3 to the POPC phase of liposomes, and the second step corresponds to the internalization of AM3 to the liposome interior to form more stable complexes as shown in Figure 3-7.

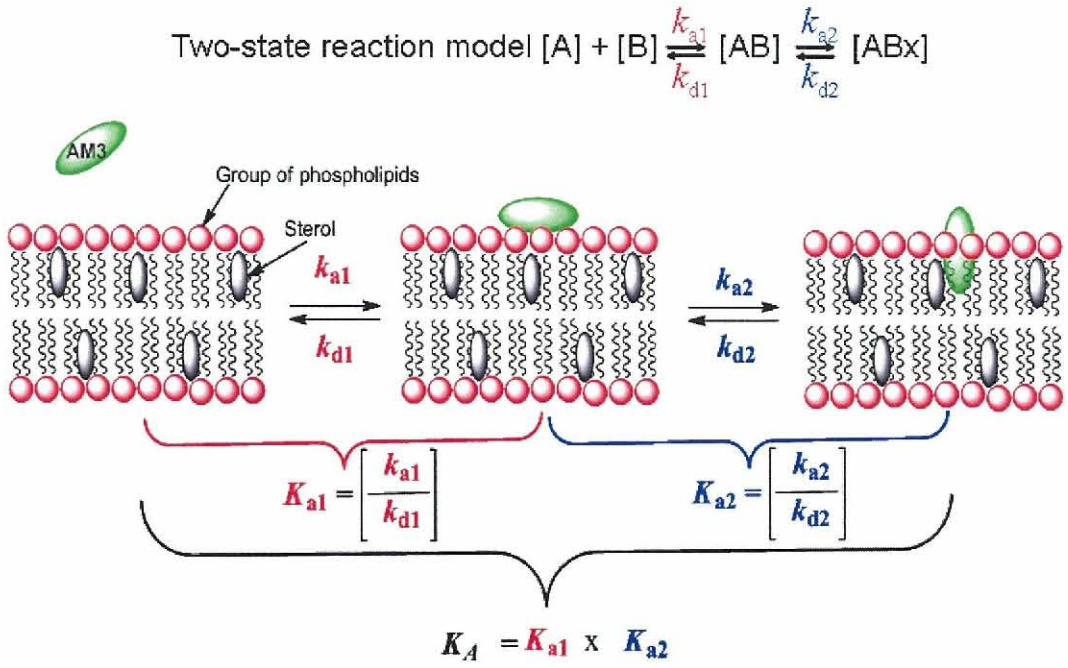

Figure 3-7. Illustration of the two-state reaction model for interaction between AM3 and sterol-containing phospholipid membranes.

Table 3-2. Kinetic and affinity constants for interactions of AM3 (10 μM) with POPC liposomes in the presence and absence of 5% sterol estimated based on the two-state reaction model.

Kinetic value	POPC + Erg	POPC + Cho	POPC
k_{a1} (x 10^3 /Ms)	1.64 ± 0.043	8.53 ± 0.61	0.0465±0.0057
k_{d1} (x10^{-3} /s)	12.5 ± 2.8	48.0 ± 6.2	51.9 ± 3.1
k_{a2} (x10^{-3} /s)	12.4 ± 3.2	7.65 ± 1.27	2.62 ± 0.23
k_{d2} (x10^{-3} /s)	0.420 ± 0.070	1.98 ± 0.13	3.96 ± 1.52
K_{A1} (x10^3 /M)	143 ± 23	180 ± 11	0.901 ± 0.121
K_{A2}	28.6 ± 2.62	3.92 ± 0.71	0.930 ± 0.380
K_A (x10^3 /M)	3970 ± 410	721 ± 169	0.764 ± 0.226

Estimation of the kinetic parameters of AM3 binding to the membranes based on the two-state reaction model[11] can be calculated using BIAevaluation® software and the result is presented in Table 3 2. In this model, k_{a1} and k_{d1} are association

and dissociation constants of analyte to membrane surface in the first step while k_{a2} and k_{d2} are association and dissociation rates for the second step. Then K_{A1}, K_{A2} and K_A represent the affinity constants for the first step, the second step and overall equilibrium, respectively, and were calculated from the association and dissociation rate constants.[29]

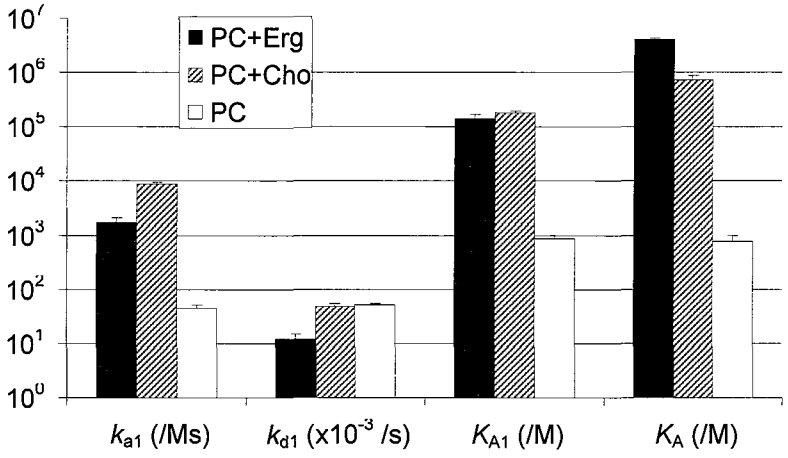

Figure 3-8. Comparison kinetic data in logarithmic scale for AM3 binding to ergosterol-containing, cholesterol-containing, and sterol-free POPC liposomes.

The sterols have the most striking effects on the initial process of AM3-binding to membrane as revealed by k_{a1}. The k_{a1} value of AM3 in 5% cholesterol- and ergosterol-containing membranes exceeds that in the sterol-free membranes by about 180- and 35-fold, respectively. This suggests that sterols play a functional role in capturing AM3 on the membrane surface. The resultant K_A value of AM3 in 5% cholesterol-containing membrane exceeds that in the sterol-free one by almost 1000-fold. The binding step to membrane is, as aforementioned, one of important features for the biological activity.[3] Although effect of ergosterol on the initial binding process is not as dramatic as that of cholesterol, ergosterol stabilizes formation of complex in the second step. As a result, the K_A value of AM3 in 5% ergosterol-containing membrane exceeds that in the sterol-free one by about 5000-fold.

The binding of AM3 to the POPC liposomal membrane is very strong. It was therefore extremely difficult to regenerate the membrane once AM3 bound to it. New liposome surface on the sensor chip has to be prepared every time before AM3 injection to replicate the experiments. Yet, similar membrane conditions were not attainable for each run, which caused relatively large standard error means on Table 3-2. Nonetheless, large differences between kinetic constants obtained in the presence and absence of sterols clearly indicate that sterols markedly enhance the membrane-binding of AM3. These effects of cholesterol, mammalian sterol, and ergosterol, fungal sterol, may account for the respective potent cytotoxicity[13,14] and antifungal activities.[2,4,13,15-17] Interestingly, AMs lack anti-bacterial activity, which is probably due to the absence of sterols in bacterial membranes. Moreover, AM3 showed higher affinity to ergosterol membrane than cholesterol one, particularly, in dissociation process; K_{A2} of the former was significantly larger than those of the latter. These observations indicate that AM3 forms more stable complex in the presence of ergosterol and may provide a clue for developing a new antifungal drug.

In conclusion, SPR experiments disclosed for the first time that sterols markedly enhance affinity of AM3 to phospholipid membrane. The present results agree with the previous findings in fluorescent-dye leakage experiments;[7] the potentiation of the activity of AM3 by sterol is prominent even at 0.5% (w/w) to the lipid, which ruled out the possibility that alteration of the membrane physical properties elicited by sterols[18] was responsible for this effect.[7] The significantly larger K_{A2} for POPC-ergosterol membrane (Table 3-2) further supports the notion that sterols, particularly ergosterol, not only accelerate partition of AM3 to membrane but also stabilize the membrane-bound complex formed by AM3, suggesting the direct interaction between AM3 and sterols in the complex. NMR-based investigations on this interaction in membrane model systems will provide information in more detail.

References:

1. Paul, G. K.; Matsumori, N.; Konoki, K.; Sasaki, M.; Murata, M.; Tachibana, K. In Harmful and Toxic Algal Blooms, Sendai, July, 1996; Intergovernmental Oceanographic Commission of UNESCO: Sendai, 1996; 503-506.
2. Paul, G. K.; Matsumori, N.; Konoki, K.; Murata, M.; Tachibana, K. *J. Mar. Biotechnol.,* **1997**, *5*, 124-128.
3. Houdai, T.; Matsuoka, S.; Morsy, N.; Matsumori, N.; Satake, M.; Murata, M. *Tetrahedron,* **2005**, *61*, 2795-2802.
4. Morsy, N.; Houdai, T.; Matsuoka, S.; Matsumori, N.; Adachi, S.; Oishi, T.; Murata, M.; Iwashita, T.; Fujita, T. *Bioorg. Med. Chem.,* **2006**, *14*, 6548-6554.
5. Houdai, T.; Matsumori, N.; Murata, M. *Org. Lett.,* **2008**, *10*, 4191-4194.
6. Houdai, T.; Matsuoka, S.; Matsumori, N.; Murata, M. *Biochim. Biophys. Acta,* **2004**, *1667*, 91-100.
7. Morsy, N.; Houdai, T.; Konoki, K.; Matsumori, N.; Oishi, T.; Murata, M. *Bioorg. Med. Chem.,* **2008**, *16*, 3084-3090.
8. Morsy, N. Structure Elucidation and Mode of Action of Amphidinol Homologues from Marine Dinoflagellate. PhD., Osaka University, Osaka, 2007.
9. Abdiche, Y. N.; Myszka, D. G. *Anal. Biochem.,* **2004**, *328*, 233-243.
10. Papo, N.; Shai, Y. *Biochemistry,* **2003**, *42*, 458-466.
11. Mozsolits, H.; Wirth, H. J.; Werkmeister, J.; Aguilar, M. I. *Biochim. Biophys. Acta,* **2001**, *1512*, 64-76.
12. Mouri, R.; Konoki, K.; Matsumori, N.; Oishi, T.; Murata, M. *Biochemistry,* **2008**, *47*, 7807-7815.
13. Echigoya, R.; Rhodes, L.; Oshima, Y.; Satake, M. *Harmful Algae,* **2005**, *4*, 383-389.
14. Qi, X.-M.; Yu, B.; Huang, X.-C.; Guo, Y., -W.; Zhai, Q.; Jin, R. *Toxicon,* **2007**, *50*, 278-282.

15. Satake, M.; Murata, M.; Yasumoto, T.; Fujita, T.; Naoki, H. *J. Am. Chem. Soc.,* **1991**, *113*, 9859-9861.
16. Morsy, N.; Matsuoka, S.; Houdai, T.; Matsumori, N.; Adachi, S.; Murata, M.; Iwashita, T.; Fujita, T. *Tetrahedron,* **2005**, *61*, 8606-8610.
17. Hoye, T. R.; Jeffrey, C. S.; Shao, F. *Nature protocols,* **2007**, *2*, 2451-2458.
18. Alvarez, F. J.; Douglas, L. M.; Konopka, J. B. *Eukaryot. Cell,* **2007**, *6*, 755-763.

Chapter 4

Conclusions

Amphidinol family (AMs) have been isolated as potent antifungal agents from the dinoflagellate *Amphidinium klebsii.* Among other homologues, AM3 has the most potent antifungal and hemolytic activities. Their structures are characterized by a linear polyhydroxyl moiety, tetrahydropyran rings and a polyolefinic chain of fourteen or sixteen carbon atoms. Unlike other natural or synthetic antifungal compounds, AMs lack nitrogenous polycycles or macrocycles in their structures. These unique features make AMs an interesting model to gain a better understanding of the molecular mechanism of antifungal action.

From the current study, it can be concluded that:

- The NMR data of peracetyl AM3 provide essential information about stereochemistry that remains uncertain in intact AM3.
- The stereochemistry of the C50-C51 and C32-C33 portions of AM3 are established as *threo* configurations. These assignments support that AM3 takes a turn structure around the two tetrahydropyran rings. This conformational preference of AM3 is considered to play a crucial role for toroidal pore formation.
- SPR experiments using a dodecylamine-modified sensor chip facilitate kinetic analysis for AM3 binding to sterol-containing and sterol-free POPC liposomes.
- Sterol, particularly ergosterol, not only accelerate partition of AM3 to membrane but also stabilize the membrane-bound complex formed by AM3, suggesting the direct interaction between AM3 and sterols in the complex.

Chapter 5

Experimental

5.1 General Experimental Procedures

5.1.1 Materials

Salt for artificial seawater, Marin Art Hi® was from Tomita Pharmaceutical. Ion exchange resin DIAION HP-20 (Mitsubishi Chemical) was purchased from Nippon Rensui Co. (Osaka, Japan) and silica gel YMC ODS-AQ was from YMC Co. (Kyoto, Japan). Pyridine and acetic anhydride were from Nacalai Tesque (Kyoto, Japan). Glass plates coated with 60 F_{254} silica gel or RP-18 F_{254} were used for normal phase or reverse phase thin layer chromatography (TLC), respectively. All NMR solvent (CD_3OD, D_2O, pyridine-d_5, and C_6D_6) were from Euriso-Top. 1-Palmitoyl-2-oleoyl-*sn*-glycero-3-phosphocholine (POPC) was purchased from NOF Corporation. (Tokyo, Japan). Cholesterol, chloroform, sodium chloride (NaCl), potassium chloride (KCl), disodium hydrogen phosphate, potassium dihydrogen phosphate, and 2-propanol were purchased from Nacalai Tesque, Inc. (Kyoto, Japan). 1-Ethyl-3-(3-dimethylaminopropyl) carbodiimide hydrochloride (EDC), *N*-hydroxysuccinimide (NHS), 10 mM acetate buffer (pH 5.0), 1 M ethanolamine hydrochloride (pH 8.5) and 50 mM sodium hydroxide (50 mM NaOH) were purchased from BIAcore AB (Uppsala, Sweden). Dodecylamine and dimethyl sulfoxide (DMSO) were purchased from Sigma-Aldrich Co. (St. Louis, MO). All of these chemicals were of the highest grade and used without further purification. Water was purified with a Millipore Simpli Lab system (Millipore Inc., Bedford, MA).

5.1.2 Instruments

HPLC system :	Shimadzu (SCL-10Avp, SPD-M10Avp, LC-10ADvp, LC-10ADvp, DGU-12A)
UV spectrofotometer :	Shimadzu UV-2500
Mass spectrometer :	LCQ deca, LTQ-Orbitrap (Thermo electron)
NMR spectrometer :	JEOL ECA500 (500 MHz) VARIAN AS600 (600 MHz)
Surface Plasmon Resonance :	BIACORE®X
Clean bench :	Sanyo MCV-710ATS
Microscope :	Olympus CK30-F100
Autoclave :	TOMY BS-325
Water purifying apparatus :	Elix-UV, Simpli Lab (MILLIPORE)
Electronic balance :	A & D GR-202, HF-3200
pH meter :	TOA HM-40S
Rotary evaporator :	N-1000, WATER BATH SB-350, COOL ACE CA-1111(EYELA) NVC-2000 (Technosigma)
Centrifugator :	KUBOTA5200, E-centrifuge (WEALTEC)
Vortex mixer :	Scientific IndustriesVORTEX GENIE-2
Sonicator :	Yamato BRANSON 1200
Micropipette :	Nichiryo Nichipet EX

5.2 Methods

5.2.1 Culture of *Amphidinium klebsii*

The dinoflagellate *Amphidinium klebsii* was separated from surface wash seaweed that were commonly abundant during spring near Aburatsubo-Bay,

Kanazawa, Japan and deposited in National Institute of Environmental Studies as NIES 613. Species identification was previously carried out by Prof. Y. Fukuyo, Faculty of Agriculture, the University of Tokyo, based on the cell morphology. The culture was unialgally grown in a 3-liter flask containing artificial seawater (Marin Art Hi, Tomita Pharmaceutical, 3% w/v) enriched with ES-1 nutrient (Table 5-1) at 25 °C for 4 weeks under 16-8 light-dark photocycle. The cells were harvested by filtration with glass filters under reduced pressure. After harvesting the cultured cells, the cultured medium was passed through an HP-20 column (15 X 5 cm) and the trapped toxins were eluted by MeOH and then combined with MeOH extract from the harvested cells for AM3 isolation.

Figure 5-1. Culture of the dinoflagellate *Amphidinium klebsii* in 3 L flask containing artificial sea water enriched with ES-1 nutrient.

5.2.2 Isolation of amphidinol 3

The harvested cells (from 60 L culture) were extracted with MeOH (1 L X 2) and then with 50% aqueous methanol (1 L). The combined extract, after the solvent was removed by a rotary evaporator at 30 °C, was subjected to lead acetate purification to remove most thanins and coloring materials, and the excess of lead acetate was eliminated using Na_2HPO_4. The supernatant was subjected to ethyl acetate/H_2O partition and the aqueous layer was then subjected to butanol/H_2O

partition. The butanol extract was dried and applied to an ODS open column and then to HPLC to furnish 6.3 mg AM3.

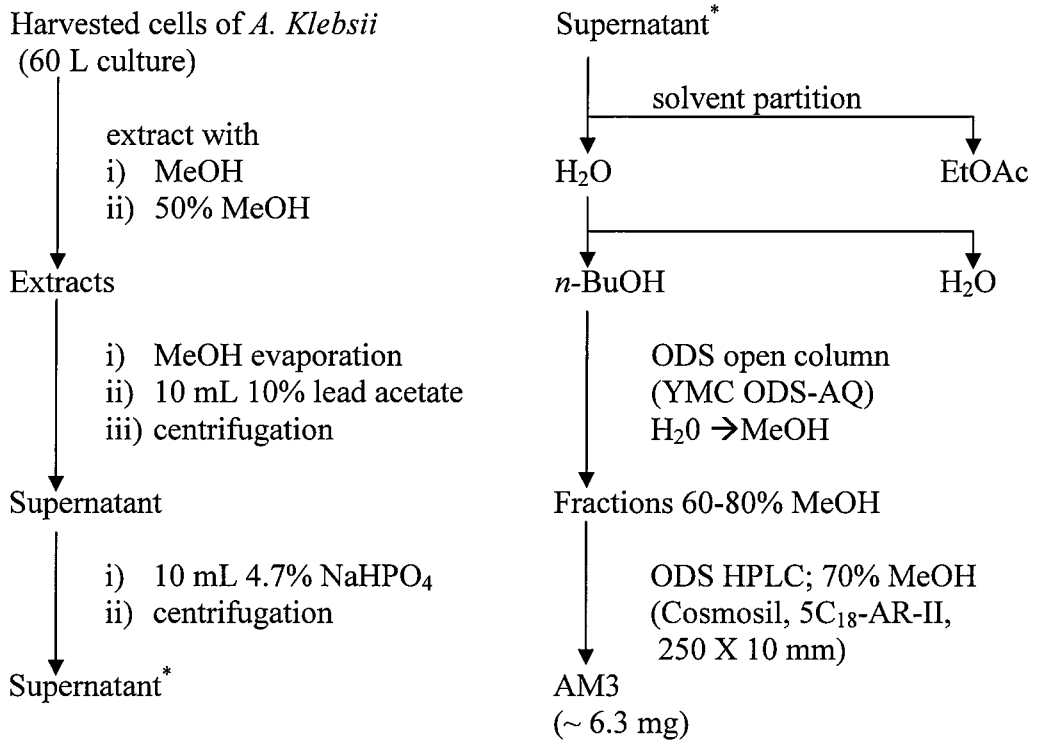

Figure 5-2. Isolation of AM3 from the cultured of *Amphidinium klebsii*

Table 5-1. ES-1 nutrient

Ingredients	Volume or Weight
Artificial sea water	1000 mL
$NaNO_3$	70 mg
$Na_2\beta$-glycerophosphate	10 mg
Tris(hydroxymethyl)aminomethane	100 mg
H_3BO_3	1 mg
$MnSO_4$	290 μg
$ZnSO_4$	25 μg
Na_2-EDTA	5 mg
Fe-EDTA	550 mg
$CoSO_4$	1 μg
Vit B_{12}	2 μg
Biotin	1 μg
Thiamine-HCl	100 μg

5.2.3 Liquid chromatography using an open column and HPLC

The *n*-butanol fractions, after evaporating the solvent by a rotary evaporator, were applied to an ODS open column chromatography (YMC Gel ODS-AQ; 12 X 2 cm) initially with 3 column volume of H_2O and then gradually increasing ratio of MeOH in H_2O (10-100%). AMs were found abundant in fractions eluted by 60-80% MeOH solution. After evaporation of the solvent, the AMs containing fractions were futher purified by HPLC.

Two pre-packed columns (Cosmosil, $5C_{18}$-AR-II, 250 X 10 mm) were connected in series on a Shimadzu HPLC system. The AMs containing fractions (200-300 μg) was injected as 50 μL aqueous solution for each separation. Aqueous methanol 70% eluent was degassed using sonicator before being introduced into the system and elution rate was 1.5 mL/min. Amphidinol 3 were collected at retention time 72 minute.

Column : $5C_{18}$-AR-II (250 X 10 mm); 2 column in series.
Eluent : 70% MeOH
Flow rate : 1.5 mL/min
Detection : 270 nm

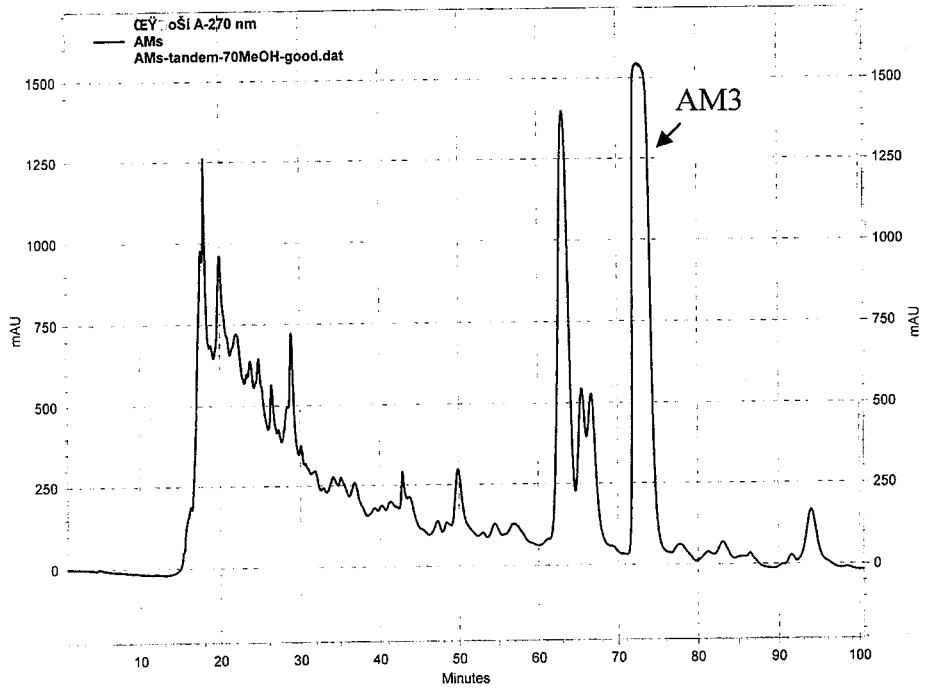

Figure 5-3. Chromatogram of AM3 isolation.

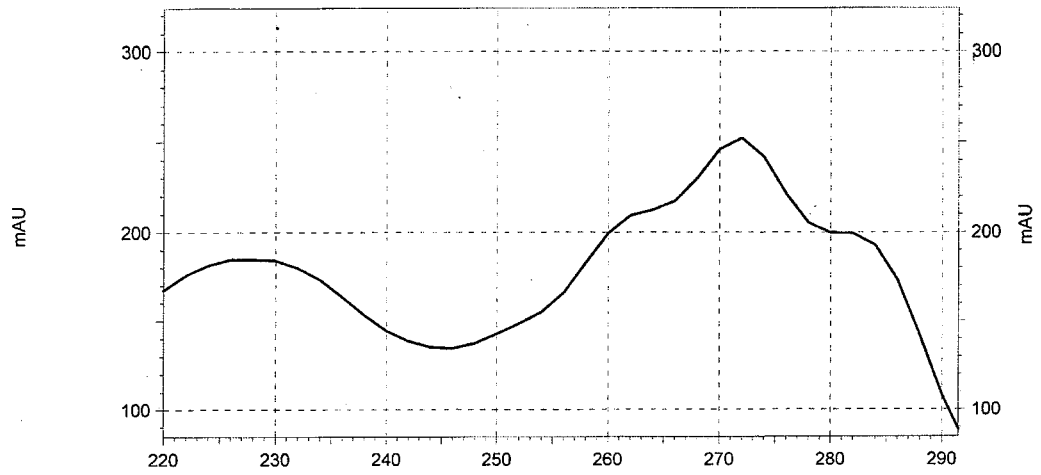

Figure 5-4. UV spectrum observed during AM3 separation by HPLC at retention time 72 minute.

5.3 Preparation of Peracetyl AM3

Peracetyl AM3 was prepared as follow; 2.00 mg (1.52 μmol) of AM3 was dissolved in 75.0 μL pyridine and stirred in a small vial. Then, 75.0 μL (794 μmol) acetic anhydride was added into the solution. Reaction was carried out for 24 hours under argon atmosphere and monitored by TLC. Pyridine and access of acetic anhydride was removed by evaporation in vacuo. Afforded product was dissolved in 200 μL perdeuterated benzene and transferred into Shigemi NMR tube for NMR studies.

5.4 NMR experiments

Nuclear magnetic resonance (NMR) spectra were recorded on JEOL ECA500 or VARIAN AS600 spectrometers at the Department of Chemistry, Osaka University. Chemical shifts (δ) were recorded in parts per million (ppm) Spectra recorded in deuterobenzene (C_6D_6) were referenced to residual protonated benzene (^1H δ 7.15 and ^{13}C 128.0 ppm). ^1H and 13C spectra recorded in

deuteromethanol (CD_3OD) or mixture of CD_3OD/pyridine-d_5 were referenced to residual protonated methanol (^1H δ 3.31 and ^{13}C 49.0 ppm). Coupling contants (J values) were measured in Hz. All ^{13}C spectra were proton decoupled unless otherwise stated.

Two dimensional NMR (2D NMR) for DQF-COSY, TOCSY, and NOESY spectra were recorded at 30 °C with a repetition time of 1s in phased-sensitive mode using states method. The spectral width in both dimensions was typically 5000 Hz or 9000 Hz. The data points were acquired using a 1K X 512 complex data matrix for NOESY and TOCSY; and 1K X 256 complex data matrix for DQF-COSY which were zero filled once in X dimension and twice in Y dimension. The data points for HETLOC were 2K X 128 which were zero filled four times in X dimension and twice in Y dimension. For DQF-COSY and NOESY, 2D data were apodized with a π/2 shifted sine-squared bell curve window function before Fourier transformation. The 2D data for HMBC were apodized with a sine bell function while HETLOC data were apodized with a sine-squared bell window function. Phase sensitive HMBC and gradient enhanced HSQC (gHSQC) spectra were acquired with 32 transients per increment. The evolution delay was set for $^nJ_{CH}$ of 8 Hz (HMBC) or $^1J_{CH}$ of 140 Hz (gHSQC). DQF-COSY spectra were acquired with 16 transients per increment and a pulse delay of 1.5 seconds. NOESY spectra were acquired with 32 transients per increment, a pulse delay of 1.5 seconds, and mixing time of 0.3 seconds. The mixing times of TOCSY and HETLOC were 80 and 50 ms.

5.5 Surface Plasmon Resonance Experiments

5.5.1 Preparation of liposome

POPC with or without sterol was dissolved in chloroform/methanol (2:1) in a round-bottom flask. The mixture was evaporated and dried in vacuo for over 2 hours, which was then hydrated with 10 mM phosphate buffer (pH 7.4) containing KCl (2.7 mM) and NaCl (137 mM) (PBS buffer, 1 mL). The mixture

was vortexed and sonicated to prepare multilamellar vesicles (MLVs). The resultant suspension was subjected to three cycles of freezing (-80 °C), thawing (60 °C) and vortexing (5 s) to form LUVs. The LUVs were passed through double 100 nm polycarbonate filters 19 times with LiposoFast™-Basic (AVESTIN Inc., Ottawa, Canada) at room temperature, and diluted with PBS buffer to furnish a LUV solution with the lipid concentration of 0.5 mM.

5.5.2 Surface plasmon resonance experiments

AM3 (1 mg, 0.75 μmol) was dissolved in water (1 mL) and stored as a 0.75 mM AM3 stock solution. For SPR measurements, the stock solution was first diluted with the PBS buffer to 250 μM AM3 and then diluted again with PBS buffer to give 10 μM AM3 solution. The experiments were performed at 25°C using the CM5 sensor chip mounted in a BIAcore X analytical system (BIAcore AB, Uppsala, Sweden). A washing solution was comprised of 50 mM sodium hydroxide and mixture 50 mM sodium hydroxide/isopropanol (3:1). After a routine pretreatment of the BIAcore instrument, the sensor chip was washed with distilled water overnight to remove trace amounts of detergent.

Dodecylamine was immobilized to one of the flow cell lanes (fc2) in the CM5 sensor chip by an amino coupling method while the other lane was left intact as a control lane. The immobilization reaction was performed at a flow of 5 μL/min; briefly, the sensor chip was activated for 7 minutes by injecting a solution mixture (1:1 v/v, 35 μL) of 390 mM EDC and 100 mM NHS. Dodecylamine (1 mg/mL) in 10 mM acetate buffer containing 10% DMSO (pH 5.0, 35 μL) was then injected for crosslinking. The remaining activated N-hydroxysuccinimide ester groups were converted to amide groups by 1 M ethanolamine hydrochloride (pH 8.5, 35 μL). The sensor chip that obtained was washed with 10% DMSO (35 μL) to remove nonspecifically bound substances.

The running buffer was PBS buffer (pH 7.4). Prior to use, the buffer was degassed by sonication. The liposome solution (0.5 mM, 80 μL) was injected to the sensor chip at a flow rate of 2 μL/min, and then 50 mM sodium hydroxide (40 μL) was added at a flow rate of 20 μL/min. The NaOH treatment was repeated

twice, resulting in a stable baseline which indicated formation of stable liposome layers on the sensor chip. AM3 in the running buffer (10 μM, 100 μL) was introduced to the sensor chip at a flow rate of 10 μL/min, and the time course of its association and dissociation was monitored. Analysis of the sensorgrams was carried out by using BIAevaluation software (Biacore AB). Kinetic parameters was estimated using provided reaction models; among those, the two-state reaction model is the best fitted with the experimental sensorgrams.

In the two-state reaction model, two steps of drug-membrane interactions are involved. This first step where AM3 (A) binds to membrane lipids (B) in a parallel manner is stoichiometric since AM3 is supposed to be surrounded by a certain number of PC molecules, and the second step involves the reorientation of the complex (AB) to another complex (ABx) which forms the inner lining of the toroidal pore.

$$A + B \underset{k_{d1}}{\overset{k_{a1}}{\rightleftarrows}} AB \underset{k_{d2}}{\overset{k_{a2}}{\rightleftarrows}} ABx$$

where k_{a1} and k_{d1} represent association and dissociation constants for free AM3 to liposome surface, respectively, and k_{a2} and k_{d2} represent distribution constants between the liposome surface and interior of the liposome. Therefore, the rate equations for this two-state reaction model are represented by:

$$dA/dt = -k_{a1}[A][B] + k_{d1}[AB]$$

$$dAB/dt = (k_{a1}[A][B] - k_{d1}[AB]) - (k_{a2}[AB] - k_{d2}[ABx])$$

$$dABx/dt = k_{a2}[AB] - k_{d2}[ABx]$$

$$K_{A1} = (k_{a1}/k_{d1}) \; ; \; K_{A2} = (k_{a2}/k_{d2}) \; ; \; K_A = (k_{a1}/k_{d1})(k_{a2}/k_{d2})$$

where [A] and [B] are concentrations of free AM3 and lipids in liposomes, and [AB] and [ABx] are concentrations of the complex before or after conformational

change, respectively. Then K_{A1}, K_{A2} and K_A represent the affinity constants for the first step, the second step and overall equilibrium, respectively.

Supplementary Materials

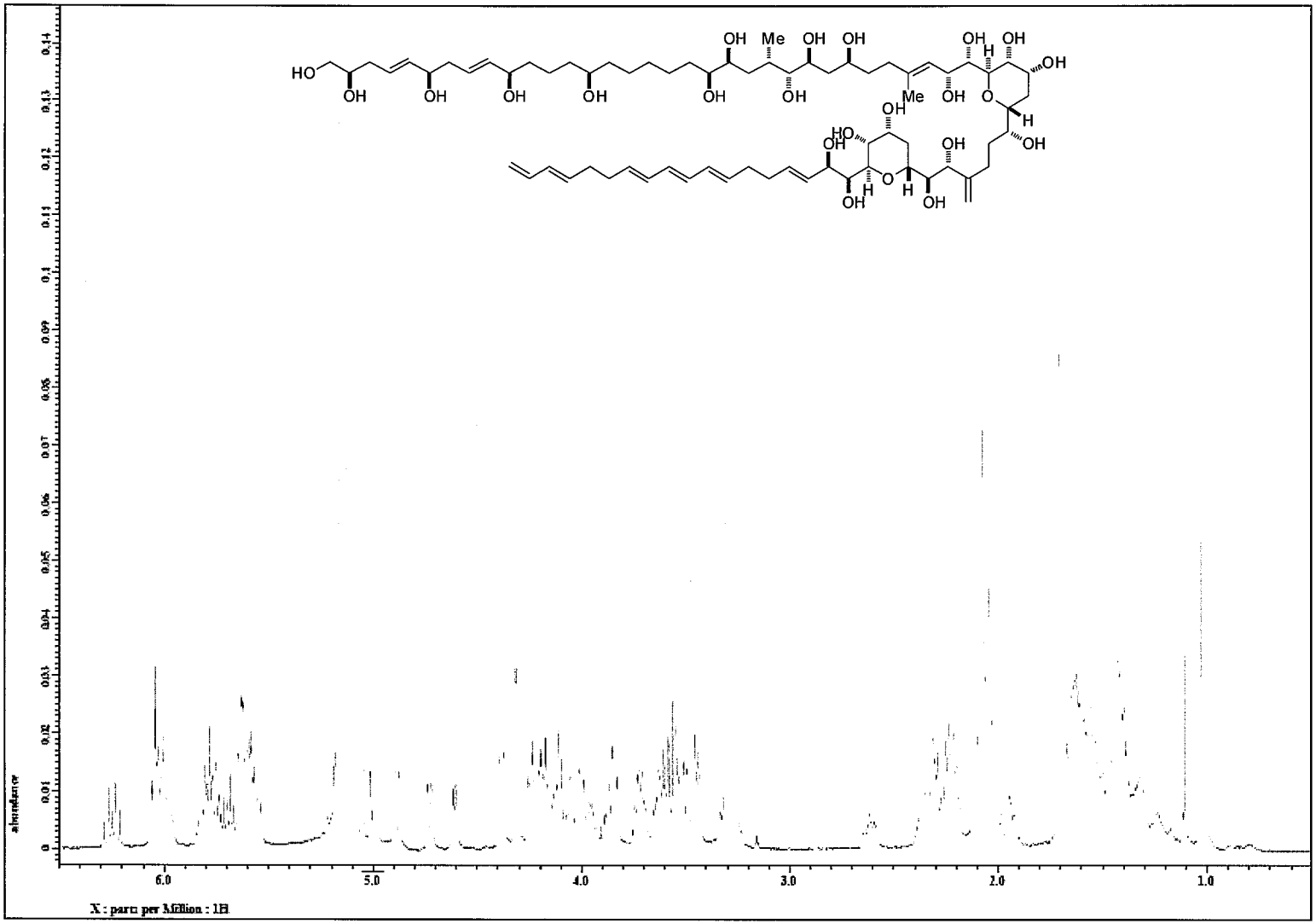

Figure S-1. ^{1}H NMR spectrum of AM3 in CD_3OD.

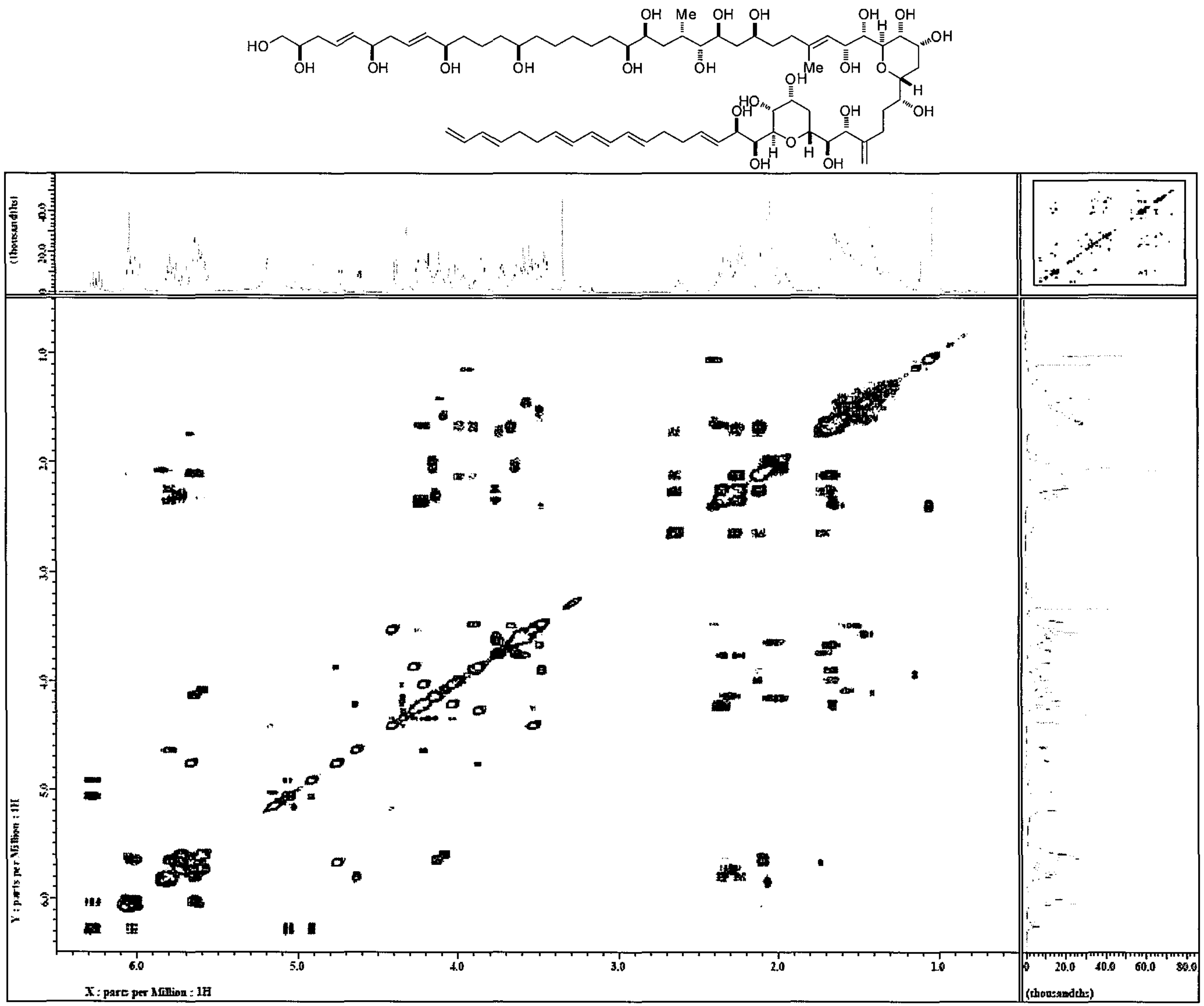

Figure S-2. DQF-COSY spectrum of AM3 in CD_3OD.

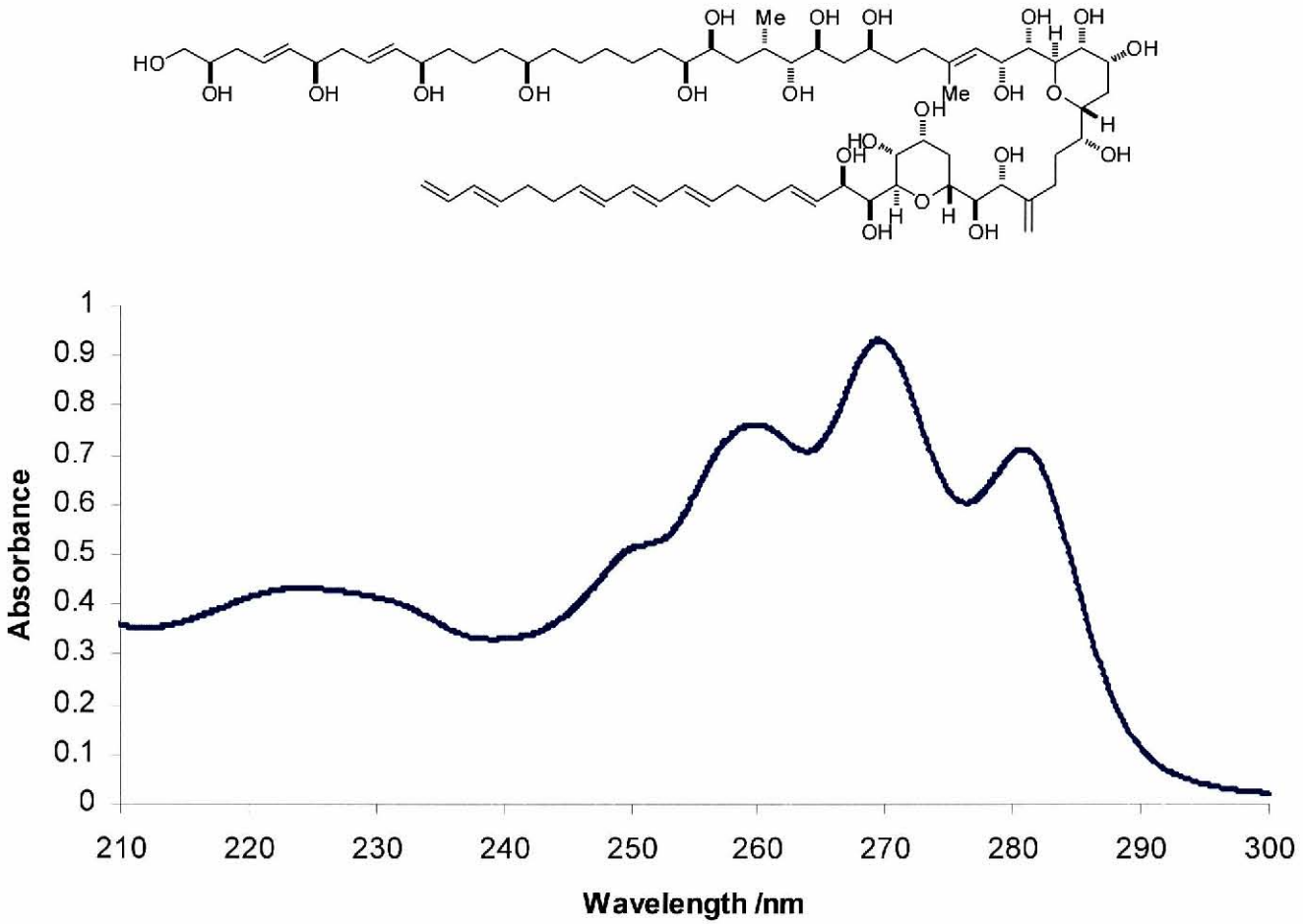

Figure S-3. UV spectrum of AM3 in MeOH.

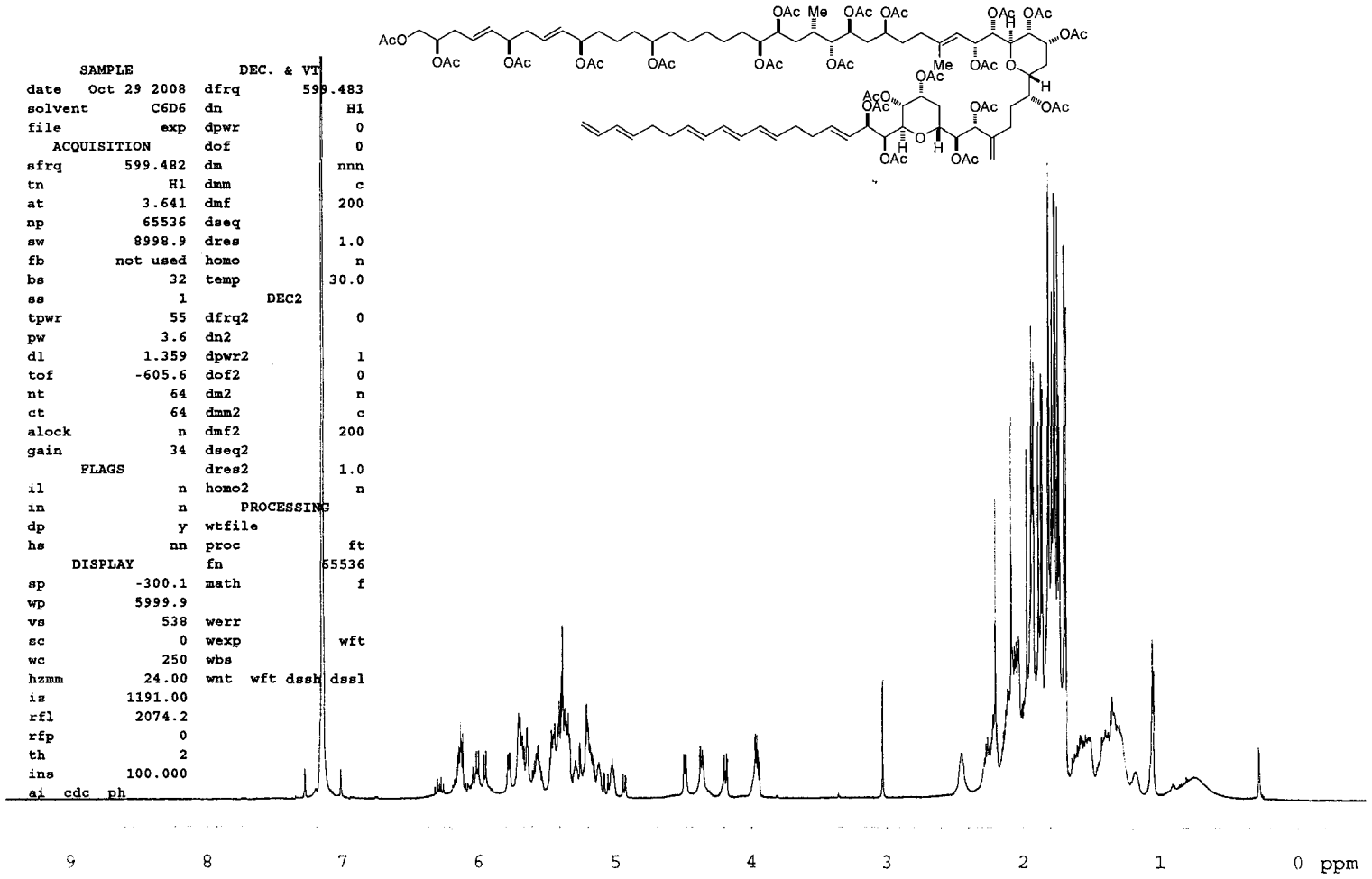

Figure S-4. 1H NMR spectrum of peracetyl AM3 in C_6D_6.

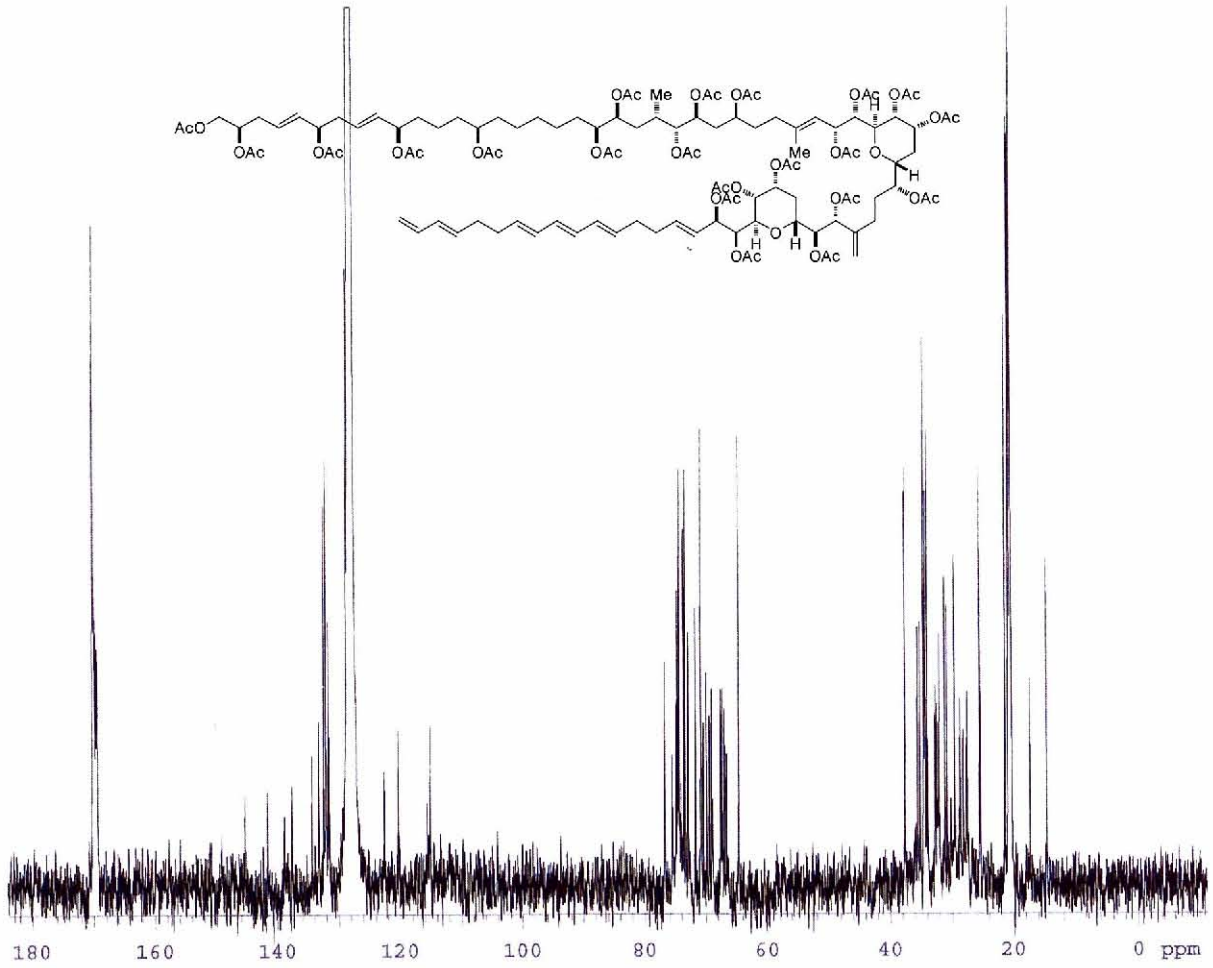

Figure S-5. ^{13}C NMR spectrum of peracetyl AM3 in C_6D_6.

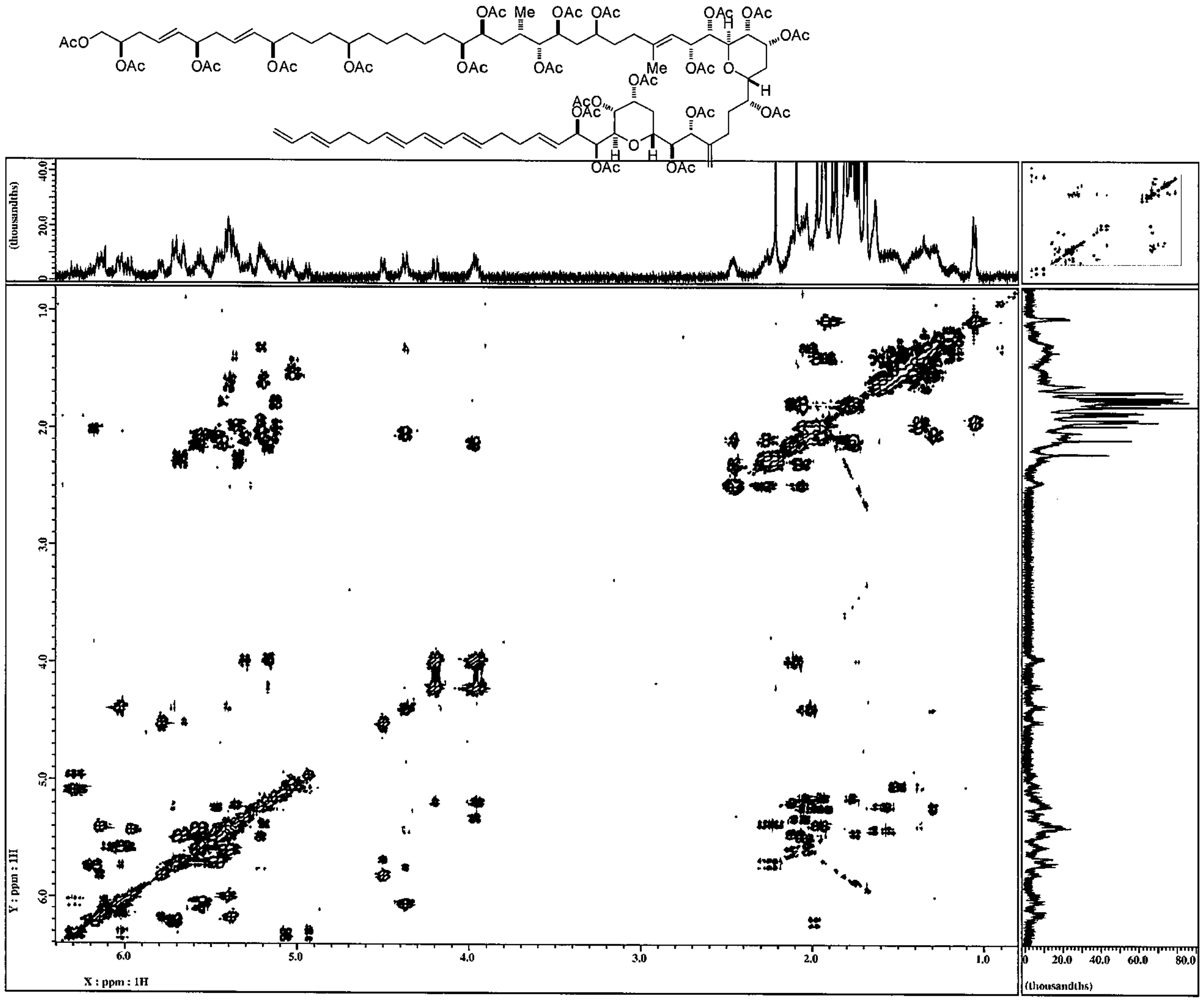

Figure S-6. DQF-COSY spectrum of peracetyl AM3 in C_6D_6.

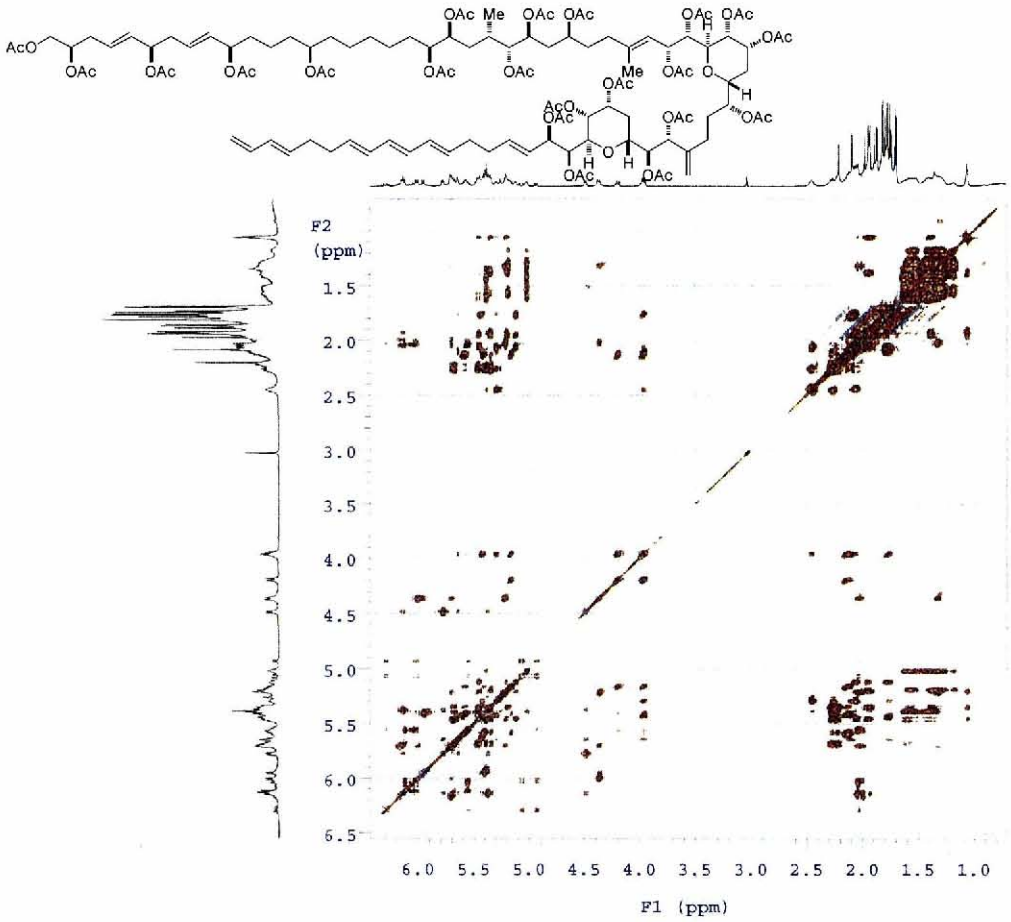

Figure S-7. TOCSY spectrum of peracetyl AM3 in C_6D_6.

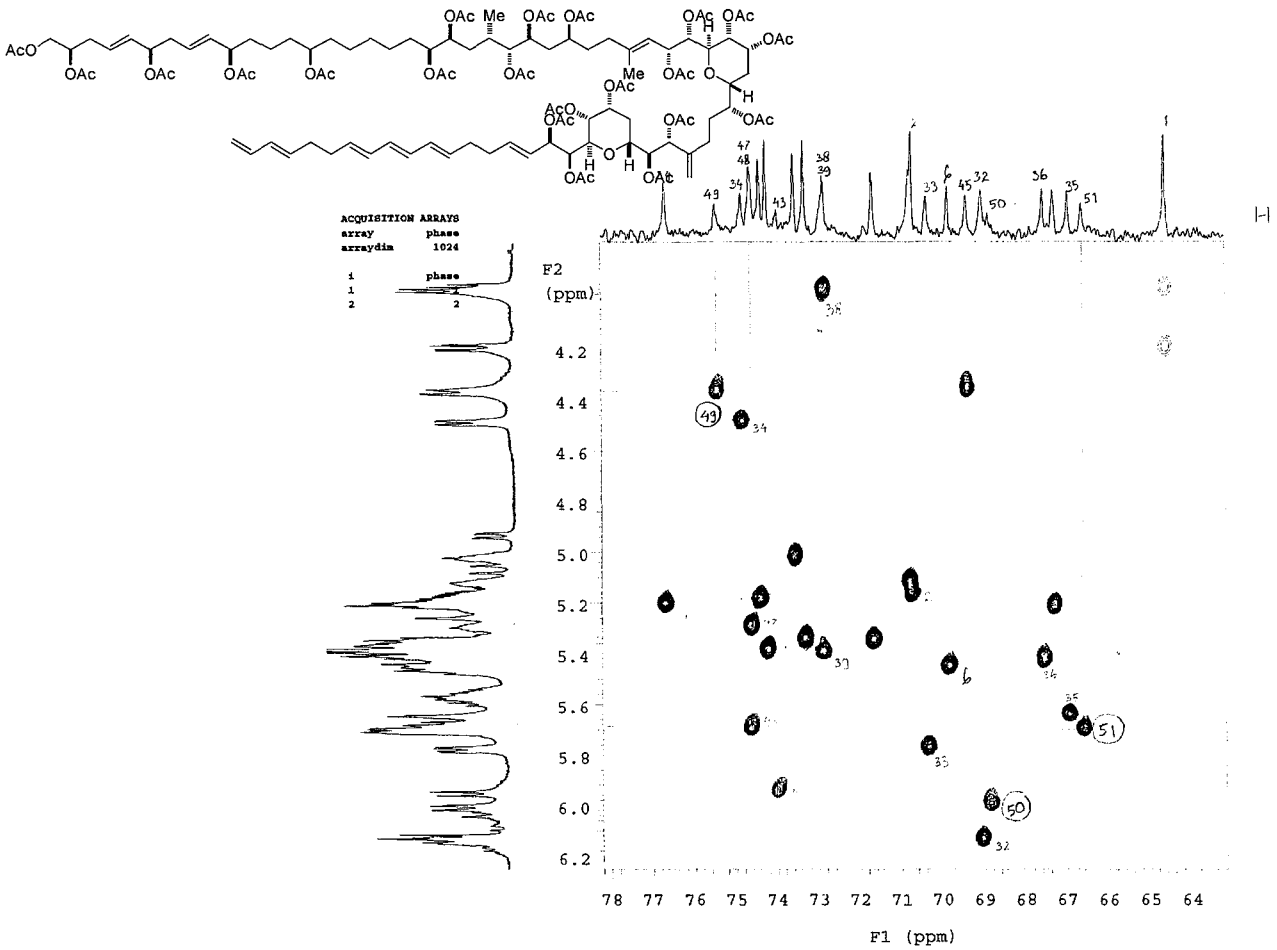

Figure S-8. Expansion of HSQC spectrum of peracetyl AM3 in C_6D_6.

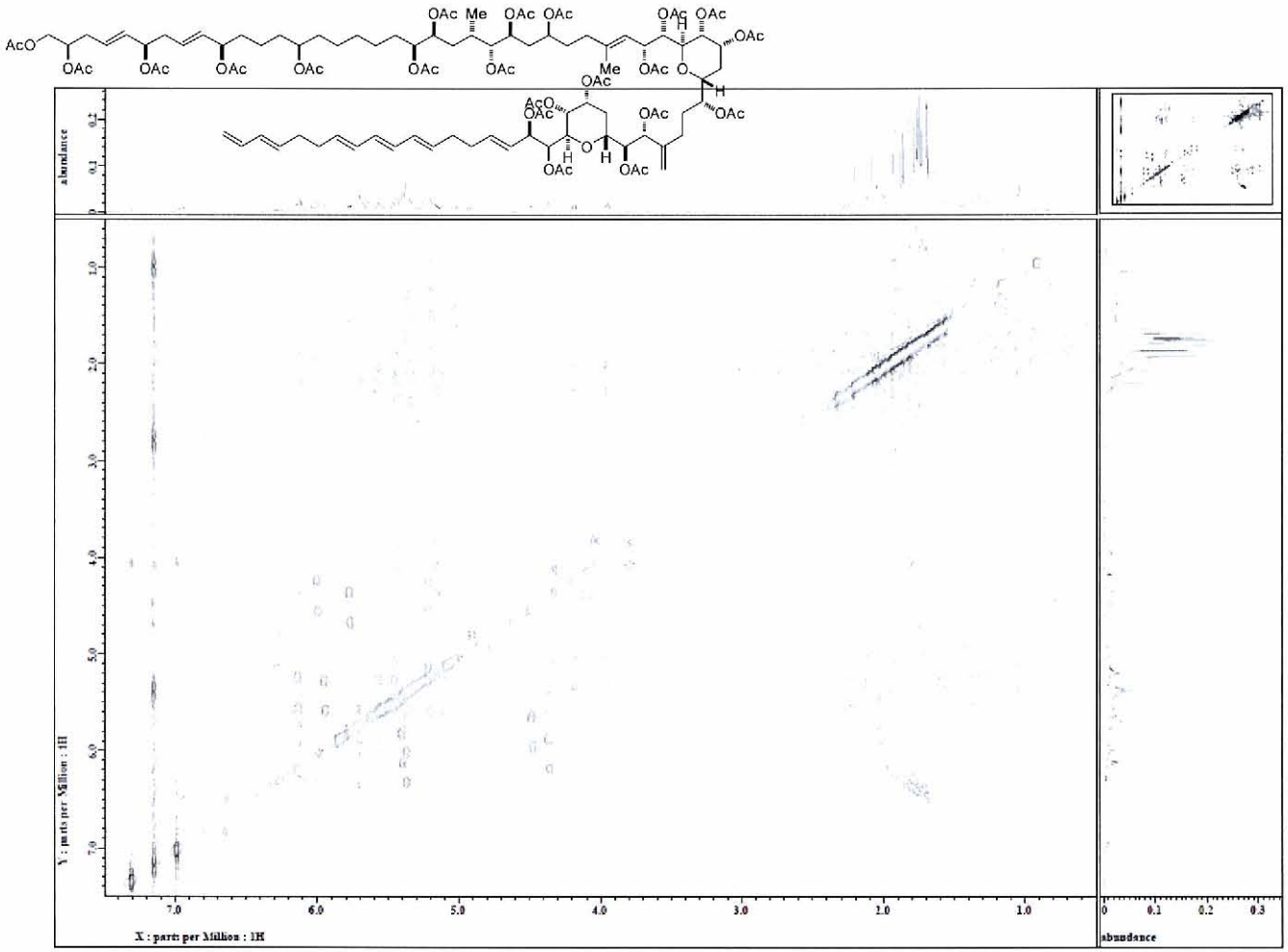

Figure S-9. HETLOC spectrum of peracetyl AM3 in C_6D_6.

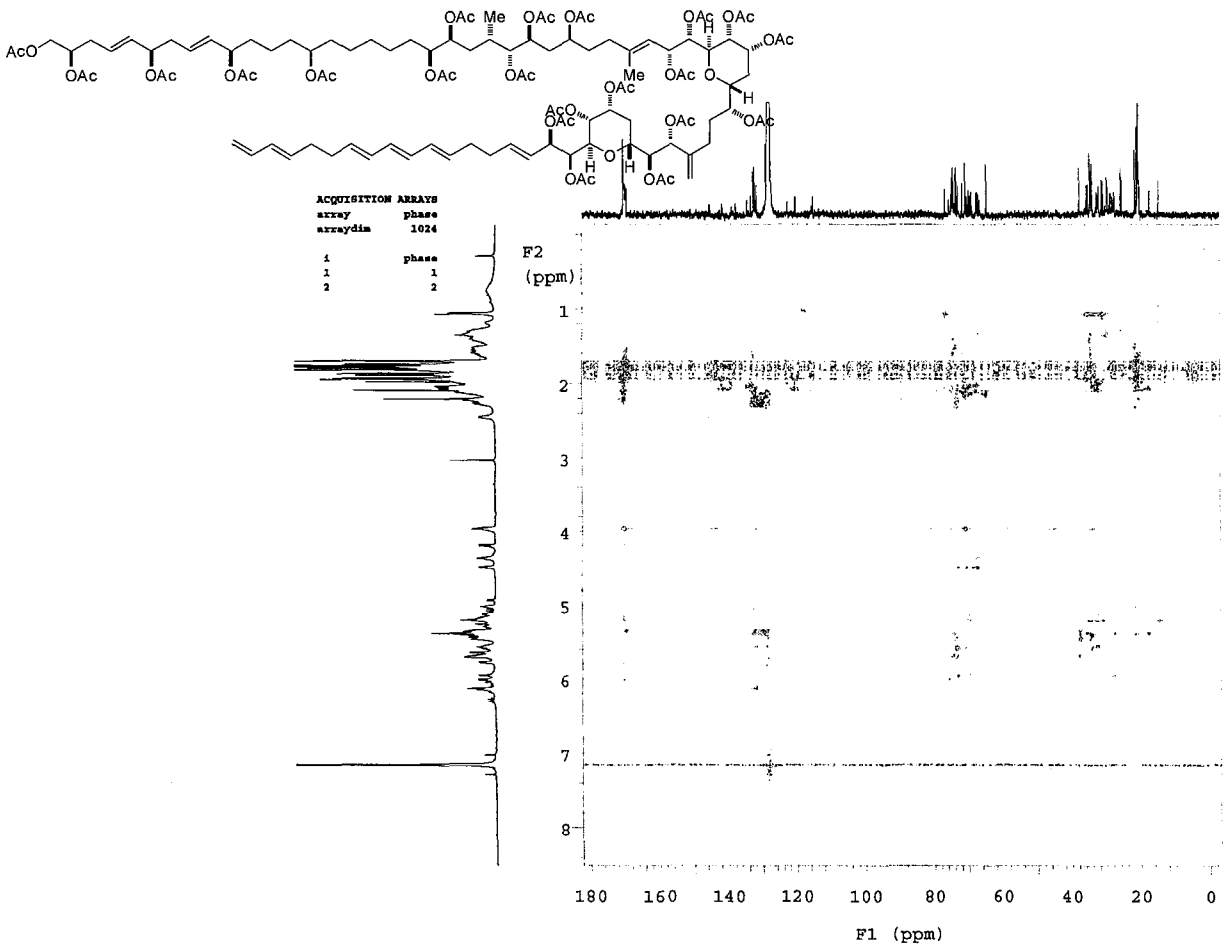

Figure S-10. HMBC spectrum of peracetyl AM3 in C_6D_6.

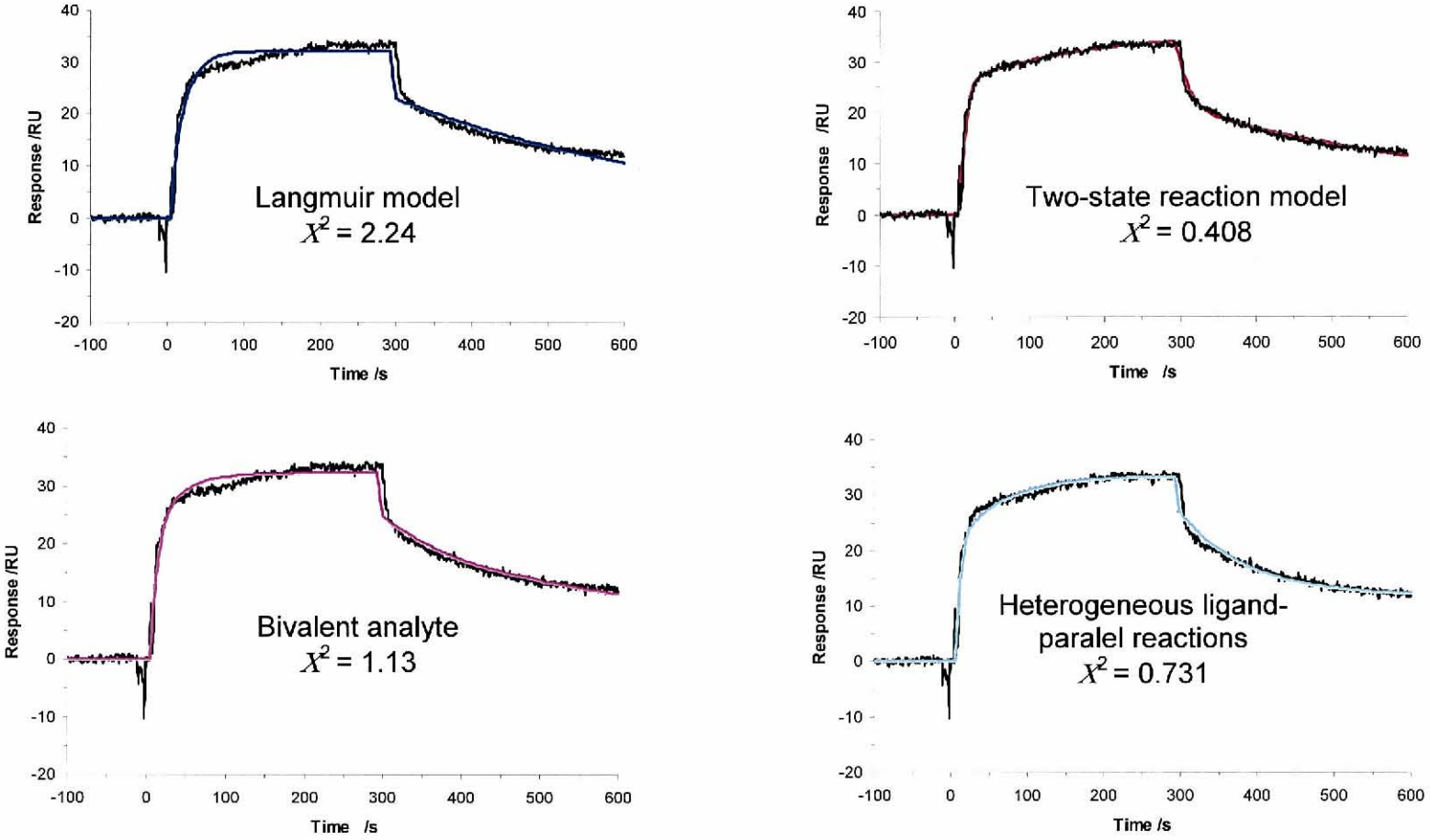

Figure S-11. Sensorgram for interaction of 10 μM AM3 and 5% cholesterol-containing POPC (black curves) and fitting curves to various reaction model (color curves). Reaction models and their X^2 values are shown.

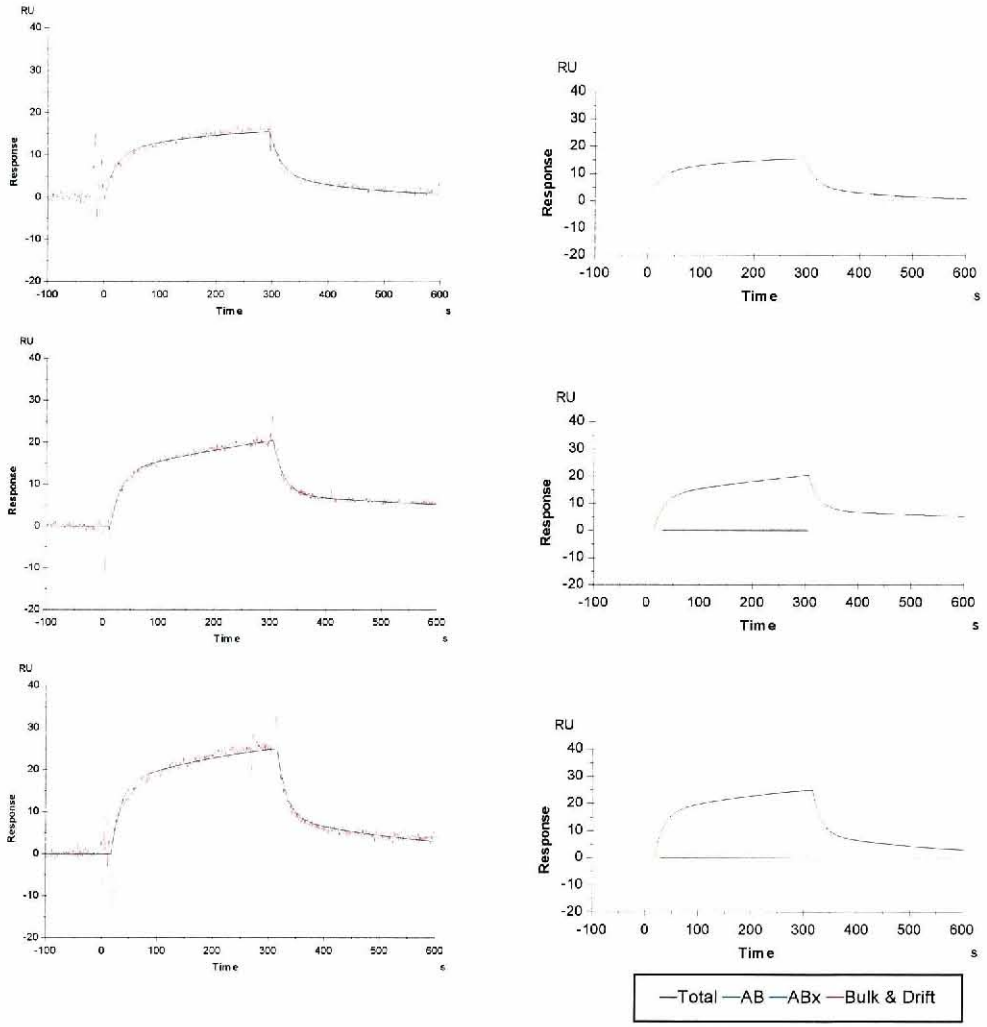

Figure S-12. SPR sensorgrams and their components for interaction of 10 μM AM3 to cholesterol-free POPC. The sensorgrams were fitted to the two-state reaction model (smooth black curves).

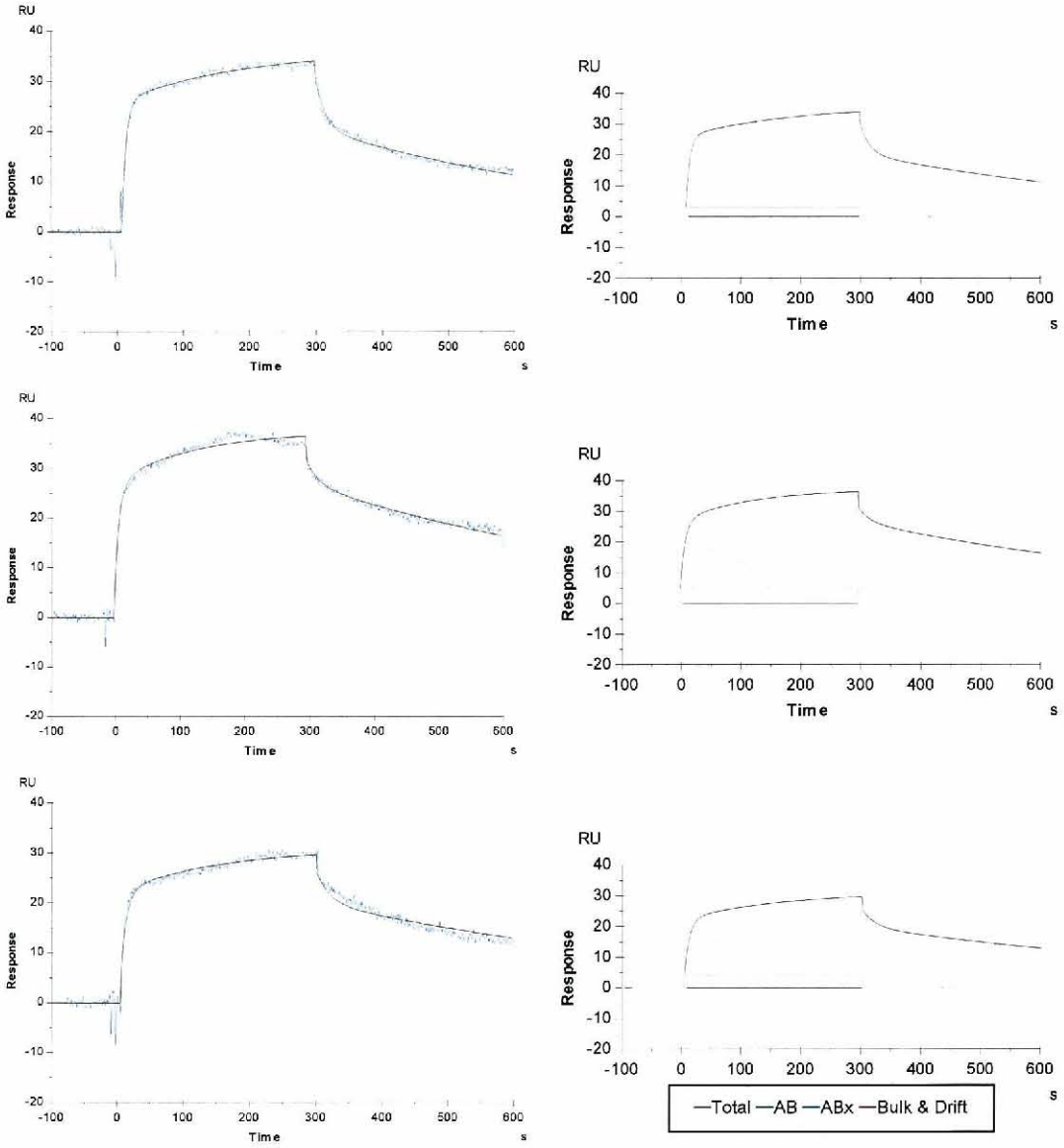

Figure S-13. SPR sensorgrams and their components for interaction of 10 μM AM3 to 5% cholesterol-containing POPC. The sensorgrams were fitted to the two-state reaction model (smooth black curves).

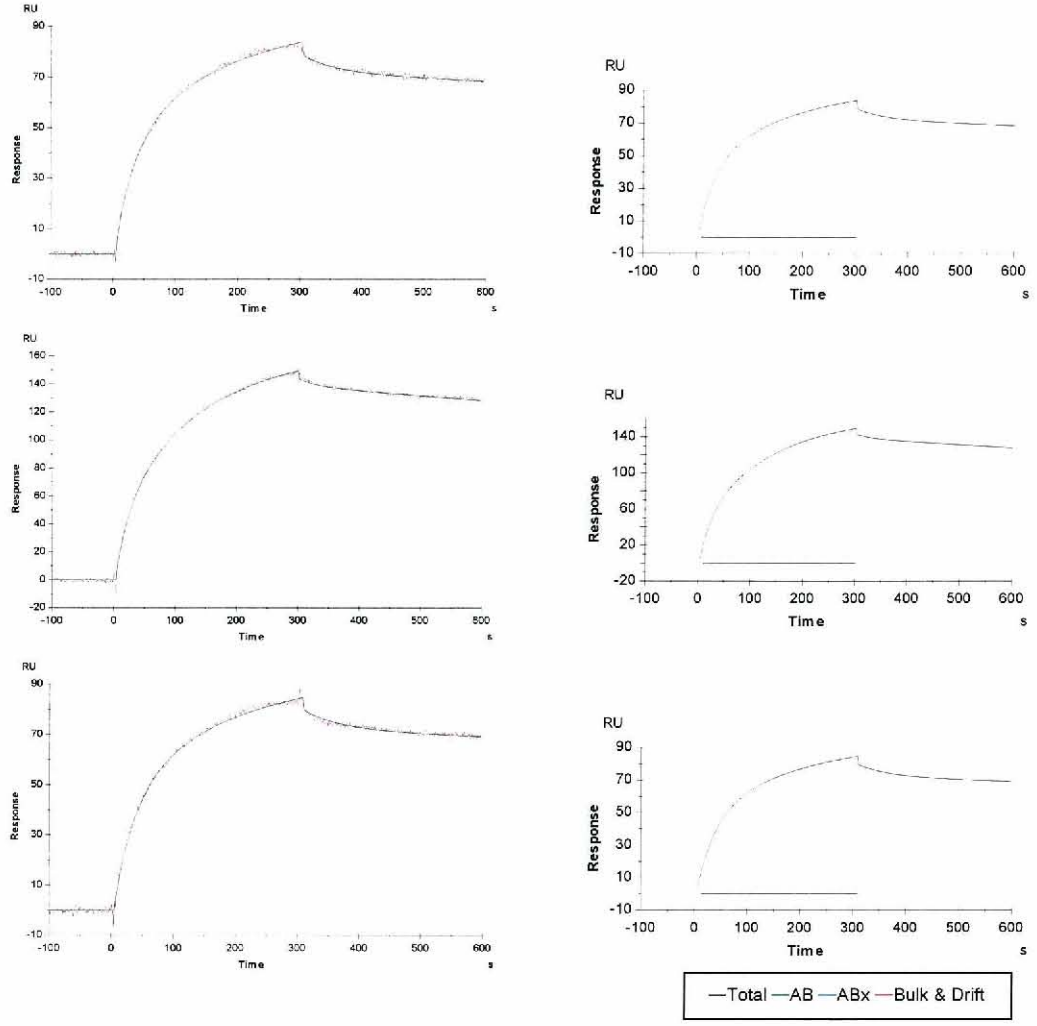

Figure S-14. SPR sensorgrams and their components for interaction of 10 μM AM3 to 5% ergosterol-containing POPC. The sensorgrams were fitted to the two-state reaction model (smooth black curves).

Table S-1. Kinetic and affinity constants of interaction between 10 μM AM3 and cholesterol-free POPC.

	k_{a1} (/Ms)	k_{d1} (x10^{-2}/s)	k_{a2} (x10^{-3}/s)	k_{d2} (x10^{-3}/s)	K_{A1} (x10^{2}/M)	K_{A2}	K_A (x10^{2}/M)
1	54.6	4.83	3.01	6.57	11.3	0.460	5.18
2	35.6	4.93	2.22	1.32	7.22	1.68	12.1
3	49.3	5.80	2.62	3.99	8.50	0.660	5.58
Mean	46.5	5.19	2.62	3.96	9.01	0.930	7.64
SEM	5.66	0.310	0.230	1.52	1.21	0.380	2.26

Table S-2. Kinetic and affinity constants of interaction between 10 μM AM3 and 5% cholesterol-containing POPC.

	k_{a1} (x10^{3}/Ms)	k_{d1} (x10^{-2}/s)	k_{a2} (x10^{-3}/s)	k_{d2} (x10^{-3}/s)	K_{A1} (x10^{3}/M)	K_{A2}	K_A (x10^{3}/M)
1	9.67	6.04	5.62	2.19	160	2.57	411
2	8.31	4.17	10.0	2.01	199	4.98	991
3	7.60	4.20	7.32	1.74	181	4.21	761
Mean	8.53	4.80	7.65	1.98	180	3.92	721
SEM	0.607	0.620	1.27	0.130	11.3	0.710	169

Table S-3. Kinetic and affinity constants of interaction between 10 μM AM3 and 5% ergosterol-containing POPC.

	k_{a1} (x10^{3}/Ms)	k_{d1} (x10^{-2}/s)	k_{a2} (x10^{-3}/s)	k_{d2} (x10^{-3}/s)	K_{A1} (x10^{4}/M)	K_{A2}	K_A (x10^{4}/M)
1	1.64	1.03	9.79	0.390	15.9	25.4	404
2	1.72	1.80	18.8	0.560	9.56	33.8	323
3	1.57	0.906	8.66	0.320	17.3	26.7	463
Mean	1.64	1.25	12.42	0.420	14.3	28.6	397
SEM	0.043	0.280	3.21	0.0700	2.39	2.62	40.6

PUBLICATIONS

List of publications related to this thesis:

Main papers:

1. Sterol effect on interaction between amphidinol 3 and liposomal membrane as evidenced by surface plasmon resonance.
   Swasono, R. T.; Mouri, R.; Morsy, N.; Matsumori, N.; Oishi, T.; Murata, M. *Bioorg. Med. Chem. Lett.*, **2010**, *20*, 2215-2218.

2 Structural reevaluations of amphidinol 3, a potent antifungal compound from dinoflagellate
   Swasono, R.T., Kanemoto, M.; Matsumori, N.; Oishi, T.; Murata, M. *Heterocycles*, 2010 in Press

Reference paper:

1. Combinatorial synthesis of the 1,5-polyol system based on cross metathesis: Structure revision of amphidinol 3.
   Oishi, T.; Kanemoto, M.; Swasono, R.; Matsumori, N.; Murata, M. *Org. Lett.*, **2008**, *10*, 5203-5206.

Bioorganic & Medicinal Chemistry Letters 20 (2010) 2215–2218

Contents lists available at ScienceDirect

Bioorganic & Medicinal Chemistry Letters

journal homepage: www.elsevier.com/locate/bmcl

Sterol effect on interaction between amphidinol 3 and liposomal membrane as evidenced by surface plasmon resonance

Respati T. Swasono, Ryota Mouri, Nagy Morsy †, Nobuaki Matsumori, Tohru Oishi, Michio Murata *

Department of Chemistry, Graduate School of Science, Osaka University, 1-1 Machikaneyama, Toyonaka, Osaka 560-0043, Japan

ARTICLE INFO

Article history:
Received 23 December 2009
Revised 4 February 2010
Accepted 5 February 2010
Available online 10 February 2010

Keywords:
Amphidinol
Surface plasmon resonance
Cholesterol
Ergosterol

ABSTRACT

The affinity of amphidinol 3 (AM3) to phospholipid membranes in the presence and absence of sterol was examined by surface plasmon resonance (SPR) experiments. The results showed that AM3 has 1000 and 5300 times higher affinity for cholesterol- and ergosterol-containing liposomes, respectively, than those without sterol. The two-state reaction model well reproduced the sensor grams, which indicated that the interaction is composed of two steps, which correspond to binding to the membrane and internalization to form stable complexes.

A family of amphidinols (AMs) have been isolated as a potent antifungal agent from the marine dinoflagellates of genus *Amphidinium*.[1–7] AM homologues including luteophanols,[8–10] lingshuiols,[11] karatungiols,[12] amphezonol A[13] and carteraol E[14] have common structural features comprising a linear polyhydroxyl moiety, tetrahydropyran rings and an alkenyl chain of 14 or 16 carbon atoms. Unlike other natural or synthetic antifungal compounds, AMs lack nitrogenous polycycles or macrocycles in their structures. These unique features make AMs an interesting model to gain a better understanding of the molecular mechanism of antifungal action.

Since amphidinol 1 (AM1) was first isolated in 1991, fifteen homologues have been reported to date.[1–7] Among those, AM3 significantly exceeds other homologues in the antifungal activity. The absolute configuration of AM3 (Fig. 1) was determined by extensive NMR experiments such as the *J*-based configuration analysis (JBCA) method, modified Mosher method, and HPLC analysis of the degradation products.[15] Recently, we have revised the stereochemistry of C2 of AM3 to be *R* by comparing synthetic specimens with a fragment of AM3 and by GC–MS.[16]

We have previously[3,4,17] revealed that AMs increase membrane permeability by directly interacting with lipid bilayers. The distinct partition coefficients (K'_m values) to multilamellar vesicle (MLV) membrane were examined by HPLC quantification for AMs[17]; the K'_m values of AM2, AM3, and AM4 in eggPC preparations were 0.77×10^3, 22.2×10^3 and 2.24×10^3, respectively. The order in K'_m values agrees well with those of the membrane-permeabilizing and antifungal activities, where AM3 with a butadiene terminus binds most efficiently to PC membrane.

Permeabilization of the phospholipid membrane by AMs is thought to be responsible for their potent antifungal activity. Moreover, AMs permeabilize the membrane more efficiently in the presence of sterol.[3,4,17–19] The size of the pore/lesion formed in the erythrocyte membrane was estimated to be 2.0–2.9 nm in diameter which was significantly larger than those of other antifungals such as amphotericin B (AmB).[18] Structure–activity relationship[7] using naturally occurring AMs and chemically modified AM derivatives has showed that the polyene and polyhydroxy moieties play respective roles in binding to the lipid bilayer membrane and in forming an ion-permeable pore/lesion across the membrane. In order to gain insight into the membrane-bound structure of AMs, conformational analysis of AM3 has been carried out on the basis of high-resolution ^{1}H NMR data measured for SDS micelles[17] and isotropic bicelles.[20] These experiments have revealed that the central region of AM3 takes a hairpin conformation while the hydrophobic polyene chain is immersed in the hydrophobic interior. The efficacies of AM2 and AM3 have been measured by fluorescent-dye leakage experiments for POPC liposomes with various cholesterol and ergosterol contents, indicating that, with increasing concentrations of the sterol, the membrane permeability are increased significantly.[19] Moreover, cholesterol and ergosterol have a similar efficacy in enhancement of the AM activities.

By using surface plasmon resonance (SPR) techniques, which are shown to be useful for membrane-bound peptides and drugs,[21–23] we successfully evaluated interaction between AmB and lipid bilayers.[24] To examine more closely the affinity of AM3 to membranes

* Corresponding author.
E-mail address: murata@ch.wani.osaka-u.ac.jp (M. Murata).
† Present address: Department of Chemistry of Natural Compounds, National Research Centre, Dokki, Cairo, Egypt.

0960-894X/$ - see front matter © 2010 Elsevier Ltd. All rights reserved.
doi:10.1016/j.bmcl.2010.02.025

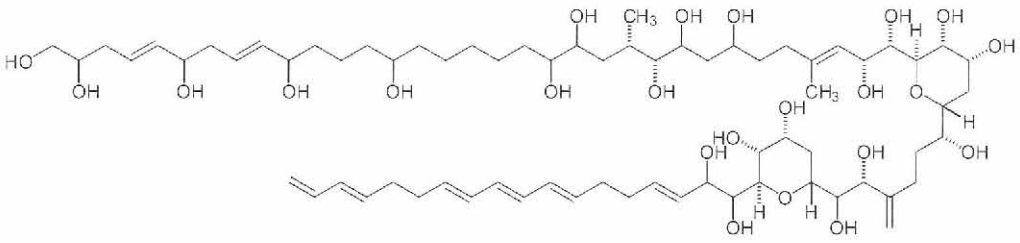

Figure 1. Amphidinol 3(AM3).

with or without sterol in this study, we utilized the same dodecylamine-modified SPR sensor chip[24] to carry out kinetic analysis for AM3 binding to sterol-containing and sterol-free palmitoyloleoylphosphatidylcholine (POPC) liposomes.

Amphidinol 3 was isolated from the marine dinoflagellate *Amphidinium klebsii* (deposited in National Institute for Environmental Studies as NIES 613) as described previously.[5] Briefly, the unialgal culture was grown in artificial seawater enriched with ES-1 supplement at 25 °C under illumination of a 16–8 light–dark photocycle for 4 weeks. Harvested cells were extracted and treated with an ODS open column and HPLC. Liposomes used in the experiments were prepared by evaporating sterol-containing or sterol-free POPC solution to form dry film, which was then suspended in PBS buffer, frozen and thawed, vortexed and finally extruded through polycarbonated membrane to predominantly yield large unilamellar vesicles with 100 nm in diameter. Details of experimental methods are described in Supplementary data.[28]

The CM5 chip of SPR was modified with dodecylamine to prepare a hydrophobic surface. One of two flow cell lanes in the CM5 chip was modified with dodecylamine, while the other lane remained intact for the use of a control run.[28] To the modified lane, POPC and POPC/sterol liposomes were stably captured. When the liposomes at the phospholipid concentration of 0.5 mM were introduced, the SPR response due to liposome association reached about 10,000 RU (Fig. 2). The sensor chip was tolerant of NaOH treatments (50 mM), and the amount of captured liposomes was essentially unchanged by repetitive washing. For kinetic analysis, the binding of AM3 to liposome membranes was standardized as an amount of AM3 in RU bound to the amount of lipids equivalent to 10,000 RU.

Detection of AM3 affinity was carried out in PBS buffer (pH 7.4) as running and injection media. AM3 dissolved in PBS buffer was then passed on the sensor chip treated with liposomes. The SPR response increased immediately after injection due to interaction between AM3 in the sample solution and POPC liposomes immobilized on the surface of the sensor chip. To evaluate AM3 binding to sterol-containing or sterol-free liposomes, the SPR response in the control lane was subtracted from that in the liposome-captured lane.[28] AM3 firmly interacted with the sensor-chip surface and a small portion of AM3 was hardly washed out during regeneration. To eliminate the effect of the remaining AM3, we always used a newly prepared sensor chip.

Typical sensorgrams for interaction of 10 μM AM3 with 5% cholesterol-containing POPC liposomes and sterol-free ones were shown in Figure 3. The RU changes upon AM3 addition are largely responsible for the drug-liposome interaction. As is evident from Figure 3, AM3 bound preferentially to cholesterol-containing liposomes. We next carried out kinetic analysis of the drug's binding to membrane using BIA evaluation software for the reaction models including Langmuir binding, bivalent analyte, and two-state reaction models. Among those, the two-state reaction model best reproduced the experimental sensorgrams as depicted in Figure 3.

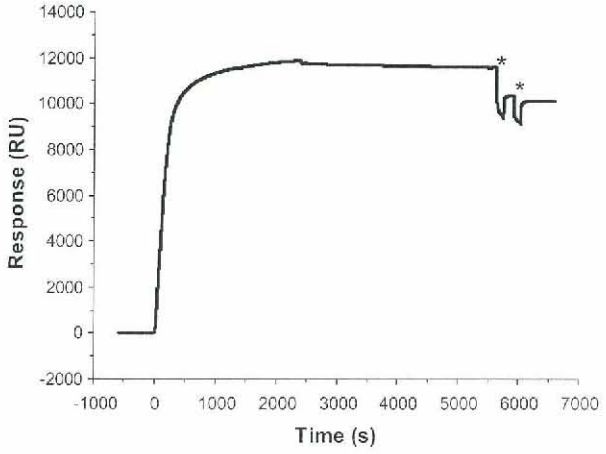

Figure 2. Immobilization of 0.5 mM POPC liposome (80 μL) on dodecylamine-modified CM5 sensor chip. Liposome-bound surface was washed twice with 50 mM NaOH for 2 min at 20 μL/min (denoted by asterisks).

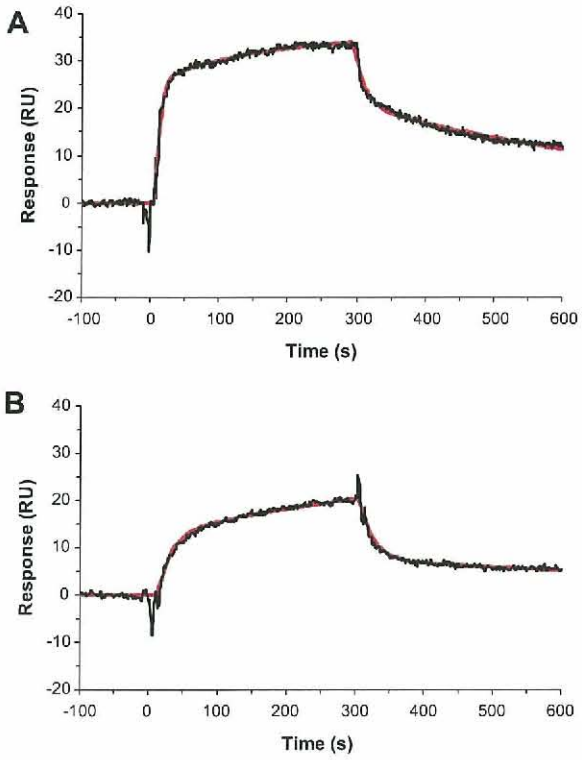

Figure 3. Typical sensorgrams for interaction of 10 μM AM3 to 5% cholesterol-containing POPC (A) and to sterol-free POPC (B). The sensorgrams were fitted to the two-state reaction model (smooth red lines).

The two-state reaction model indicates that the interaction is composed of subsequent two steps; the first step is partition of AM3 to the POPC phase of liposomes, and the second step probably corresponds to the internalization of AM3 to the liposome interior to form more stable complexes.

Then, we estimated the kinetic parameters of AM3 binding to the membranes based on the two-state reaction model[23] as presented in Table 1. In this model, k_{a1} and k_{d1} are association and dissociation constants of analyte to membrane surface in the first step while k_{a2} and k_{d2} are association and dissociation rates for the second step. Then K_{A1}, K_{A2} and K_A represent the affinity constants for the first step, the second step and overall equilibrium, respectively, and were calculated from the association and dissociation rate constants[29] (see Supplementary data for details).

As depicted in Figure 4, sterols have the most striking effects on the initial process of AM3 binding to membrane as revealed by k_{a1}. The k_{a1} value of AM3 in 5% cholesterol- and ergosterol-containing membranes exceeds that in the sterol-free membranes by about 180- and 35-fold, respectively. This suggests that sterols play a functional role in capturing AM3 on the membrane surface. The resultant K_A value of AM3 in 5% cholesterol-containing membrane exceeds that in the sterol-free one by almost 1000-fold. The binding step to membrane is, as aforementioned, one of important features for the biological activity.[17] Although effect of ergosterol on the initial binding process is not as dramatic as that of cholesterol, ergosterol stabilizes formation of complex in the second step. As a result, the K_A value of AM3 in 5% ergosterol-containing membrane exceeds that in the sterol-free one by about 5000-fold.

The binding of AM3 to the POPC liposomal membrane is very strong. It was therefore extremely difficult to regenerate the membrane once AM3 bound to it. We had to prepare the new liposome surface on the sensor chip each time to replicate the experiments. As a result, similar membrane conditions were not attainable for each run, which caused relatively large standard error means in Table 1. Nonetheless, large differences between kinetic constants obtained in the presence and absence of sterols clearly indicate that sterols markedly enhance the membrane-binding of AM3.

Table 1
Kinetic and affinity constants for interactions of AM3 (10 μM) with POPC liposomes in the presence and absence of 5% sterol estimated from the two-state reaction model

Kinetic value	POPC + Erg	POPC + Cho	POPC
k_{a1} ($\times 10^3$/Ms)	1.64 ± 0.43	8.53 ± 0.61	0.0465 ± 0.0057
k_{d1} ($\times 10^{-3}$/s)	12.5 ± 2.8	48.0 ± 6.2	51.9 ± 3.1
k_{a2} ($\times 10^{-3}$/s)	12.4 ± 3.2	7.65 ± 1.27	2.62 ± 0.23
k_{d2} ($\times 10^{-3}$/s)	0.420 ± 0.070	1.98 ± 0.13	3.96 ± 1.52
K_{A1} ($\times 10^3$/M)	143 ± 23	180 ± 11	0.901 ± 0.121
K_{A2}	28.6 ± 2.62	3.92 ± 0.71	0.930 ± 0.380
K_A ($\times 10^3$/M)	3970 ± 410	721 ± 169	0.764 ± 0.226

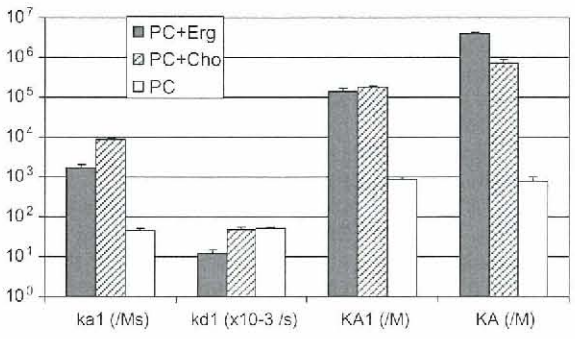

Figure 4. Comparison kinetic data in logarithmic scale for AM3 binding to ergosterol-, cholesterol-containing and sterol-free POPC liposomes.

These effects of cholesterol, mammalian sterol, and ergosterol, fungal sterol,[25] may account for the respective potent cytotoxicity[6,26] and antifungal activities.[1–7] Interestingly, AMs lack anti-bacterial activity, which is probably due to the absence of sterols in bacterial membranes. Moreover, AM3 showed higher affinity to ergosterol membrane than cholesterol one, particularly, in dissociation process; K_{A2} of the former was significantly larger than those of the latter. These observations indicate that AM3 forms more stable complex in the presence of ergosterol and may provide a clue for developing a new antifungal drug.

In conclusion, we disclosed that sterols markedly enhance affinity of AM3 to phospholipid membrane. The present results support previous findings in fluorescent-dye leakage experiments;[19] the potentiation of the activity of AM3 by sterol is prominent even at 0.5% (w/w) to the lipid, which ruled out the possibility that alteration of the membrane physical properties elicited by sterols[27] was responsible for this effect.[19] The significantly larger K_{A2} for POPC-ergosterol membrane (Table 1) further supports the notion that sterols, particularly ergosterol, not only accelerate partition of AM3 to membrane but also stabilize the membrane-bound complex formed by AM3, suggesting the direct interaction between AM3 and sterols in the complex. NMR-based investigations on this interaction in membrane model systems are now in progress in our laboratory.

Acknowledgements

This work was supported by Grants-in-Aid for Scientific Research (S) (No. 18101010), for Priority Area (A) (No. 16073211), and for Young Scientists (A) (No. 17681027) from MEXT, Japan as well as by The Naito Foundation. A Monbukagakusho scholarship to R.T.S. is also greatly acknowledged.

Supplementary data

Supplementary data associated with this article can be found, in the online version, at doi:10.1016/j.bmcl.2010.02.025.

References and notes

1. Satake, M.; Murata, M.; Yasumoto, T.; Fujita, T.; Naoki, H. *J. Am. Chem. Soc.* **1991**, *113*, 9859.
2. Paul, G. K.; Matsumori, N.; Murata, M.; Tachibana, K. *Tetrahedron Lett.* **1995**, *36*, 6279.
3. Paul, G. K.; Matsumori, N.; Konoki, K.; Sasaki, M.; Murata, M.; Tachibana, K. In *Harmful and Toxic Algal Blooms*, Sendai, July, 1995; Intergovermental Oceanographic Commission of UNESCO: Sendai, 1995; 503.
4. Paul, G. K.; Matsumori, N.; Konoki, K.; Murata, M.; Tachibana, K. *J. Mar. Biotechnol.* **1997**, *5*, 124.
5. Morsy, N.; Matsuoka, S.; Houdai, T.; Matsumori, N.; Adachi, S.; Murata, M.; Iwashita, T.; Fujita, T. *Tetrahedron* **2005**, *61*, 8606.
6. Echigoya, R.; Rhodes, L.; Oshima, Y.; Satake, M. *Harmful Algae* **2005**, *4*, 383.
7. Morsy, N.; Houdai, T.; Matsuoka, S.; Matsumori, N.; Adachi, S.; Oishi, T.; Murata, M.; Iwashita, T.; Fujita, T. *Bioorg. Med. Chem.* **2006**, *14*, 6548.
8. Doi, Y.; Ishibashi, M.; Nakamichi, H.; Kosaka, T.; Ishikawa, T.; Kobayashi, J. *J. Org. Chem.* **1997**, *62*, 3820.
9. Kubota, T.; Tsuda, M.; Doi, Y.; Takahashi, A.; Nakamichi, H.; Ishibashi, M.; Fukushi, E.; Kawabata, J.; Kobayashi, J. *Tetrahedron* **1998**, *54*, 14455.
10. Kubota, T.; Takahashi, A.; Tsuda, M.; Kobayashi, J. *Mar. Drugs* **2005**, *3*, 113.
11. Huang, X.-C.; Zhao, D.; Guo, Y.-W.; Wu, H.-M.; Trivellone, E.; Cimino, G. *Tetrahedron Lett.* **2004**, *45*, 5501.
12. Washida, K.; Koyama, T.; Yamada, K.; Kita, M.; Uemura, D. *Tetrahedron Lett.* **2006**, *47*, 2521.
13. Kubota, T.; Sakuma, Y.; Shimbo, K.; Tsuda, M.; Nakano, M.; Uozumi, Y.; Kobayashi, J. *Tetrahedron Lett.* **2006**, *47*, 4369.
14. Huang, S.-J.; Kuo, C.-M.; Lin, Y.-C.; Chen, Y.-M.; Lu, C.-K. *Tetrahedron Lett.* **2009**, *50*, 2512.
15. Murata, M.; Matsuoka, S.; Matsumori, N.; Paul, G. K.; Tachibana, K. *J. Am. Chem. Soc.* **1999**, *121*, 870.
16. Oishi, T.; Kanemoto, M.; Swasono, R.; Matsumori, N.; Murata, M. *Org. Lett.* **2008**, *10*, 5203.
17. Houdai, T.; Matsuoka, S.; Morsy, N.; Matsumori, N.; Satake, M.; Murata, M. *Tetrahedron* **2005**, *61*, 2795.

18. Houdai, T.; Matsuoka, S.; Matsumori, N.; Murata, M. *Biochim. Biophys. Acta* **2004**, *1667*, 91.
19. Morsy, N.; Houdai, T.; Konoki, K.; Matsumori, N.; Oishi, T.; Murata, M. *Bioorg. Med. Chem.* **2008**, *16*, 3084.
20. Houdai, T.; Matsumori, N.; Murata, M. *Org. Lett.* **2008**, *10*, 4191.
21. Abdiche, Y. N.; Myszka, D. G. *Anal. Biochem.* **2004**, *328*, 233.
22. Papo, N.; Shai, Y. *Biochemistry* **2003**, *42*, 458.
23. Mozsolits, H.; Wirth, H. J.; Werkmeister, J.; Aguilar, M. I. *Biochim. Biophys. Acta* **2001**, *1512*, 64.
24. Mouri, R.; Konoki, K.; Matsuoka, S.; Oishi, T.; Murata, M. *Biochemistry* **2008**, *47*, 7807.
25. Bolard, J. *Biochim. Biophys. Acta* **1986**, *864*, 257.
26. Qi, X.-M.; Yu, B.; Huang, X.-C.; Guo, Y.-W.; Zhai, Q.; Jin, R. *Toxicon* **2007**, *50*, 278.
27. Alvarez, F. J.; Douglas, L. M.; Konopka, J. B. *Eukaryot. Cell* **2007**, *6*, 755.
28. Supplementary data is available on the online version
29. The association rate constants (k_{a1} and k_{a2}), the dissociation rate constants (k_{d1} and k_{d2}) and the equilibration constants K_{A1} (k_{a1}/k_{d1}), K_{A2} (k_{a2}/k_{d2}) and K_A ($k_{a1}/k_{d1} \times k_{a2}/k_{d2}$).

HETEROCYCLES, Vol. 82, No. 2, 2011, pp. -. © The Japan Institute of Heterocyclic Chemistry
Received, 1st July, 2010, Accepted, 20th August, 2010, Published online, 24th August, 2010
DOI: 10.3987/COM-10-S(E)86

STRUCTURAL REEVALUATIONS OF AMPHIDINOL 3, A POTENT ANTIFUNGAL COMPOUND FROM DINOFLAGELLATE

Respati T. Swasono, Mitsunori Kanemoto, Nobuaki Matsumori, Tohru Oishi, and Michio Murata*

Department of Chemistry, Graduate School of Science, Osaka University, 1-1 Machikaneyama, Toyonaka, Osaka, 560-0043, Japan (E-mail address: murata@chem.sci.osaka-u.ac.jp)

Abstract – Among other homologues, amphidinol 3 (AM3) is the most potent antifungal compound isolated from the dinoflagellate *Amphidinium klebsii.* AM3 undergoes conformational changes in organic solvents while it takes relatively fixed configuration in a membrane model. By using NMR data of peracetyl AM3, we were able to confirm the configuration of C50-C51 of AM3 which remained uncertain in our previous study.

INTRODUCTION

Marine dinoflagellates are a rich source of bioactive substances with diverse structures and highly specific activities.[1] The dinoflagellates of the genus *Amphidinium* attract much attention because of their production of bioactive compounds, such as luteophanols,[2] lingshuiols,[3] karatungiols[4], and carteraol E.[5] An early report by Yasumoto's group on hemolytic and antifungal activities from extracts of *Amphidinium klebsii* led to the isolation and identification of the first member of the family, amphidinol 1 (AM1).[6] Since then, about 17 homologues known as the amphidinols (AMs) have been isolated from the same genus.[7-9] Amphidinols largely exhibit potent antifungal, cytotoxic and hemolytic activity, and possess common structural features comprising a linear polyhydroxyl moiety, two heterocycles and an olefinic chain. These unique features make AMs an interesting model to gain a better understanding of the molecular mechanism of antifungal action. Among AM homologues, AM3 significantly exceeds other homologues in the antifungal activity. The absolute configuration of AM3 was previously determined by extensive NMR experiments such as the *J*-based configuration analysis (JBCA) method, modified Mosher method, and HPLC analysis of the degradation products.[10] Recently, we have revised the

---

This paper is dedicated to Prof. Albert Eschenmoser on the occasion of his 85th birthday

stereochemistry of C2 of AM3 to be *R* by comparing synthetic specimens with a fragment of AM3 and by GC-MS.[11] Thus, extensive synthetic studies of AM3 have been carried out by several groups all over the world.[11-16]

AMs increase membrane permeability by directly interacting with membrane lipids (Figure 1). Structure-activity relationship using naturally occurring AMs and chemically modified AM derivatives has disclosed that the polyene and polyhydroxy moieties play respective roles in binding to the lipid bilayer membrane and in forming an ion-permeable pore/lesion across lipid bilayer membranes.[8,9,17] In order to gain insight into the membrane-bound structure of AMs, conformational analysis of amphidinol 3 (AM3) has been carried out on the basis of high-resolution ^{1}H NMR data measured for SDS micelles[18] and isotropic bicelles[19] (Figure 1). These experiments have revealed that the central region of AM3 takes a hairpin conformation while the hydrophobic polyene chain is immersed in the hydrophobic interior. The stereochemistry in the central part, thus, is of great interest for not only synthetic chemistry but also mechanism of action studies; In particular, configurations of two tetrahydropyran rings and *anti/gauche* orientation of 1,2-dihydroxy moieties greatly influence the 3D structure of the AM3 molecule. Nevertheless, the configuration and conformation with respect to the C50-C51 bond remained ambiguous due to an intermediate ^2J(C50, H-51) value, which could be interpreted as alternating rotamers either in *threo-* or in *erythro-* interaction (Figure 2**a**); according to our previous data,[10] we thought that the upper pair was more likely than the bottom in bracket.

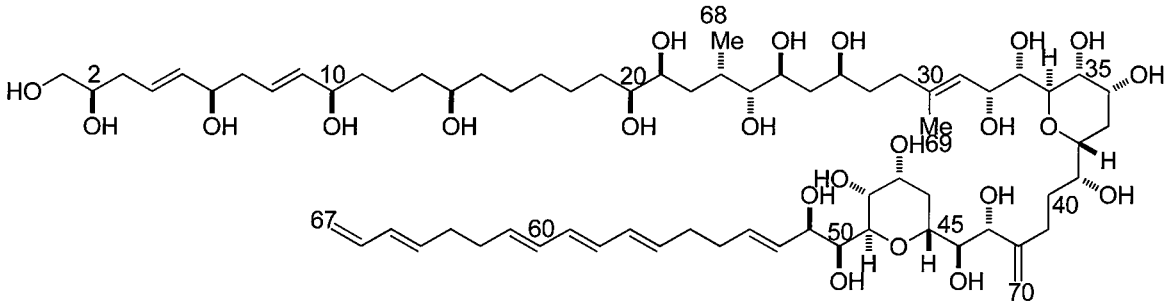

amphidinol 3 (AM3)[10]

peracetyl AM3 (All the 21 hydroxyl groups are acetylated)

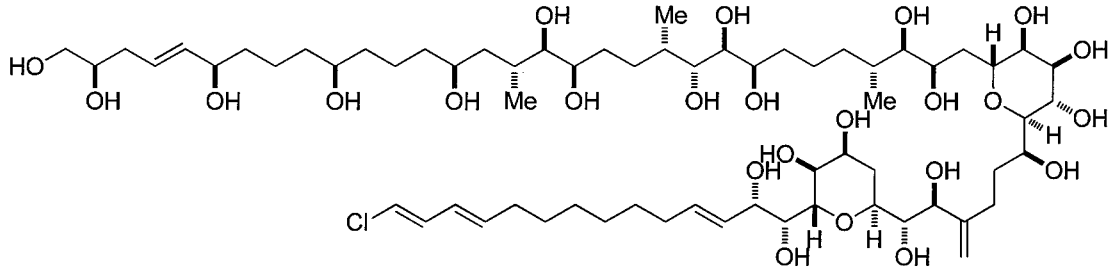

karlotoxin 2 (KmTx2)[20]

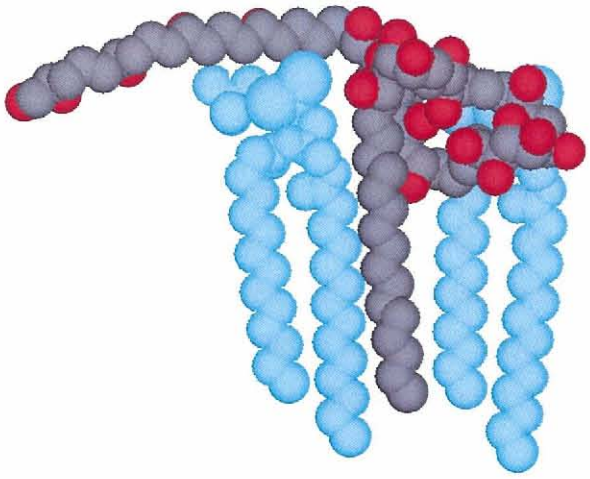

Figure 1. Proposed model for membrane-bound structure of AM3. Blue molecules represent DMPC interacting with AM3. The long and hairpin-shaped polyhydroxy chain of AM3 is likely to effectively capture the polar headgroups of lipids, which may form the inner lining of the toroidal pore (see text for details). The conformation of AM3 in the figure has been deduced from our proposed configuration and conformational analysis in micelles[18] and bicelles.[19]

Moreover, karlotoxin 2 (KmTx2), a congener isolated from the dinoflagellate *Karlodinium veneficum* that shows close structural similarities to AM3, has been reported to have the different absolute configuration for the C34-C51 unit where all the asymmetric centers have opposite configuration to those in AM3.[20] These circumstances prompted us to do further structural confirmation of AM3, in particular for the contentious portions around the tetrahedropyran rings (C32-C51), which play an essential role in the hairpin conformation of the whole molecule. In this study, we focus on the configurational/ conformational study of this region.

RESULTS AND DISCUSSION

The potent antifungal activity of AM3 likely results from its effective membrane-permeabilizing activity, which can be accounted for by ion-permeable pores or lesions formation. We have previously revealed that the size of pore or lesion in erythrocyte formed by AM3 is approximately 2.0 to 2.9 nm, which is much larger than that of amphotericin B, 0.8 nm.[17] Moreover, we have determined the conformation of AM3 in isotropic micelles[18] and bicelles[19] on the basis of the NOEs and $^{3}J_{HH}$ values obtained from the NOESY and DQF-COSY experiments, respectively. The results show that AM3 adopt a turn structure in the portion of the two tetrahydropyran rings. The polyhydroxy chain of AM3 resides in hydrophilic water-accessible region while hydrophobic polyolefin penetrates into the membrane interior. In such structures, confirmation of the stereochemistry of 1,2 diol systems adjacent to the tetrahydropyran rings is

crucial, in particular for C50-C51 portion whose conformation remains uncertain. Although intramolecular hydrogen bonding hardly causes significant conformational aberration, structural arrangements of six member ring in the region may stabilize formation of intramolecular hydrogen bonding, and as a result, alter the configuration. To eliminate the effect of this intramolecular hydrogen bond, we prepared peracetyl AM3 to confirm the stereostructure on the basis of its NMR data. Assignments of ^{1}H and ^{13}C NMR signals were based on DQF-COSY and HSQC spectra. For measuring $^{2,3}J_{C,H}$ values, we relied on HETLOC; In case of small magnetization transfer by TOCSY, intensities of HMBC cross peaks were used to deduce the coupling constant values.

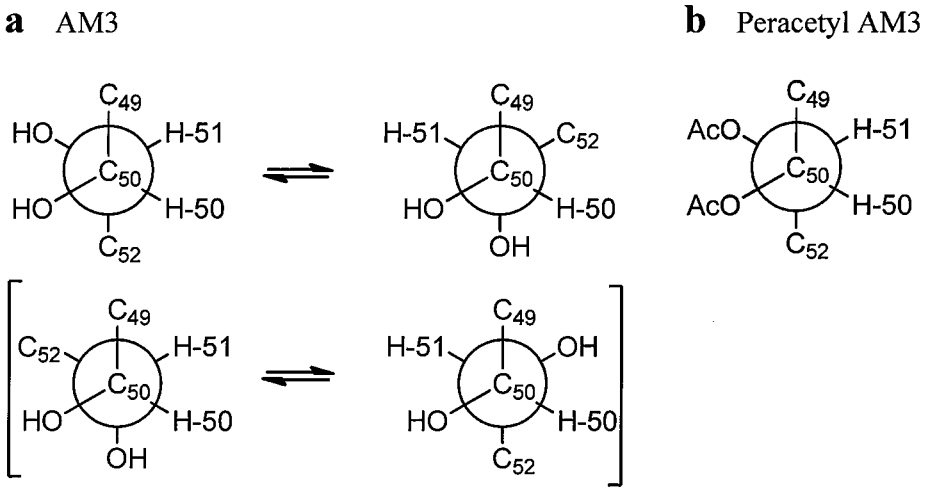

^{3}J(H-50, H-51) = 3.4 Hz
^{2}J(C51, H-50) = −2.5 Hz
^{3}J(C49, H-51) = 1 Hz

^{3}J(H-50, H-51) = 1.8 Hz
^{2}J(C50, H-51) ≅ 0 Hz
^{2}J(C51, H-50) ≅ 0 Hz
^{3}J(C49, H-51) = 0 Hz

Figure 2. Coupling constants and rotamers for C50-C51 of AM3 and peracetyl AM3. The Newman projections in **a** depict that two dominant rotamers alternate each other to give rise to intermediate *J* values.

Configuration of C50-C51 of intact AM3 in CD_3OD/C_5D_5N (2:1) underwent conformational change as depicted in Figure 2**a**, where an intermediate value of ^{3}J(H-50, H-51) suggested the presence of two alternating conformers with *gauche* or *anti* orientation for H-50/H-51. Meanwhile, ^{3}J(C49, H-51) showed only typical *gauche* interaction. The intermediate value of ^{2}J(C51, H-50) could possibly be interpreted as alternating *gauche* and *anti* orientations of H50 to C51-OH. Yet, this assignment left some ambiguity due to the inaccuracy of $^{2,3}J_{C,H}$ values as was often seen in exchanging conformers.

In contrast to AM3, the C50-C51 portion of peracetyl AM3 did not show conformational alternation. As depicted in Figure 2**b**, the small ^{3}J(H-50, H-51) value indicated the *gauche* orientation of these two protons to be predominant. The small $^{2}J_{C,H}$ values between C51/H-50 and C50/H-51 further suggested that both H-50/C51-OAc and H-51/C50-OAc adopt *anti* orientation. This was further confirmed by the small ^{3}J(C49, H-51), which indicated the *gauche* relationship between H-51/C49. Therefore, the *threo* configuration of C50-C51 was unequivocally established.

Similar assignment could also be applied for C32-C33, which is another key part for the hairpin conformation of AM3. As shown in Figure 3, typical *gauche* interaction between H-32/H-33 was revealed by the small ^{3}J(H-32, H-33) values. The values for ^{2}J(C32, H-33) and ^{3}J(C34, H-32) are small, indicating that H-33 is *anti* orientation to C32-OAc and H-32 is *gauche* to C34, respectively. These interactions clearly reveal the *threo* configuration for C32-C33.

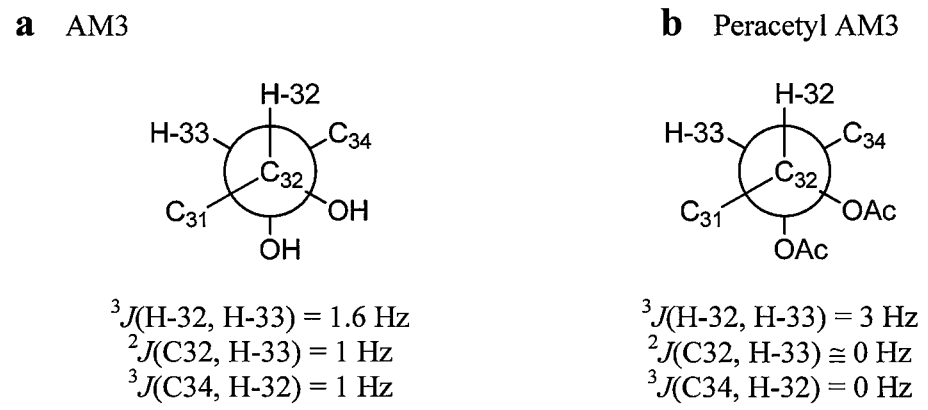

^{3}J(H-32, H-33) = 1.6 Hz
^{2}J(C32, H-33) = 1 Hz
^{3}J(C34, H-32) = 1 Hz

^{3}J(H-32, H-33) = 3 Hz
^{2}J(C32, H-33) ≅ 0 Hz
^{3}J(C34, H-32) = 0 Hz

Figure 3. Coupling constants and rotamers for C32-C33 of AM3 and peracetyl AM3

The relative configurations of the two tetrahydropyran rings (Figure 4) and the C39-C45 tether (Figure 5) were determined mainly using NOEs and *J*-based configuration analysis[21] for peracetyl AM3. Coupling constants of peracetyl AM3 used for the configuration study are listed in the Table 1 in comparison with those of AM3. The large ^{3}J(H-33, H-34) and ^{3}J(H-50, H-49) indicated the *anti* orientation of their adjacent protons; in this case, NOEs are required for the determination of the relative configuration.[21] In a *threo* configuration, an H/H-anti orientation allows C/C-gauche relationship. The prominent NOEs should be observed on for protons on these *gauche*-oriented carbons. For exo-cyclic bonds C33-C34 and C49-C50, NOEs across the ether bonds H-32/H-38 and H-45/H-51 unambiguously show their relative configurations, as previously assigned (Figure 4).

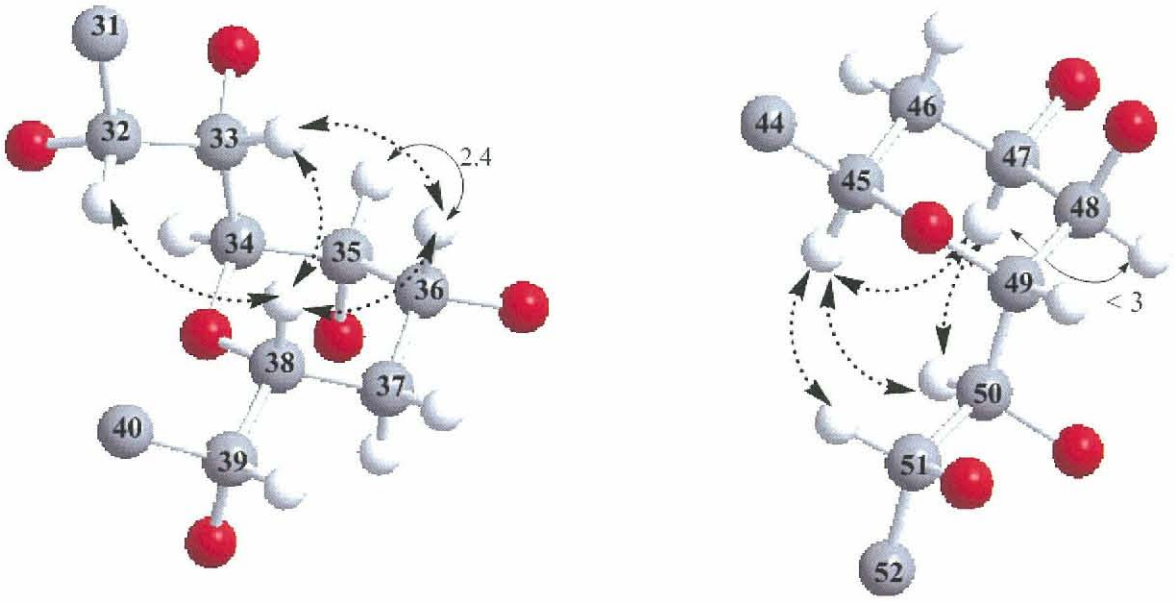

Figure 4. Configuration of tetrahydropyran rings of peracetyl AM3 with key NOEs (dashed arrow) and $^{3}J_{HH}$ in Hz (small plain arrow). Acetyl groups on oxygen atoms were omitted for clarity.

Table 1. $^{3}J_{H,H}$ and $^{2,3}J_{C,H}$ values of AM3 and peracetyl AM3

Bond	AM3[10]		Peracetyl AM3	
	$^{3}J_{H,H}$	$^{2,3}J_{C,H}$	$^{3}J_{H,H}$	$^{2,3}J_{C,H}$
C32-C33	1.6	C32-H33 = 1	3	C32-H33 ≅ 0
		C34-H32 = 1		C34-H32 = 0
C33-C34	9.5		9	
C35-C36	3.1		2.4	
C38-C39	5.1	C37-H39 = 1	4.6	C37-H39 = 0
		C40-H38 = 1		C40-H38 = 1
C39-C40	9.4 (H^S)		9.2 (H^S)	
	3.4 (H^R)		< 3 (H^R)	
C40-C41	10.2	($H\text{-}40^S$-$H\text{-}41^R$)	9	($H\text{-}40^S$-$H\text{-}41^R$)
	11.1	($H\text{-}40^R$-$H\text{-}41^S$)	9.1	($H\text{-}40^R$-$H\text{-}41^S$)
C42-C43		C41, H-43 > 5		C41, H-43 > 5
C44-C45	1.7	C44, H-45 = 0	< 3	C44, H-45 ≅ 0
		C45, H-44 = 1		C45, H-44 ≅ 0
C48-C47	3.3		<3	
C49-C50	10.0		9.2	
C50-C51	3.4	C50-H-51 = 0	1.8	C50-H-51 ≅ 0
		C51-H-50 = -3		C51-H-50 ≅ 0
				C49-H-51 = 0

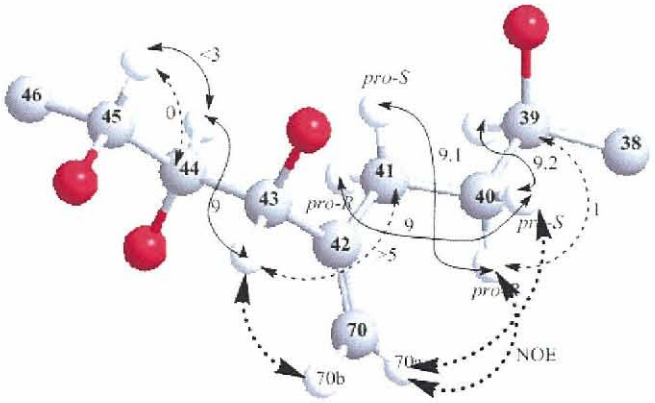

Figure 5. Configuration of C39-C45 unit of peracetyl AM3 with key NOEs (dashed arrow) $^{3}J_{HH}$ (small plain arrow), and $^{2,3}J_{CH}$ (dashed line) in Hz. Acetyl groups were omitted for clarity.

Table 2. NMR data of positions 31-52 of peracetyl AM3

Position	δ_H	δ_C	NOE
31	5.38	132.1	H-32, 33, 34
32	6.14 dd (9.0, 3.0)	69.0	H-31, 33, 34, 38
33	5.78 dd(9.0, 3.0)	70.4	H-33, 34, 35, 36, 38
34	4.49 dd (8.4, 2.4)	74.8	H-32, 33, 35
35	5.64	66.9	H-33, 34, 36
36	5.42	67.5	H-33, 37, 38
37	1.70, 2.10	28.2	H-36, 38
38	3.96	72.9	H-32, 33, 36, 37
39	5.39	72.9	H-40, 41
40	2.05, 2.26	28.7	H-39, 41, 70
41	2.22, 2.46	27.6	H-39, 40, 43, 44
42	-	145.3	
43	5.95	74.2	H-44, 70
44	5.38	74.4	H-43, 45
45	4.36	69.4	H-44, 46, 47, 50, 51
46	1.26, 1.96	27.5	H-44, 45, 47
47	5.21	74.6	H-45, 48, 50
48	5.70	74.8	H-47, 49
49	4.37 dd(9.6, 1.2)	75.5	H-48
50	6.01 dd(10.2, 1.8)	68.9	H-45, 47
51	5.71 dd (6.0, 1.8)	66.6	H-45, 50, 52, 53
52	6.18 dd(13.2, 7.2)	131.5	H-51, 53

We reported that the central region of AM3 (C20-C52) in membrane model takes a hairpin conformation.[18,19] The hydrophilic polyhydroxy portion of AM3 mainly resides on the surface, while the hydrophobic polyolefinic region penetrated in the membrane interior (Figure 1). Conformation research experiments on and around tetrahydropyran rings with the confirmed configuration in this study allows us to deduce the orientation of the polyene side chain with respect to the central hairpin portion and also to the membrane surface. Recently, we have found that the membrane-permeabilizing activity of AM3 is hardly affected by membrane thickness.[22] The finding supports the toroidal pore formation by AM3 rather than barrel-stave pore because the stability of a barrel-stave pore as exemplified by an ion channel of AmB is influenced by the membrane thickness to much greater extent than that of a toroidal pore. As aforementioned, large difference in diameter of pores formed by AM3 and AmB also infers the different mechanism of pore formation. In contrast to a barrel-stave assembly, a toroidal-pore involves lipid headgroups as pore lining even when they partially penetrate in the lipid bilayer. In the toroidal assembly, the lipid monolayer continues from the outer leaflet to inner one so that the pore is lined by both the detergents and the lipid headgroups. From this consideration, the amphiphilic structure of AM3 is apparently suitable for forming a toroidal pore where the long hydrophilic polyhydorxy chain can induce a positive curvature strain to effectively capture the polar headgroups of membrane surface (Figure 1). Finally, the hydrophilic chain of AM3 associates with lipid headgroups to form the inner lining of the toroidal pore.

In conclusion, using the detailed NMR data obtained for peracetyl AM3, we successfully confirmed the stereochemistry of the C50-C51 and C32-C33 portions of AM3 which hampered unambiguous assignments in an intact form. The current results support the previous finding that AM3 takes a turn structure around the two tetrahydropyran rings. This conformation may account for formation of a toroidal pore in biological membranes. In our previous report, the absolute configuration of C34-C51 portion of AM3 was determined on the correlation with C39, whose absolute configuration was deduced from Mosher's esters of the C33-C50 unit of HIO_4 degradation products.[10] Similarly, the absolute configuration of C34-C51 unit of karlotoxin 2 was determined on the correlation with C30;[20] the interpretation of ^3J(H-31, H-30) = 7.3 Hz as an intermediate or large coupling constant is somewhat controversial, which may possibly give an effect on assignment of relative configuration of C30-C31 and, eventually on the absolute configuration of C34-C51 unit of karlotoxin 2. To confirm the absolute configuration of C34-C51 portions of AM3, the synthetic fragments corresponding to this unit are currently being built in our laboratory to compare their stereochemistry with those of degradation products from AM3.

EXPERIMENTAL

Materials

AM3 was obtained from cultured marine dinoflagellate *Amphidinium klebsii* as previously reported;[9] Briefly, the dinoflagellate *Amphidinium klebsii* was separated from Aburatsubo-Bay, Kanazawa, Japan and deposited in National Institute of Environmental Studies (NIES 613). The unialgal culture was grown in artificial seawater (Marin Art Hi, Tomita Pharmaceutical, 3% w/v) enriched with 2% ES-1 supplement at 25 °C for 4 weeks under 16-8 light-dark photocycle. The cells (from 60 L culture) were extracted with MeOH and then with 50% aqueous MeOH. The combined extract, after the solvent was removed, was subjected to lead acetate purification, and the excess of lead acetate was eliminated using Na_2HPO_4. The supernatant was subjected to EtOAc/H_2O partition and the aqueous layer was then subjected to BuOH/H_2O partition. The butanol extract was dried and applied to an ODS open column and then to HPLC (Cosmosil, 5C_{18}-AR-II, Waters, 250 x 10 mm; 70% aqueous MeOH; UV 270 nm) to furnish 6.3 mg AM3. Pyridine and acetic anhydride were purchased from Nacalai Tesque (Osaka, Japan). Thin-layer chromatography (TLC) of silica gel 60 F254 pre-coated plates (0.25-mm thickness) was used for the reaction analyses. Perdeuterated benzene (C_6D_6) was from Euriso-Top. Other chemicals were from standard commercial sources and used without further purification.

Methods

Peracetyl AM3 was prepared as follow; 2.00 mg (1.52 μmol) of AM3 was dissolved in 75.0 μL pyridine and stirred in a small vial. Then, 75.0 μL (794 μmol) acetic anhydride was added into the solution. Reaction was carried out for 24 h under argon atmosphere. Pyridine and excess of acetic anhydride was removed by evaporation in vacuo. Afforded product was dissolved in 200 μL perdeuterated C_6D_6 and transferred into Shigemi NMR tube for NMR studies. ^1H, ^{13}C, and 2D NMR (DQF-COSY, TOCSY, HSQC, HMBC, NOESY, and HETLOC) spectra of peracetyl AM3 were recorded in benzene (C_6D_6) on a JEOL ECA500 (500 MHz) or a VARIAN AS600 (600 MHz) spectrometer. Two dimensional NMR (2D NMR) for DQF-COSY, TOCSY, and NOESY spectra were recorded at 30 °C with a repetition time of 1s in phased-sensitive mode using states method. The spectral width in both dimensions was typically 5000 Hz or 9000 Hz. The data points were acquired using a 1K X 512 complex data matrix for NOESY and TOCSY; and 1K X 256 complex data matrix for DQF-COSY which were zero filled once in X dimension and twice in Y dimension. The data points for HETLOC were 2K X 128 which were zero filled four times in X dimension and twice in Y dimension. For DQF-COSY and NOESY, 2D data were apodized with a $\pi/2$ shifted sine-squared bell curve window function before Fourier transformation. The 2D data for HMBC were apodized with a sine bell function while HETLOC data were apodized with a sine-squared bell window function. Phase sensitive HMBC and gradient enhanced HSQC (gHSQC) spectra were acquired with 32 transients per increment. The evolution delay was set for $^nJ_{CH}$ of 8 Hz (HMBC) or $^1J_{CH}$

of 140 Hz (gHSQC). DQF-COSY spectra were acquired with 16 transients per increment and a pulse delay of 1.5 seconds. NOESY spectra were acquired with 32 transients per increment, a pulse delay of 1.5 seconds, and mixing time of 0.3 seconds. The mixing times of TOCSY and HETLOC were 80 and 50 ms. In all spectra, chemical shifts were referenced to the solvent peaks (δ_H 7.15 ppm and δ_C 128.0).

ACKNOWLEDGEMENTS

This work was supported by Grants-in-Aid for Scientific Research (S) (No. 18101010), for Priority Area (A) (No. 16073211), and for Young Scientists (A) (No. 17681027) from MEXT, Japan as well as by The Naito Foundation. We thank to Mr. Seiji Adachi and Dr. Naoya Inazumi at Department of Chemistry, Osaka University for assistance in measuring NMR spectra and Mr. Toshiyuki Yamaguchi in our laboratory for the discussions and his help. R.T.S. is also grateful for a Monbukagakusho scholarship from Japanese Government.

REFERENCES

1. Y. Shimizu, *Chem. Rev.*, 1993, **93**, 1685; J. Kobayashi and T. Kubota, *J. Nat. Prod.*, 2007, **70**, 451.
2. Y. Doi, M. Ishibashi, H. Nakamichi, T. Kosaka, T. Ishikawa, and J. Kobayashi, *J. Org. Chem.*, 1997, **62**, 3820; T. Kubota, M. Tsuda, Y. Doi, A. Takahashi, H. Nakamichi, M. Ishibashi, E. Fukushi, J. Kawabata, and J. Kobayashi, *Tetrahedron*, 1998, **54**, 14455; T. Kubota, A. Takahashi, M. Tsuda, and J. Kobayashi, *Mar. Drugs*, 2005, **3**, 113.
3. X.-C. Huang, D. Zhao, Y.-W. Guo, H.-M. Wu, Y.-C. Lin, Z.-H. Wang, J. Ding, and Y.-S. Lin, *Bioorg. Med. Chem. Lett.*, 2004, **14**, 3117; X.-C. Huang, D. Zhao, Y.-W. Guo, H.-M. Wu, E. Trivellone, and G. Cimino, *Tetrahedron Lett.*, 2004, **45**, 5501.
4. K. Washida, T. Koyama, K. Yamada, M. Kita, and D. Uemura, *Tetrahedron Lett.*, 2006, **47**, 2521.
5. S.-J. Huang, C.-M. Kuo, Y.-C. Lin, Y.-M. Chen, C.-K. Lu, *Tetrahedron Lett.*, 2009, **50**, 2512.
6. M. Satake, M. Murata, T. Yasumoto, T. Fujita, and H. Naoki, *J. Am. Chem. Soc.*, 1991, **113**, 9859.
7. G. K. Paul, N. Matsumori, M. Murata, and K. Tachibana, *Tetrahedron Lett.*, 1995, **36**, 6279; G. K. Paul, N. Matsumori, K. Konoki, M. Sasaki, M. Murata, and K. Tachibana, 'Harmful and Toxic Algal Blooms: Structure of Amphidinol 3 and Its Cholesterol-dependent Membrane Perturbation: A Strong Antifungal Metabolite Produce by Dinoflagellate, *Amphidinium klebsii,*' Vol. 7, ed. by T. Yasumoto, Y. Oshima, Y. Fukuyo, Intergovernmental Oceanographic Commission of UNESCO, Sendai, 1996, pp. 503-506; R. Echigoya, L. Rhodes, Y. Oshima, and M. Satake, *Harmful Algae*, 2005, **4**, 383; Y. Meng, R. M. V. Wagoner, I. Misner, C. Tomas, and J. L. C. Wright, *J. Nat. Prod.*, 2010, **73**, 409.

8. G. K. Paul, N. Matsumori, K. Konoki, M. Murata, and K. Tachibana, *J. Mar. Biotechnol.*, 1997, **5**, 124; N. Morsy, T. Houdai, S. Matsuoka, N. Matsumori, S. Adachi, T. Oishi, M. Murata, T. Iwashita, and T. Fujita, *Bioorg. Med. Chem.*, 2006, **14**, 6548.
9. N. Morsy, S. Matsuoka, T. Houdai, N. Matsumori, S. Adachi, M. Murata, T. Iwashita, and T. Fujita, *Tetrahedron*, 2005, **61**, 8606.
10. M. Murata, S. Matsuoka, N. Matsumori, G. K. Paul, and K. Tachibana, *J. Am. Chem. Soc.*, 1999, **121**, 870.
11. T. Oishi, M. Kanemoto, R. Swasono, N. Matsumori, and M. Murata, *Org. Lett.*, 2008, **10**, 5203.
12. S. BouzBouz and J. Cossy, *Org. Lett.*, 2001, **3**, 1451; J. Cossy, T. Tsuchiya, L. Ferrie, S. Reymond, T. Kreuzer, F. Colobert, P. Jourdain, and I. E. Markó, *Synlett*, 2007, **14**, 2286; F. Colobert, T. Kreuzer, J. Cossy, S. Reymond, T. Tsuchiya, L. Ferrie, I. E. Markó, and P. Jourdain, *Synlett*, 2007, **15**, 2351.
13. E. M. Flamme and W. R. Roush, *Org. Lett.*, 2005, **7**, 1411; J. D. Hicks, E. M. Flamme, and R. Roush, *Org. Lett.*, 2005, **7**, 5509; J. D. Hicks and W. R. Roush, *Org. Lett.*, 2008, **10**, 681.
14. J. de Vicente, B. Betzemeier, and S. D. Rychnovsky, *Org. Lett.*, 2005, **7**, 1853; J. de Vicente, J. R. Huckins, and S. D. Rychnovsky, *Angew. Chem. Int. Ed.*, 2006, **45**, 7258; J. R. Huckins, J. de Vicente, and S. D. Rychnovsky, *Org. Lett.*, 2007, **9**, 4757.
15. L. A. Paquette and S.-K. Chang, *Org. Lett.*, 2005, **7**, 3111; S.-K. Chang and L. A. Paquette, *Synlett*, 2005, **19**, 2915; M. W. Bedore, S.-K. Chang, and L. A. Paquette, *Org. Lett.*, 2007, **9**, 513.
16. C. Dubost, I. E. Markó, and J. Bryans, *Tetrahedron Lett.*, 2005, **46**, 4005.
17. T. Houdai, S. Matsuoka, N. Matsumori, and M. Murata, *Biochim. Biophys. Acta*, 2004, **1667**, 91.
18. T. Houdai, S. Matsuoka, N. Morsy, N. Matsumori, M. Satake, and M. Murata, *Tetrahedron*, 2005, **61**, 2795.
19. T. Houdai, N. Matsumori, and M. Murata, *Org. Lett.*, 2008, **10**, 4191.
20. J. Peng, A. R. Place, W. Yoshida, C. Anklin, and M. T. Hamann, *J. Am. Chem. Soc.*, 2010, **132**, 3277.
21. N. Matsumori, D. Kaneno, M. Murata, H. Nakamura, and K. Tachibana, *J. Org. Chem.*, 1999, **64**, 866.
22. N. Morsy, T. Houdai, K. Konoki, N. Matsumori, T. Oishi, and M. Murata, *Bioorg. Med. Chem.*, 2008, **16**, 3084.

Acknowledgement

Praise be to Allah, the Cherisher and Sustainer of the Worlds. Firstly, I would like to thank the Mighty God for giving me the strength and perseverance to pursue my study and for teaching me a little "wisdom of Nature".

I would like to express my sincere gratitude to my supervisor, Professor Michio Murata, for the opportunities, guidance, support, and patience he provided me during my Ph.D. He has provided both excellent scientific and working facilities and always has time for questions and discussions.

My deep appreciation extends to Associate Professor Nobuaki Matsumori and Professor Tohru Oishi, who gave me invaluable guidance and advice throughout this study. I am especially thankful for their kind willingness to discuss on both experimental setups and interpretation of the data.

I am really grateful for the assistance from Mr. Seiji Adachi and Dr. Naoya Inazumi for their assistance on NMR measurements and processing some 2D spectra.

I would like to thank the Department of Chemistry, School of Graduate Science, Osaka University for use of their excellent research facilities. I am also grateful for a Ph.D scholarship from Monbukagakusho (MEXT).

I would like to extend my appreciation to past and present members of the Laboratory for Biomolecular Chemistry at the Osaka University who have assisted me during my studies. I would especially like to thank Mr. Toshiyuki Yamaguchi, Mr. Tetsuro Takano, Mr. Mitsunori Kanemoto, Ms. Asuka Kitamura, Dr. Keiichi Konoki, Dr. Ryota Mouri, Dr. Sarah Goretta, and Dr. Nagy Morsy who have helped my life inside and outside the lab.

My warmest regards to members of the PPI Osaka-Nara for the friendship and I especially thank to Ambara R. Pradipta who assisted me during my life in Osaka

Finally, I greatly indebted and deeply grateful to my parents, my wife-Anin, and my daughters-Caca and Lisha for their pray, love, support, encouragement, and understanding during my current study.